# ENGINEERING AN IMPROVED CARTILAGE REPAIR STRATEGY COMBINING CELLS AND ECM-DERIVED MATERIALS

A Dissertation
Presented to
The Academic Faculty

by

Olivia A. Burnsed

In Partial Fulfillment
of the Requirements for the Degree
Doctor of Philosophy in BioEngineering

Georgia Institute of Technology
December 2017

**ENGINEERING AN IMPROVED CARTILAGE REPAIR STRATEGY**

**COMBINING CELLS AND ECM-DERIVED MATERIALS**

Approved by:

Dr. Robert E. Guldberg, Advisor
School of Mechanical Engineering
*Georgia Institute of Technology*

Dr. Todd McDevitt, Advisor
*Gladstone Institute of*
*Cardiovascular Disease*

Dr. Krishnendu Roy
School of Biomedical Engineering
*Georgia Institute of Technology*

Dr. Johnna S. Temenoff
School of Biomedical Engineering
*Georgia Institute of Technology*

Dr. Thomas J. Koob
Chief Scientific Officer
*MiMedx Group, Inc*

Date Approved: November 1, 2017

*To my dad, Noel, for telling me "I am a winner" and teaching me to believe in myself;*

*to my mom, Alicia, for teaching me the importance of balance;*

*and to my fiancé, Roger, for his unconditional love, support, and encouragement.*

# ACKNOWLEDGEMENTS

Many people have contributed to various aspects of my projects over the past 6 years and have made the work presented in this thesis possible. To my mentors, mentees, colleagues, friends, and family – I cannot thank you enough.

First and foremost, I would like to thank my advisors, Robert Guldberg and Todd McDevitt. Todd has been a wonderful teacher and mentor throughout my PhD career. Todd's encouragement empowered me to pursue and drive research projects that were interesting to me although they were quite different from other research areas in his lab. I have learned so much about research design and interpretation through Todd, and have discovered firsthand how unexpected results can lead to interesting findings. Todd's high standards for writing and aesthetics has taught me to be more critical of my own work and the work of others, and I am so fortunate to have been a part of his lab. Despite all of the changes and many new demands on his time through moving to Gladstone Institutes, Todd has always been incredibly supportive and eager to "go to bat" for me and any of his other students whenever we need. I will always cherish my time in his lab and his mentorship.

I was so excited when Bob Guldberg agreed to take me on in the middle of my PhD after Todd decided moved to Gladstone Institutes. I had wanted to work with Bob for many years, even as an undergraduate, and was thrilled to join his group. I quickly felt at home in the Guldberg lab thanks to Bob's charismatic personality and the collaborative environment he has fostered in the lab. Through Bob's mentorship, I saw firsthand the impact and relevance of translational research and developed a passion for working with industry. Bob was incredibly encouraging even through some of my greatest mishaps

(*note: make sure you don't decalcify tibias before EPIC-μCT). Bob has taught me the importance of thinking outside the box and that by critically analyzing potential solutions to various problems, you may come up with an even better approach than originally planned. Seeing Bob interact with his peers, mentees, collaborators, and industry partners shows he has more than just a vested interest in our work, but genuinely cares about our success. I am constantly impressed by his passion for his work, care for his students, and his ability to balance so many leadership roles.

I am also incredibly grateful for the valuable feedback and poignant questions asked by my other thesis committee members: Johnna Temenoff, Krishendu Roy, and Thomas Koob. Johnna's extensive background in biomaterials and osteoarthritis helped me to think about my work in relation to the current direction of both fields. She and her lab members (particularly Torri Rinker, Jennifer Lei, and Liane Tellier) have been incredibly helpful in exchanging protocols, equipment, and ideas in many aspects of this project. Krish Roy's expertise on immunology gave me a new perspective on immunomodulation for OA and taught me that conventional paradigms of pro- and anti-inflammatory mediators are incomplete. Kirsten Parratt, Michael Nelson, Nate Dwarshuis, Alex Atalis, and Joscelyn Mejias in the Roy lab were especially helpful and collaborated to share lab space and equipment for the MSC studies described in this thesis. Moreover, both Johnna and Krish have provided invaluable insights on cell manufacturing and translatability of my projects. Working with Tom Koob from MiMedx has also allowed me to consider the effect of my project on clinical translation. Although our groups have actively collaborated for years, working directly in the MiMedx facility was extremely eye-opening and ultimately led me to develop and characterize a new in vitro system for osteoarthritis inflammation. Insights

from Tom, Jen Lei, Lauren Priddy, and my own undergraduate mentee, Lizzie Marr, who was an intern at MiMedx, shaped many aspects of this project and my (high) opinion of industry collaboration.

In addition to Lizzie, I also mentored 3 other students: Apoorv Sarogee, Nadiya Zafar, and Clinton Smith. Lizzie Marr was my first undergraduate mentee, and she helped design, plan, and perform the experiments with our decellularized cartilage microcarriers. Lizzie was completely invested in the project, always eager to learn, and never lost sight of her goals through many failed (or at least unexpected) experiments. I am forever grateful for her investments in lab (particularly the experiments that lasted late into the night) and am so proud of the biomedical engineer she has become today through her position at Draper. Apoorv Saraogee also suffered through many experiments with unexpected results when comparing chondrogenic differentiation protocols for MSCs. Although most of this work remains unpublished, Apoorv's contributions have helped shape multiple research laboratories at Georgia Tech through our collaborative MSC subgroup meetings, where his comparisons of different media types, donors, and growth factors have been shared. I am especially encouraged that Apoorv recently started as a doctoral student himself and look forward to watching him progress as a scientist and engineer. Nadiya Zafar performed multiple analyses via EPIC-μCT and helped our lab test and develop a more standardized approach for quantifying changes due to OA progression in rats. Nadiya was always interested in the clinical aspects of our work and am confident she will be a successful and nurturing medical doctor when she graduates from the Medical College of Georgia in a few years. Clinton Smith worked tirelessly in our histology core in my last semester of graduate school. Clinton was fun to work with and his understanding of the project and work ethic

are especially impressive as he is a high school intern. His interest in biomedical research is inspiring and I look forward to watching him progress into an independent scientist.

In addition to the mentors I have had in graduate school, I must also thank the multiple mentors that trained me through my undergraduate career. Chris Lee was my graduate mentor as a Petit Scholar in the Boyan/Schwartz Laboratory at Georgia Tech. Chris taught me so much in my first two years with him, including basic laboratory techniques, cell culture, PCR, statistical analysis, writing, and even aesthetics of presentation. Although I started in the laboratory as a volunteer to learn in preparation for medical school, I changed my career plans after just one semester of working with Chris. He has always been incredibly fun to work with, but also instilled high standards for quality research. Dr. Barbara Boyan was also very supportive during my time in her lab. I am constantly impressed by her passion for research and willingness to stand up for her students. I cannot emphasize enough the impact that having a strong, female role model who was (and is) a leader in the field has had on me, particularly at the start of my research endeavors. Dr. Schwartz taught me to question the status quo and probe into the mechanisms underlying each technique and protocol in lab. Dr. René Olivares-Navarrete mentored me through my senior thesis project and inspired me to dream big and ask the basic but probing questions that are so often forgotten when we're "in the trenches" of research. Sharon Hyzy also collaborated on my independent senior thesis project, and I was consistently impressed with her analytical and organizational skills. I must also thank Matthew Wolf, my NSF REU mentor in Stephen Badylak's laboratory. My experience working with decellularized matrices in the Badylak lab shaped my entire PhD, and I am incredibly thankful to Matt for his help understanding decellularization and the importance

of the extracellular matrix as it relates to inflammation. Dr. Badylak was an amazing mentor and I was encouraged and inspired by the niche he created for himself through his collaborations with industry, academia, and clinicians.

Throughout my time at Georgia Tech I have worked with the best group of colleagues, including fellow graduate students, postdocs, undergrads, and staff who have made work a fun place to be. The lab manager of the Guldberg lab, Hazel Stevens performed some of the single cell and spheroids comparisons described in this thesis. Hazel was a great sounding board for many of my experimental questions and problems. She also provided great comic relief with her English vernacular. Giuli Salazar-Noratto was often my late-night comrade in lab, training me on numerous surgical and lab techniques, and I will never forget our lab chocolate experience! Brennan Torstrick was a great carpool partner and friend, and our conversations to and from lab helped frame my perspective for the work presented in this thesis. David Reece developed the surface roughness algorithm described in this work, trained me and my undergraduate to do the EPIC-μCT analysis, and collaborated on the in vitro synoviocyte model of OA-associated inflammation. David also brought his precious little girl Jane to the graduate lair occasionally, which was a welcome respite from lab work. Laxmi Krishnan was incredibly helpful with the cryoembedding and sectioning, and I enjoyed our many conversations as neighbors in the lair. Lina Maria Mancipe Castro has been a huge asset to myself and our lab throughout her time here. I felt I could call on her for urgent help that I needed at the last minute, is a great friend, and I have thoroughly enjoyed our salsa nights! Angela Lin's expertise was absolutely essential for the micro-CT analysis presented in this thesis and both she and Nick Willet were instrumental in the experimental design of the animal studies presented in this thesis.

Angela and Nick have both been very helpful when troubleshooting problems and were extremely patient when teaching me various techniques for in vivo analyses. I am glad I got to interact with Ramesh Subbiah at the end of my PhD and have especially enjoyed the daily lab lunches he has organized. I enjoyed taking many classes with Albert Cheng as a fellow IGERT trainee and he has been a most gracious and helpful while we have figured out advanced statistical analysis together. Lauren Priddy was also very helpful in our collaboration with MiMedx group even after her graduation and I look forward to learning from her as a fellow instructor. I first delivered spheroids in vivo in a project with Ashley Allen, whose help with retroviral transfection and bioluminescent tracking later aided in my own animal studies. I've enjoyed discussing teaching aspirations and curriculum development with fellow labmate Jason Wang, and have especially appreciated his help with vermicomposting and gardening! Both Brett Klosterhoff and Marissa Ruehle have been amazing colleagues. I enjoyed co-mentoring Clinton with Brett during my last semester, when I grew to appreciate the many moving parts (literally) to his sensor work. Marissa was especially helpful during tedious preparations for MSC injections, and her friendly demeanor always made lab work more fun. Casey Vantucci is not only a talented researcher, but also a very engaging presenter and conversationalists. I enjoyed working with labmates Ryan Akman, Lina Castro, and Fabrice Bernard both in lab and as vice chairs for Biomaterials Day. Fabrice is extremely outgoing, Lina is very organized, and Ryan's fun, even keeled personality rounds out this incredible team that I know will put together another amazing Southeastern Biomaterials Day. I am glad that Gilad Doran will continue to build on this work comparing MSC culture formats and donors for osteoarthritis. Gilad is a capable researcher and I look forward to his progress with great anticipation.

Alex McKinlay and I started in the McDevitt lab together and I enjoyed collaborating on projects, our late-night homework sessions with MATLAB coding, and especially his sarcastic banter. Denise Sullivan was a year ahead of me and was very helpful in learning new laboratory techniques, but I especially loved that Denise was always up for some tension-relieving activity like kickboxing or dancing. Melissa Kinney was a senior graduate student during my time in McDevitt lab, and I continue to look up to her. Melissa manages to be incredibly fun, organized many lab activities (most were food related – yum!), and an incredible biomedical engineer. Jenna Wilson was also very helpful, a wonderful baker, and her help organizing our IGERT trainee meetings fostered collaborations and exchange of valuable information for myself and the other trainees. Joshua Zimmermann in the McDevitt lab performed a lot of the preliminary research on MSC single cells and spheroids that inspired us to consider MSC spheroids as a potential therapeutic for OA. Josh taught me so much about MSC culture, spheroid formation, and was a huge help when I was designing and developing my own experiments. Josh was fun to work with and I especially appreciated his banter with both Marian and Denise. Marian was also co-advised by Bob and Todd and helped me transition into the Guldberg lab with ease. Marian is so friendly to everyone (perhaps because of her Canadian-ness). I'll never forget how Doug White (also in the McDevitt lab) made a point to follow up with me after a particularly difficult lab meeting presentation to encourage me. Doug and Megan White were both encouraging, supportive, friends that provided lots of comic relief. Lab Managers Alex Ortiz and Marissa Cooke were so helpful when learning laboratory techniques and I enjoyed walking and carpooling with Alex while we were neighbors. Tracy Hookway did an excellent job standardizing training for McDevitt lab, and helped

me develop the immunohistochemical staining protocols used in this thesis. Yun Wang was a postdoc with me in both the McDevitt and Boyan/Schwartz labs. Yun's expertise in cartilage tissue engineering provided necessary insights for the experimental design of my first aim and she aided in early writing for grants with this project. Melissa Goude's work with cartilage tissue engineering and particularly chondrogenic culture was also very helpful. While I didn't work closely with postdocs Lindsay Fitzpatrick, Krista Fridley, Ankur Singh, or Sarah Griffiths, I really enjoyed their contributions to group discussions and their unique perspectives and contributions to the lab. Jessica Butts, Chad Glen, and Emily Jackson are all incredibly talented researchers, but also extremely friendly and fun to work with. I especially enjoyed Chad's comic relief in lab meetings with his scientific poems. Anh Nguyen was also an excellent researcher, flexible yogi, and had the best taste in music! Katy Hammersmith and I started at Georgia Tech together as undergraduates, and she was the first McDevitt lab member I met. I couldn't have had a higher opinion from Katy's description and was so pleased that the lab was a friendly, inclusive, and collaborative as Katy described.

Levi Wood, Sitara Sankar, and Laura Weinstock have also been instrumental in the Luminex bead assays and partial least squares discriminate analysis detailed in this thesis. Levi's lab developed much of the MATLAB code that I used to analyze the secretome of MSCs and synoviocytes and Levi was particularly helpful and approachable throughout the development of this project. I am so thankful for Sitara's thoughtful training for the Luminex system that contributed to a large portion of this thesis. Both Sitara and Laura provided crucial help with the equipment and analysis and they made me feel at home each time I popped in their lab for advice.

One of my favorite things about the BME department at Georgia Tech is the collaboration with Emory University. Luke Brewster, a vascular surgeon at Emory, graciously provided the human femurs that were used to isolate primary chondrocytes for the microcarrier expansion comparisons. Heidi Kloefkorn, now at Emory, and Kyle Allen (from the University of Florida) developed the semi-automated OARSI GUI scoring system that significantly reduced the time required to analyze a large number of samples. Heidi was especially helpful in training our lab on OARSI scoring techniques and how to use the GUI she developed.

The Petit Institute and BME department have also provided immeasurable support on various aspects of this project. Research staff in core facilities – Aqua Asberry, Andrew Shaw, Allen the PRL staff – provide us with functional, high quality researches that make the Petit Institute a great place to do research. The additional support of Petit Institute staff – Colly Mitchell, Meg McDevitt, Laura Paige, Vivian Johnson, Rose Brito, Karen Ethier, Angela Barros, Floyd Wood, Courtney Ferencik, James Echols, Steve Woodard, Angela Ayers, Maria Pinto, and Randy Johnson – have been so helpful throughout my PhD and I am thankful that I got to know all of them throughout my time at Tech. I am especially thankful that I got to know the late Christopher Ruffin, who was an extremely generous and kind director for the BioEngineering program and made the transition to the BioE department easy. Laura Paige had huge shoes to fill and has left everyone impressed! Laura is so friendly and encouraging to students, and I don't know what our program would do without her support. I would also thank Dr. Andrés Garcia for his encouragement and for being the facilitator for our first two Biomaterials Days. He has continued to support me through recommendations for my future endeavors in academia. His passion for research,

curriculum, and people is contagious and I enjoyed serving on the BioEngineering Graduate Association. I would also like to especially thank Meg McDevitt for everything she has done to encourage and support me. She not only supports the lab through her amazing marketing and event planning, but she also helped me immeasurably in organizing the inaugural Georgia Tech Biomaterials Day. I similarly wish to thank Colly Mitchell, who helped bring our ideas for a Southeastern Biomaterials Day to life. Since my time as a Petit Scholar, I have enjoyed working with Colly and am so appreciative of her support, encouragement, and friendship.

Finally, to my family – my parents, my brother, my grandparents, and my cousin have all been so supportive throughout this process. Thank you for your constant guidance and encouragement. Growing up, my father constantly told me that "I am a winner" and nurtured my skills as an engineer, critical thinker, and communicator. My grandparents were all incredibly supportive of my education, both financially and emotionally, and words cannot express my gratitude for their unconditional love and support. My mom helped me to understand the importance of balance in life, and without her help I am sure I would have "burned out" and missed out on the many extracurricular activities that are some of the highlights of my time at Tech. I am most proud of my "buddy" and brother, Stephen. Watching him grow into a great dad in the last few months of my PhD has been an incredible experience and I am so excited to spoil my new niece, Paisley Olivia Burnsed. My cousin, best friend, and maid of honor has also been a life line throughout my PhD, and her snapchat videos have gotten me through many late nights in lab. I am constantly impressed by the balance she has in life, her compassion, and especially her traveling, gypsy soul. I would also like to thank my soon to be in-laws, Jack, Eve, and Bryan – who

have taken me in as one of their own and supported Roger and me throughout our PhDs. Through the many rough times, my family has helped me to maintain my perspective on the important things in life and has rejoiced in my successes.

Perhaps most importantly, this work would not be possible without the love, support, and encouragement of my fiancé, Roger White. Roger has been my rock, my best friend, my proof-reader, my statistician, and my shoulder to cry on throughout my doctorate. Words cannot express how thankful I am for him and our relationship, particularly over the last year when we have been 1,800 miles apart. I am so excited to close that gap soon and continue to learn and growth together as his wife.

# TABLE OF CONTENTS

# LIST OF TABLES

# LIST OF FIGURES

# LIST OF SYMBOLS AND ABBREVIATIONS

| | |
|---|---|
| **µC(s)** | Microcarrier(s) |
| **2D/3D** | 2-dimensional/3-dimensional |
| **A** | Amnion |
| **Acan** | Aggrecan or aggregating proteoglycan |
| **ACI** | Autologous chondrocyte implantation |
| **ADAMTS** | A disintegrin and metalloproteinase with thrombospondin motifs |
| **AKT** | Protein kinase B |
| **AM** | Amniotic membrane |
| **ANOVA** | Analysis of variance |
| **aSYN** | Activated synoviocytes |
| **AtSPH** | Amnion separated from spheroids by transwell |
| **BLI** | Bioluminescent imaging |
| **BMP** | Bone morphogenetic protein |
| **CCL5/RANTES** | Chemokine ligand 5 (regulated on activation, normal T cell expressed and secreted) |
| **CD** | Cluster of differentiation |
| **cDNA** | Complimentary DNA |

| | |
|---|---|
| **CG-µCs** | CultiSpher®G gelatin microcarriers |
| **Col1/Col I** | Type-I collagen alpha 1 |
| **Col10/Col X** | Type-X collagen |
| **Col2/Col II** | Type-II collagen alpha 1 |
| **Comp** | Cartilage oligomeric matrix protein |
| **CTXII** | C-terminus telopeptide of type II collagen |
| **DAPI** | 4',6-diamidino-2-phenylindole |
| **DC-µCs** | Decellularized cartilage microcarriers |
| **DMEM** | Dulbecco's modified Eagle's medium |
| **DMOAD** | Disease modifying osteoarthritis drug |
| **DNA** | Deoxyribonucleic acid |
| **DPBS** | Dulbecco's phosphate buffered saline |
| **ECM** | Extracellular matrix |
| **EDTA** | Ethylenediaminetetraacetic acid |
| **EGF** | Epidermal growth factor |
| **ELISA** | Enzyme-linked immunosorbent assay |
| **EPIC-µCT** | Equilibrium partitioning of an ionic contrast agent – microcomputed tomography |

**ERK** Extracellular signal–regulated kinases

**EtD-1** Ethidium homodimer-1

**EtOH** Ethanol

**FBS** Fetal bovine serum

**FDA** Federal drug administration

**FGF2** Basic fibroblast growth factor

**Flt-3L** FMS-like tyrosine kinase 3 ligand

**Fmod** Fibromodulin

**GAG** Glycosaminoglycan

**G-CSF** Granulocyte-colony stimulating factor

**GFP** Green fluorescent protein

**GM-CSF** Granulocyte-macrophage colony-stimulating factor

**GRO** Growth-regulated oncogene

**H&E** Hematoxylin & eosin

**HEK** Human embryonic kidney cells

**HGF** Hepatocyte growth factor

**hMSCs** Human mesenchymal stem cells

**IDO** Indolamine-2,3-Dioxygenase

| | |
|---|---|
| **IFN** | Interferon |
| **IGF-1** | Insulin-like growth factor 1 |
| **IL** | Interleukin |
| **iNOS** | Inducible nitric oxide synthases |
| **IP-10** | Interferon gamma-induced protein 10 |
| **IVIS** | In vivo imaging system |
| **LPS** | Lipopolysaccharides also known as lipoglycans and endotoxins |
| **LV** | Latent variable |
| **MACI** | Matrix assisted autologous chondrocyte implantation |
| **MCL** | Medial collateral ligament |
| **MCP** | Monocyte chemotactic proteins |
| **MDC** | Macrophage-derived chemokine |
| **MEMα** | Minimum essential medium alpha |
| **MIA** | Monoiodoacetate |
| **MIP** | Macrophage inflammatory proteins |
| **MMP** | Matrix metallopeptidase |
| **MMPi** | Matrix metallopeptidase inhibitors |
| **MMT** | Medial meniscal transection |

**MSC** Mesenchymal stem/stromal cell

**MSCGM** MSC growth media

**N** Normal seeding density

**NSAIDs** Non-steroidal anti-inflammatory drugs

**OA** Osteoarthritis

**OARSI** Osteoarthrtis research society international

**Opn/Spp1** Osteopontin

**P** Pooled

**P1/P2** Passage1/2

**PBS** Phosphate buffered saline

**PC** Principal component

**PDGF** Platelet-derived growth factor

**PDL** Passage doubling level

**PDO** Polydioxanone

**PGE2** Prostaglandin E2

**PL** Platelet lysate

**PLA** Polylactic acid or polylactide

**PLGA** Poly(lactic-*co*-glycolic acid)

**PLSDA** Partial least squares discriminate analysis

**PLSR** Partial least squares regression

**R** Rotary

**RA** Rheumatoid arthritis

**RNA** Ribonucleic acid

**RPM** Revolutions per minute

**Rps18** Ribosomal protein S18

**Runx2** Runt-related transcription factor 2

**S** Static

**SafO** Safranin-O

**SC** Single cells

**sCD40L** Soluble CD40 ligand

**SDF-1** Stromal cell-derived factor 1

**sGAG** Sulfated glycosaminoglycan

**SGM** Synoviocyte growth medium

**SLP** Secretory leukocyte protease

**Sox9** SRY (sex determining region Y)-box 9

**SPH** Spheroids

**SPHwA** MSC spheroids with amnion pre-incorporated

**t** Transwell

**TCPS** Tissue culture polystyrene

**TGF-β** Transforming growth factor-β

**TLR** Toll-like receptor

**TNFα** Tumor necrosis factor alpha

**TSG-6** Tumor necrosis factor-inducible gene 6 protein (TNF-stimulated gene 6 protein)

**uSYN** Unactivated synoviocytes

**VEGF** Vascular endothelial growth factor

**VOI** Volume of interest

# SUMMARY

Osteoarthritis (OA) is the leading cause of disability in the US and one in two people are expected to develop knee OA by age 85. OA is disease of the entire joint, affecting not only the cartilage, but also the bone and synovium. The avascularity, low cellularity, and slow proliferation of chondrocytes all limit the natural regenerative capacity of cartilage in addition to the chronic inflammation prevalent in the joint space.

Cell therapies, such as autologous chondrocyte implantation (ACI), offer promising options for treating persistent cartilage lesions, but the inability to expand chondrocytes to sufficient numbers without adversely affecting their phenotype remains a significant problem. While synthetic microcarrier culture can improve the scalability of chondrocyte expansion over conventional monolayer methods by providing a high surface area-to-volume ratio, de-differentiation remains a problem for long-term expansion. Therefore, decellularized cartilage microcarriers (DC-μCs) that retain structural and biochemical cues of the native extracellular matrix (ECM) may provide an improved means to culture and deliver chondrocytes for ACI therapies. While ACI is promising, it is not indicated for cartilage damage associated with OA or other inflammatory diseases of the joint and is better for defects resulting from trauma. This lack of efficacy of cellular therapies is likely due to the inflammatory environment cells are exposed to upon implantation since multiple inflammatory mediators have been shown to play a pivotal role in the initiation and perpetuation of OA. Anti-inflammatory therapies with single molecular inhibitors do not effectively modulate the complex inflammatory environment presented in OA. Thus, novel therapies capable of modulating multiple signaling pathways and cell types are needed.

Mesenchymal stem cells (MSCs) are an adult multipotent stem cell population that can regulate multiple immune cells involved in innate and adaptive immunity, largely through paracrine mechanisms. Additionally, human amniotic membrane (AM) has emerged as a potential therapy for OA as it provides an abundant source of multiple immunoregulatory proteins, promotes stem cells proliferation, promotes pro-healing macrophage phenotype, and modulates cell secretion *in vivo*.

Therefore, the objective of this proposal was to engineer an improved cartilage repair strategy by combining cells and ECM materials to address problems with both cartilage repair and OA-associated inflammation. In Chapter 3, we developed decellularized cartilage microcarriers that retain endogenous extracellular matrix proteins to both expand and deliver chondrocytes while retaining their phenotype. In Chapter 4, robust characterization of the influence of culture format, donor variability, and media composition demonstrated that aggregated MSCS have enhanced sensitivity to changes in the local microenvironment, which can be tailored to enhance immunomodulatory paracrine activity. Moreover, MSC single cells and spheroids reduced inflammation in activated synoviocyte cultures in a dose-dependent manner and reduced OA progression when delivered to a rodent model of OA. Finally, in Chapter 5, we investigated the interaction between MSCs and human amniotic membrane and the influence of cell-cell and cell-ECM therein on the modulation of inflammation, both in vitro and in vivo. Overall, this work broadens current understanding of cartilage tissue engineering and immunomodulation, providing valuable information that can be used to develop strategies to improve efficacy of osteoarthritis treatments.

# CHAPTER 1. INTRODUCTION

Articular cartilage defects due to degeneration or trauma are one of the most common causes of chronic pain, stiffness, and loss of joint movement in all age populations. Cell therapies, such as autologous chondrocyte implantation (ACI), offer promising options for treating persistent cartilage lesions, but the inability to expand chondrocytes to sufficient numbers without adversely affecting their phenotype remains a significant problem. While synthetic microcarrier culture can improve the scalability of chondrocyte expansion over conventional monolayer by providing a high surface area-to-volume ratio, de-differentiation remains a problem for long-term expansion, which may be due to the lack of pro-chondrogenic properties within the system. Therefore, decellularized cartilage microcarriers (DC-μCs) that retain structural and biochemical cues of the native extracellular matrix (ECM) may provide an improved means to culture and deliver chondrocytes for ACI therapies.

While ACI has good clinical outcomes when the defect repair is hyaline cartilage as opposed to fibrocartilage, ACI is not indicated for cartilage damage associated with osteoarthritis (OA) or other inflammatory diseases of the joint and is better suited for defects resulting from trauma. This lack of efficacy of cellular therapies may be due to the inflammatory environment cells are exposed to upon implantation since multiple inflammatory mediators have been shown to play a pivotal role in the initiation and perpetuation of OA. Although non-steroidal anti-inflammatory drugs are often administered for pain management in OA, they inhibit proteoglycan secretion and are not recommended for cartilage cell therapies. Other, more targeted, anti-inflammatory

therapies, including use of systemic and intra-articular biologic agents to inhibit TNF-α and IL-1β, have also proved disappointing and were unable to effectively modulate the complex inflammatory environment presented in OA. Thus, novel therapies that are capable of modulating multiple signaling pathways and cell types are an attractive alternative to address OA-associated inflammation that is currently unachievable with available drug treatment regimens.

Mesenchymal stem cells (MSCs) are an adult multipotent stem cell population that can regulate multiple immune cells involved in innate and adaptive immunity, largely through paracrine mechanisms. Additionally, human amniotic membrane (AM) has emerged as a potential therapy for OA as it provides an abundant source of multiple immunoregulatory proteins, promotes stem cells proliferation, and promotes pro-healing macrophage phenotype *in vivo*.

The **overall objective** of this proposal is to engineer an improved cartilage repair strategy by combining cells and ECM materials in order to address problems with both cartilage repair and OA-associated inflammation. The **central hypothesis** is that cartilage and amniotic membrane ECM-based materials will provide a matrix-specific microenvironment that will enhance cellular response in terms of stimulating an appropriate phenotype and cytokine production, respectively. The **rationale** for this hypothesis is that decellularized cartilage represents a structurally and functionally appropriate microenvironment to promote chondrogenesis and retention of cartilage-specific phenotype, and amniotic membrane contains multiple cytokines that may have a synergistic effect on paracrine activity of MSCs. The central hypothesis will be tested with the following specific aims:

**Specific Aim 1:** Determine the ability of decellularized cartilage microcarriers (DC-µCs) to promote the phenotypic stability & ex vivo expansion of human chondrocytes. The working hypothesis for this aim was that *ex vivo* expansion of human chondrocytes on DC-µCs would yield a more stable chondrogenic phenotype than tissue-culture treated polystyrene (plated) or gelatin CultiSpher-G microcarrier (CG-µC) expansion. DC-µCs were fabricated and characterized; and primary human chondrocytes were cultured on the DC-µCs, G-µCs, or plated up to 14 days. Cell viability, yield, and gene expression were analyzed and principal component analysis was performed. DC-µCs constructs were an effective method of expanding human chondrocytes while enhancing retention of their endogenous phenotype that could be suitable for direct implantation.

**Specific Aim 2**: Characterize the effects of culture parameters on MSC immunomodulation of OA. The working hypothesis for this aim is that the MSC secretome can be manipulated by altering environmental conditions, such as three-dimensional aggregation to enhance inherent immunomodulatory activity. The impact of the culture format (2D monolayer or 3D spheroids), donor variability, seeding density, and media composition on MSC immunomodulation was assessed by quantification of MSC paracrine factors and suppression of activated synoviocyte proliferation in co-culture and trans-well studies. MSC delivery as single cells and spheroids were then compared in the rat medial meniscal transection (MMT) rat model of OA and evaluated through histological analysis and equilibrium partitioning of an ionic contrast (EPIC) agent via µCT analysis.

**Specific Aim 3:** Evaluate the ability of MSCs and amnion to modulate inflammation & OA progression. The working hypotheses is that amnion culture can modulate and enhance MSC paracrine activity and enhance immunomodulation. Amnion incorporated into

spheroids during formation was compared to co-delivering amnion with the spheroids and transwell culture of amnion and spheroids. MSC spheroids with or without amnion were also compared to amnion or amnion alone in transwell and co-culture studies with activated synoviocytes. Finally, MSCs with or without amnion were intra-articularly delivered to MMT rats and OA progression was evaluated via EPIC-μCT and semi-automated histopathological scoring.

This project is *innovative* because it examines the ability to engineer the physical and biochemical elements of transplantable cell-ECM constructs to direct cell phenotype and/or modulate cytokine production. Through the completion of this project, we have addressed multiple shortcomings in current osteoarthritis therapies by both developing a novel tissue engineering strategy to replace damaged cartilage and combatting the complex inflammatory environment associated with OA. We constructed transplantable decellularized cartilage microcarriers capable of supporting chondrocyte expansion and sustaining the chondrogenic phenotype, laying the ground work for countless other applications of transplantable ECM microcarrier platforms. By characterizing an *in vitro* model using activated synoviocytes, we provide insights into the mechanisms governing OA-associated inflammation and developed a useful tool for screening potential therapies. Finally, the results of this project have yielded novel scientific insights into the mechanisms governing amniotic membrane particles, MSC paracrine activity, and their utility for osteoarthritis therapies.

# CHAPTER 2. BACKGROUND

## 2.1 Cartilage Biology

Cartilage is the tough but flexible tissue that cushions bones, providing mechanical support to the joints, allowing bones to glide easily over one another. It differs from other tissues because it is avascular, has a low cell density, and contains specialized cells, chondrocytes, which produce large amounts of extracellular matrix. There are three types of cartilage tissue: fibrous, elastic, and hyaline. The meniscus and intervertebral discs are composed of fibrous cartilage that allows for higher stress than hyaline cartilage. This fibrous cartilage has mechanical properties more similar to ligaments and tendons [1]. Elastic cartilage, like the auricular cartilage found in the ear, has more elastin, allowing the tissue to deform more elastically but does not have the same compressive strength as articular cartilage. Hyaline cartilage is a type of cartilage found on many joint surfaces that is very strong but still flexible and elastic. The focus of articular cartilage repair treatments is to restore the surface of an articular joint's hyaline cartilage after osteoarthritis damage.

In the developing embryo, chondrogenic cells arise primarily from the mesoderm, and cell-cell and cell-matrix interactions lead to differentiation of mesenchymal stem cells into chondroblasts and osteoblasts (bone forming cells). Chondrogenesis is marked by the expression of cartilage-specific proteins, the earliest and most important being transcription factor Sox9 [2, 3]. Sox9 then upregulates collagen type II and increases synthesis of aggrecan [3]. In response to biological and mechanical signals, the proliferating chondrocytes then undergo many mitotic divisions and align [3, 4]. As chondrocytes are further stimulated and mature, they progress away from proliferating

zone toward the middle zone and have a greater concentration of proteoglycans, are more spherical, and have an increased density of synthetic organelles indicating a greater role in matrix production [3, 4]. When chondrocytes stop dividing and begin to increase in size, they undergo hypertrophic differentiation, characterized by the expression of collagen type X, which induces calcification of the matrix [3]. The chondrocytes undergo apoptosis, allowing for subsequent osteogenesis causing the calcified cartilage to be replaced by subchondral bone and bone marrow in osteochondral bone formation [2]. Although cartilage has a low cell density of only 5-10% of the total cartilage tissue volume, chondrocytes are responsible for the production and maintenance of the dense extracellular matrix that provides the tissue its primary mechanical function [2, 4].

## 2.2 The Extracellular Matrix

The extracellular matrix of cartilage is composed mainly of water (60-87%) [5], collagens (10-30%), and proteoglycans (3-10%) [4]. Each type of cartilage has different compositions of collagens, proteoglycans, and other matrix components. Collagen complexes form the scaffold that gives cartilage its tensile strength. There are multiple types of collagens, which contribute to over 50% of the dry weight of cartilage. The major cartilage collagen is collagen type II, which accounts for 90-95% of the total collagen in most cartilage tissues [4, 5]. Collagen fibers are also important because of their ability to anchor proteoglycans in the cartilage matrix.

Proteoglycans are macromolecules consisting of a core protein covalently attached to glycosaminoglycan chains. These proteoglycans allow cartilage to resist compressive load. The most abundant protein core in cartilage is aggrecan, a cartilage-specific,

aggregating proteoglycan. The disaccharide chains of proteoglycans are heavily sulfated, producing a negatively charged matrix that is able to hold large amounts of water [6]. Cartilage oligomeric matrix protein (COMP) is another important extracellular matrix component found in cartilage that is thought to be involved in cartilage differentiation, pathogenesis, and cartilage turnover [7]. The extracellular matrix also sequesters cellular growth factors, and acts as a local depot for them. Changes in physiological conditions can trigger protease activities that cause local release of growth factors and allow the rapid and local growth factor-mediated activation of cellular functions [8].

## 2.3 Osteoarthritis

### *2.3.1 Prevalence*

Cartilage defect repair is extremely challenging due to the innate inability of cartilage tissue to regenerate properly [9]. Osteoarthritis (OA) is the degenerative joint disease characterized by joint pain, swelling, and stiffness due to cartilage loss. In 2006, an estimated 46 million in the US had doctor-diagnosed osteoarthritis [10]. Approximately 80 to 90 percent of the population is afflicted with degenerative joint disease by age 65 and nearly 1 in 2 people are expected to develop symptomatic knee OA by age 85 [11, 12]. With a rapidly aging population and an increase in the prevalence of obesity, the number of patients afflicted with osteoarthritis is expected to grow to 67 million by 2030 [12]. The direct costs of OA treatment to US insurers and individuals is more than $185 billion annually [13]. In order to develop a treatment for osteoarthritis, causes and symptoms of the disease should be considered, along with problems with current treatment options.

### *2.3.2 Disease Progression*

Osteoarthritis begins with damage and progressive degradation of articular hyaline cartilage structure and function [14]. Chondropenia is the early stage of degenerative joint disease and is defined by the loss of articular cartilage volume. As this chondropenia progresses, stress increases across the entire joint leading to further erosion of the cartilage. If OA progresses to full thickness cartilage loss, it results in abnormal remodeling of bone and the formation of osteophytes, or bone spurs that project along joints [14]. This progression may eventually lead to joint malalignment, which hastens structural deterioration of the joint by increasing localized loading forces [15]. The symptoms associated wish OA results from these abnormal stresses, which become worse and more frequent with increasing age [16].

### *2.3.3 Types of Osteoarthritis*

Osteoarthritis is categorized as primary (idiopathic) or secondary. Primary OA occurs with no apparent initial cause or abnormality and has a direct correlation with aging [16]. Secondary OA of the knee occurs as the result of trauma or repetitive motion or from congenital conditions and underlying diseases. While the initial causes of these categories of OA differ, this distinction does not alter clinical practices and therapeutic choices.

### *2.3.4 Inflammation and Osteoarthritis*

Autologous chondrocyte implantation is the first and only FDA-approved cell therapy product used to repair articular cartilage injuries, but it is not approved for patients with OA or inflammatory diseases [17]. The lack of efficacy of cell therapies is due in part

to the inflammatory environment cells are exposed to upon implantation since multiple inflammatory mediators have been shown to play a pivotal role in the initiation and persistence of OA. OA chondrocytes express an array of cytokines, chemokines, alarmins, damage-associated molecular pattern molecules, and adipokines that act as paracrine factors and initiate cartilage degradation locally, but also reach the synovium to increase cytokine production by synovial macrophages and fibroblasts, which promote inflammation and further enhance cartilage damage [18].

In fact, synovial inflammation precedes detectable structural changes and is an indicator of future medial cartilage loss [19-22]. Healthy synovium is normally two to three layers thick and lacks inflammatory cells, but the onset of inflammation is marked with hyperplasia of the lining cells and infiltration of macrophages, T and B cells [23], mast cells [24], and natural killer cells [25]. Although multiple tissues are involved in OA-related inflammation, the synovium is a major site of gross and microscopic changes that occur early in disease progression [26]. These findings suggest that targeting the inflammatory process may be critical for improving the efficacy of disease-modifying OA therapies [27].

Interleukin-1 beta (IL-1β) is one of the key cytokines involved in the pathogenesis of OA, capable of inducing inflammatory reactions and catabolic effects independently as well as being combined with other mediators. It interferes with chondrocyte synthesis of type-II collagen and aggrecan [28, 29] and increases chondrocyte synthesis of matrix metalloproteinases (MMPs) 1,3, and 13 [30-32]. In addition to inducing its own secretion in an autocrine manner, IL-β also stimulates synthesis of other inflammatory cytokines involved in OA including TNFα, IL-6, IL-8, and CCL5 [33-37].

Both IL-1β and TNFα are increased in the synovial fluid, synovial membrane, cartilage, and subchondral bone in OA, and the expression of TNF-R1 isotype membrane receptors are increased in fibroblast-like synoviocytes [38-43]. IL-1β and TNFα exposure also speed up chondrocyte aging and induces apoptosis [44-46]. More specifically, TNFα alone blocks chondrocyte synthesis of proteoglycan components, proteins binding proteoglycans, and type II collagen, and increases IL-6, IL-8, RANTES, VEGF, MMP-1, MMP-3, MMP-13, and ADAMTS-4 [34-36, 47-52].

Although non-steroidal anti-inflammatory drugs (NSAIDs) are often administered for pain management in OA, they inhibit proteoglycan secretion and are not recommended for cartilage cell therapies [53]. Inflammation is a complex biological process involving many molecules and signaling pathways, thus current drug treatment regimens for immune diseases targeting a single molecule or pathway are often ineffective and insufficient to suppress chronic inflammation due to inherent compensatory pro-inflammatory pathways, causing patient success to vary greatly [54]. The inherent immunomodulatory capabilities of MSCs offer a potent alternative to conventional drug treatment regimens due to their ability to regulate multiple signaling pathways and cell types of innate and adaptive immunity.

## 2.4 Current Treatments for Osteoarthritis

### *2.4.1 Non-surgical Treatments*

A number of non-surgical treatment options exist to alleviate pain and improve function for patients with osteoarthritis. Some of these treatments include exercise, weight loss, anti-inflammatory drugs, painkillers, and nutritional supplements like glucosamine and chondroitin [55-57]. Glucosamine is a precursor for the formation of glycosaminoglycans, proteoglycans, and glycolipid. Chondroitin sulfate is a glycosaminoglycan, which constitutes a major component of cartilage. A study by Clegg *et al*. tested the efficacy of glucosamine and chondroitin sulfate daily supplements in treating the pain symptoms of osteoarthritis. In patients with moderate to severe arthritis pain, the placebo yielded a patient reported improvement in pain or function of 54.3%, while combination therapy with glucosamine and chondroitin sulfate had a response of 79.2% [56]. Though Clegg *et al.* showed improvement in self-reported patient pain and function, it is unknown if these compounds are able to localize to the area of osteoarthritis inflammation and are then incorporated to enhance cartilage formation. These non-surgical treatments for osteoarthritis aim to alleviate pain and improve function, but most treatments do not modify the natural history or progression of OA. When these treatments are ineffective, operative treatments are required [58].

### *2.4.2 Surgical Treatments*

Some surgical procedures intend to repair or restore cartilage. Microfracture is one of the treatments of choice and involves drilling into the subchondral bone to cause bleeding to release progenitor cells and regenerative factors. The tissue formed, however,

is a scar-like fibrocartilage that is mechanically inadequate and often results in lesions reappearing [58].

Allografts of healthy cartilage plugs with subchondral bone harvested from cadavers have also been used to repair cartilage defects. The implanted hyaline cartilage/bone is initially more stable than the fibrocartilage formed in the previous methods, but donor disease transfer, rejection, and integration are constant issues with allografts. Autografts from non-load bearing areas of the patient have also been used, but can also lead to donor site morbidity [58].

Autologous chondrocyte implantation (ACI), which involves transplanting a patients' own chondrocytes after *ex vivo* expansion, is the most widely used cell-based surgical procedure for the repair of traumatic cartilage defects [59]. Large number of cells (1.6 million cells per $cm^2$ defect) are typically needed due to the direct positive correlation between implanted cell density and the final clinical outcome [60]. Although ACI has good clinical outcomes for defect repairs resulting in hyaline cartilage, autologous chondrocyte repairs composed of fibrocartilage showed more morphologic abnormalities and became symptomatic earlier than patients requiring reoperations for other reasons and 72% of patients requiring reoperation due to macroscopically abnormal cartilage had chondral defects composed of fibrocartilage rather than hyaline cartilage [61]. Additionally, inadequate chondrocyte viability [62], inefficient cell retention [59], hypertrophic differentiation, delamination, and poor tissue integration [63] at cartilage defect sites following *in vivo* implantation of single chondrocyte suspension are impediments to successful outcomes of traditional ACI therapies. Therefore, the need for rapid and

efficient cell expansion while maintaining appropriate phenotype presents a predominant challenge for this regenerative medicine approach.

These surgical attempts to repair or regenerate cartilage are often ineffective and the disease continues to progress. Pain relievers and anti-inflammatory drugs are used to alleviate pain until total joint replacement is required, 450,000 of which were performed annually in 2004 alone [12]. Although hip and knee replacement can improve quality of life [64-66], these major surgical procedures have multiple associated risks, can fail with wear and tear, often require revision surgeries throughout the lifetime of the patient [67, 68]. There is especially a concern for long-term outcomes in younger patients [69, 70]. This overview of osteoarthritis demonstrates that even though many treatments exist to relieve the symptoms associated with OA, there is an increasing demand to find an effective source for disease modifying therapies before total joint arthroplasty is necessary.

## 2.5 Tissue Engineering Strategies

### *2.5.1 In vitro vs In Vivo*

Some tissue engineering approaches focus on creating tissue *in vitro* for later implantation into the body, while other areas of regenerative medicine focus on how to stimulate chondrogenesis *in vivo*. *In vitro* tissue engineering allows for greater control and alteration of the environment, is less expensive to study, and easier to measure. On the other hand, regenerative medicine strategies *in vivo* provide the complex biochemical and mechanical properties that are difficult to replicate *in vitro*. While both of these strategies have inherent difficulties and benefits, techniques that utilize aspects of both may have the most clinical relevance.

### *2.5.2 Cell Sources*

Focus of cartilage tissue engineering and regenerative medicine strategies primarily relies on one or a combination of cells and scaffolds. A range of cell sources ranging from embryonic stem cells to differentiated adult chondrocytes, have been analyzed for their usefulness in cartilage regeneration. Each cell source has advantages and disadvantages. Adult chondrocytes are already the appropriate cell type, but harvesting these cells is difficult, can lead to increased donor site morbidity, and can have decreased proliferative capacity. Allogeneic cell sources from cadavers eliminate the problem of donor site morbidity but raise immunological obstacles. Stem cells have a more proliferative capacity, but these must be stimulated to become chondrocytes to produce the necessary cartilage matrix components. Many current efforts in regenerating cartilage involve treating adult mesenchymal stem cells with growth factors that stimulate chondrogenesis, like TGF-β and BMP [71-74]. Many chondrogenic growth factors stimulate both chondrogenesis and osteogenesis, however [73, 74]. Over time, mesenchymal stem cells that have been stimulated with these growth factors can undergo hypertrophy and calcification [75].

### *2.5.3 Scaffolds*

Multiple synthetic and biological materials have been investigated for their usefulness as a scaffold to provide mechanical support and enhance cartilage tissue regeneration. Biomaterials evaluated for cartilage regeneration include sponges, hydrogels, electrospun fibers, and microparticles. Each of these materials provides unique properties for chondrogenesis, but few of them promote quick and functional cartilage

regeneration.[76] Scaffolds made of natural biomaterials (agarose, alginate, gelatin, collagen, silk, etc.) are biocompatible, but do not provide mechanical strength and degrade quickly *in vivo*.[77] Degradation rates are more controllable in synthetic polymers, and many of these have high mechanical strength, but cell integration is limited.[78] Some composite scaffolds of synthetic polymers and natural materials are currently on the market, but natural materials are still preferred.[76] Functional biomaterials that respond to changes in their environment are an attractive source for cartilage tissue engineering, but developing a functional biomaterial that resembles the mechanical and biochemical capabilities of cartilage is a complex obstacle.[76]

### *2.5.4 Decellularized Matrices*

A new focus in regenerative medicine involves the use of extracellular matrix materials, typically from a xenogeneic source, for use as a scaffold.[79, 80] Cellular antigens from the tissues can be removed to avoid adverse immune responses while preserving ECM components, which are conserved among species [79, 81-86]. Acellular ECM materials have been used clinically for the regeneration of a range of different tissues and offer attractive strategies for regenerative purposes due to their 3D presentation of bioactive molecules capable of promoting tissue homeostasis and regeneration [87-98]. [99]. These ECM scaffolds are biocompatible, biodegradable, and provide varying amounts of mechanical support [82-85, 100]. Previous studies have also shown that decellularized scaffolds are able to recruit immune cells and promote endogenous tissue repair [101]. ECM materials have shown to significantly improve cell viability and retention at implantation sites [102].

Furthermore, results from studies using tissue-specific ECM have shown that cells exhibit a better cell retention and phenotype when seeded on decellularized matrices from the same origin as that from which the cells are isolated [103], indicating that decellularized articular cartilage ECM might be beneficial to the acute survival and longer-term integration of chondrocytes delivered to treat cartilage defects. Both allogeneic and xenogeneic cartilage ECM-based scaffolds have been shown to support chondrocyte phenotype and promote chondrogenic differentiation [104-106]. However, implantation of cartilage matrix alone fails to repair cartilage defects due to inadequate cellular infiltration and tissue integration [107]. Therefore, decreasing scaffold size and increasing the surface-area-to-volume ratio via microcarrier fabrication may increase scalability of chondrogenic culture on decellularized cartilage matrix for the application of ACI.

### *2.5.5 Microcarrier Culture*

Microcarriers (μCs) are commonly used for scalable culture of anchorage-dependent cells because of their high surface- area-to-volume ratio [108, 109]. Microcarriers made from plastic [110, 111], dextran [110, 112], gelatin [113-116], or poly(lactide) and its co-polymers [117, 118] have been employed to expand chondrocytes and have shown more beneficial effects in terms of cell yield and chondrogenic phenotype compared to conventional 2D culture on tissue-culture polystyrene [110, 114, 115]. However, chondrocytes display a gradual decrease in synthesis of cartilaginous ECM after prolonged culture on microcarriers and fail to re-differentiate under chondrogenic culture conditions [112], suggesting that currently used microcarrier materials are not able to recapitulate the complex cartilage microenvironment seen *in vivo* by proliferating chondrocytes. Additionally, current microcarriers are often non-degradable or have limited

degradability, which poses another barrier for direct implantation of these cell-laden microcarriers *in vivo* [119]. Alternatively, expanded chondrocytes that need to be enzymatically harvested from microcarriers or monolayers before implantation separates the cells from the ECM they produce during *in vitro* culture [120] and can damage remaining ECM [121]. Therefore, the development of implantable microcarriers for chondrocyte expansion could significantly improve ACI-based cartilage regenerative applications.

## 2.6 Immunomodulation

### *2.6.1 MSC Immunomodulation*

MSC-secreted immunomodulatory paracrine factors (PGE2, IDO, TGFβ1, HGF, & IL-6) can affect multiple cell types, rendering MSCs an attractive cell therapy for regulating the complex pathogenesis of OA. Specifically, MSCs inhibit inflammatory cytokine secretion, promote anti-inflammatory M2 macrophages and tolerogenic dendritic cell phenotypes [122-124], regulate antigen presentation [125, 126], regulate B and T cell proliferation and cytokine secretion [127-129], and modulate the balance of inflammatory and regulatory T-helper cell phenotypes [130-132]. Furthermore, MSCs can prevent or resolve chronic inflammation by directing immune cells towards anti-inflammatory and tolerogenic phenotypes [122-124].

MSC immunomodulation is regulated by the inflammatory state of their microenvironment, and inflammatory cytokines including interferon gamma (IFN-ɣ), tumor necrosis factor alpha (TNF-α), and interleukin 1 beta (IL-1β) can all activate MSC expression of immunomodulatory factors such as PGE2, IDO, and HGF [133-135].

Ligands for toll-like receptors TLR3 and TLR4 can also regulate MSC immunomodulation by altering paracrine factor secretion of MSCs [136, 137].

### *2.6.2 Three-dimensional Culture of MSCs*

Spheroidal aggregate culture of MSCs has been used to mimic the cell-cell and cell-matrix interactions and 3D nature of the endogenous MSC niche. Aggregation of MSCs through hanging drop, forced aggregation, or culture on non-adherent surfaces promotes self-assembly of MSC spheroids via cadherin binding [138-141]. Spheroid culture has been shown to maintain or even induce a more multipotent state of MSCs in comparison to monolayer cultures [142-144]. Spheroid delivery of MSCs *in vivo* has also improved cell retention and survival, yielding better engraftment and treatment in cardiac and skeletal muscle models, colitis models, as well as bone defects [139, 145-148]. Spheroid culture can increase paracrine factor production of multiple cytokines *in* vitro including VEGF, FGF-2, HGF, EGF, SDF-1, BMP2, TSG-6, PGE-2, and angiogenin in comparison to monolayer culture [149-154].

The McDevitt lab has previously developed a 3-D MSC aggregate culture platform that enhances the immunomodulatory factor secretion of IDO, PGE2, and IL-6 in comparison to adherent MSCs [155]. Moreover, MSC spheroids subsequently co-cultured with lipo-polysaccharide (LPS) and IFN-γ activated macrophages for 24 hours (8:1 macrophage-to-MSC ratio) enhanced suppression of macrophage TNFα production compared to adherent MSC monolayers [155]. Incorporation of IFN-γ-loaded heparin microparticles into MSC spheroids sustained immunomodulatory paracrine production and increased the polarization of co-cultured macrophages to a less inflammatory M2

phenotype [156]. In this study, we propose to harness these anti-inflammatory properties of aggregating MSCs in order to treat OA.

### *2.6.3 Amniotic Membrane*

In addition to cellular MSC therapies for modulating inflammation, some ECM materials contain immunomodulatory properties [157, 158]. The amniotic membrane is the innermost layer of the placenta and exhibits immunosuppressant and anti-inflammatory activity in order to protect the fetus and ensure acceptance by the mother's immune system. Micronized dehydrated human amnion/chorion membrane has been shown to be immunomodulatory and non-immunogenic [158, 159]; contains a number of beneficial growth factors, including platelet derived growth factor (PDGF), fibroblast growth factor (FGF), and transforming growth factor beta (TGF-β) [160, 161]; and improves maintenance of chondrocyte phenotype [162, 163]. The multiple factors eluted from the amnion can modulate stem cell paracrine activity and proliferation [164]. Cryopreserved amnion hastens macrophage infiltration and promotes a pro-healing phenotype in wounds of diabetic mice [165]. These properties are potentially beneficial in a treatment for the inflammatory, degenerated environment of an osteoarthritic joint and previous work in the Guldberg lab has demonstrated that intra-articular injection of micronized amnion attenuates osteoarthritis development in the medial meniscal transection (MMT) rat model of OA [166]. There are, however, a number of factors in the treatment of OA with amnion that have yet to be explored, including the effect of particles on MSC trophic factor production and cross-talk between cells and the amnion matrix, and efficacy of combinatorial MSC and amnion treatment in a therapeutic model of OA.

## 2.7 Medial Meniscal Transection (MMT) Model of OA

The medial meniscal transection model (MMT) rat model is a well- accepted small animal model for evaluating new pharmacologic agents for post-traumatic OA. The medial collateral ligament is cut to expose the joint space and then the medial meniscus is transected at the narrowest point, which destabilizes the joint, resulting in fibrillation of the articular cartilage, proteoglycan loss, cartilage degeneration, and osteophyte development within 21 days [167, 168]. MMT also increases local expression of inflammatory genes, macrophage infiltration, synovial lining thickness, and joint swelling [169, 170]. In addition to using traditional methods to characterize the disease progression based on histology, the Guldberg lab has developed a technique to quantitatively assess 3D microstructural changes in the articular cartilage using contrast enhanced microcomputed tomography known as equilibrium partitioning of an ionic contrast agent via μCT (EPIC-μCT). This technique is based on the principle that compared to healthy cartilage degenerated cartilage contains a lower proteoglycan content and, therefore, a higher concentration of a negatively charged contrast agent at equilibrium. With this technique, we have shown that we can quantify 3D changes in articular cartilage morphology, lesion volume, proteoglycan composition, subchondral bone thickening, osteophyte formation, and surface fibrillation and erosions [171].

Histopathological scoring methods have also been utilized to assess changes in the MMT model. An Osteoarthritis Research Society International (OARSI) working group has developed a standardized scoring system based on six grades that reflect depth of the lesion and four stages assessing extent of OA over the joint surface [172]. In addition to

OARSI scoring, changes in the synovium are also quantifiable via immunohistochemical staining of inflammatory cells and measurement of the synovial lining [170].

# CHAPTER 3. DECELLULARIZED CARTILAGE MICROCARRIERS SUPPORT *EX VIVO* EXPANSION OF HUMAN CHONDROCYTES

## 3.1 Introduction

Cartilage regeneration is limited by its avascularity, low cellularity, and the slow proliferation of chondrocytes [173]. Autologous chondrocyte implantation (ACI), in which chondrocytes are isolated and expanded and then re-implanted, is one of the only FDA approved treatments that aims to regenerate cartilage [174]. Current chondrocyte expansion procedures can take up to four weeks on tissue-culture treated polystyrene, follow typical cell culture procedures, and utilize enzymatic release of attached cells [174]. Unfortunately, chondrocytes dedifferentiate rapidly using existing *ex vivo* expansion methods, marked by changes in collagen expression from a healthy collagen type II production to a more fibrotic collagen type I [175]. The dedifferentiation induced by *ex vivo* culture results in fibrocartilage formation upon re-implantation, calcification, and subsequent growth of bone *in vivo* instead of hyaline cartilage, resulting in additional pain and bone-on-bone contact [175]. Thus, new methods to expand chondrocytes while preserving their phenotype are needed, and may significantly decrease the cost and time of current expansion techniques, while improving physiological outcomes.

The need for a relatively large arthrotomy associated with traditional ACI as well as a desire to improve repair tissue have spurred the development of Matrix-induced ACI (MACI) membranes in which expanded chondrocytes are seeded onto a three-dimensional

scaffold that is directly implanted [176-178]. Various scaffolds derived from a porcine collagen I/III [179], collagen I-chondroitin-sulfate [180], hyaluronic acid [181], fibrin/PLA/PGA/PDO [182], or an agarose-alginate hydrogel [183] have been developed for MACI. Although seeding the cells in these three-dimensional scaffolds slightly improves their phenotype, chondrocytes are still expanded on plastic surfaces prior to scaffold seeding, and hypertrophy of the repair site, incomplete filling, and limited integration with surrounding normal cartilage continues to result in complications [184].

Like most cells, chondrocyte phenotype and function are influenced by exposure (or lack thereof) to various biochemical and biomechanical factors. Most chondrogenic culture strategies are unable to recapitulate the complex milieu of growth factors involved in chondrocyte homeostasis, and culture methods often promote either expansion or a chondrogenic phenotype in a mutually exclusive fashion. While the exact mechanisms of environmental parameters on the regulation of chondrocyte phenotype are not yet fully understood, both biochemical and physical components of the local cartilage microenvironment contribute to chondrocyte phenotype retention *in vitro*. Several studies have observed enhanced chondrocyte phenotype when cultured on decellularized cartilage [105, 185-187]. Decellularized cartilage matrix is quite dense, however, and sheets of the ECM exhibited a lack of successful tissue integration and cellular infiltration in chondral defects in vivo in an ovine model [107]. Therefore, reducing decellularized cartilage scaffold size may improve tissue integration and therapeutic applicability.

Microcarriers enhance proliferation when compared to monolayer culture due to their high surface area-to-volume ratio, which allows for culture of large amounts of cells with decreased requirements for space and nutrients. Manufactured microcarriers can be

produced with many different materials, and chondrocyte expansion has been demonstrated on polystyrene microcarriers, polymer-coated glass microcarriers, and gelatin based microcarriers [110]. Most of these materials are neither biodegradable nor manufactured for direct use, often requiring enzymatic harvest. Recently, some microcarriers have been used as delivery devices for cells or chemical compounds *in vivo*. Subcutaneous injection in a mouse model with chondrocytes seeded on gelatinous Cultispher®-G microcarriers (CGμCs) resulted in higher glycosaminoglycan content than plated chondrocytes [110]. Although microcarriers enhance chondrocyte proliferation, synthetic microcarriers do not prevent dedifferentiation and gelatin microcarriers are composed primarily of denatured collagen I, which may contribute to a fibrocartilage phenotype and microenvironment.

Thus, microcarriers composed of decellularized cartilage (DC-μCs) that retain structural and biochemical cues of the native extracellular matrix (ECM) may provide an improved means to culture chondrocytes for MACI therapies in a delivery format. Herein, we present a method of fabricating decellularized cartilage microcarriers from porcine articular cartilage. Chondrocyte seeding, expansion, and phenotype on decellularized cartilage microcarriers was compared to gelatin microcarriers and tissue culture polystyrene. Additionally, principal component analysis of gene expression was performed to elucidate the effects of the different materials on chondrocyte phenotype. Overall, this study marks a first step in developing chondrocyte-laden microcarrier constructs as a versatile expansion platform for chondrocyte phenotype retention that could be used to fill chondral defects for ACI.

## 3.2 Materials and Methods

### *3.2.1 Cartilage Decellularization*

Fresh porcine cartilage was isolated from the interphalangeal joints in the feet of eight market weight pigs obtained from a local meat processor. Extraneous tissue was removed to expose the articular cartilage surface and care was taken to avoid removing subchondral bone during isolation of the articular cartilage. Cartilage was cut into small pieces (approximately 2 mm x 2 mm), rinsed in Dulbecco's phosphate-buffered saline (DPBS), and liquid was aspirated before cartilage samples were stored at -80°C. The tissue phenotype was verified using haematoxylin and eosin (H&E) and safranin-O (Saf-O) stained sections of specimen biopsies according to histological staining methods described below.

Frozen cartilage pieces were thawed at room temperature and washed on a rotary orbital shaker at 250 RPM and 37°C in 500 mL of a series of chemical and enzymatic washes. The decellularization protocol was similar to that of Reing *et al*. with modifications of TrypLE Express (a purified, recombinant cell-dissociation enzyme) in place of trypsin and the addition of a twenty-four hour DNase and RNase wash [188]. All decellularization solution was aspirated and decellularized cartilage was frozen at -80°C until further use. The final decellularization protocol is shown in Table 1.

To quantify decellularization, frozen cartilage pieces (roughly 2 mm x 2 mm) were lyophilized, digested in proteinase K (600 mAU/ml) according to the Quiagen® DNeasy protocol, and DNA was quantified with PicoGreen® reagent and DNA gel electrophoresis. Histological samples were also stained with H&E, DAPI, and SafO to show lack of visible nuclei and GAG retention as described in the following histological staining section.

Table 1. Decellularization Protocol

| Wash Solution | Time |
|---|---|
| TrypLE Express | 6 h |
| Deionized water | 15 min, 3x |
| 70% ethanol | 15 h |
| 3% hydrogen peroxide | 15 min |
| Deionized water | 15 min, twice |
| 1% Triton X-100 in EDTA/Trizma | 6 h |
| 1% Triton X-100 in EDTA/Trizma | 15 h |
| Deionized water | 15 min, 3x |
| DNase/RNase Solution | 24 h |
| Deionized water | 15 min, twice |
| 0.1% PAA/4% ethanol | 2 h |
| Sterile DPBS | 15 min, 3x |

### *3.2.2 Cartilage Microcarrier Formation and Characterization*

The decellularized cartilage pieces were lyophilized, flash-frozen in liquid nitrogen, and milled with a Thomas Wiley Mini-Mill™ using a 400μm mesh screen. The milled cartilage was then sifted overnight at 4ºC to separate microcarriers by size in sieve meshes ranging from 180 μm – 250 μm and 250 μm – 400 μm. The dry weight of cartilage samples after each step was recorded to determine yield efficiency. After sieving, 3mg of each size microcarrier were stained with eosin for 15 minutes, washed five times with 0.1% TritonX-100 in D-PBS, and imaged with a confocal microscope (Zeiss 700 LSM). Size was quantified in ImageJ® by determining the largest and smallest cross-sectional distances, approximate diameter, and aspect ratio of each microcarrier. Commercially

available gelatin microcarriers, Cultispher®-G were also stained and used as a control for comparison.

### *3.2.3 Cell Seeding on Microcarriers*

ATDC5 cells, a mouse teratocarcinoma cell line that mimics mesenchymal condensation and chondrogenic differentiation [189], was used for preliminary cell-loading experiments. ATDC5 cells were expanded in ATDC5 growth media consisting of DMEM/F-12 media with L-glutamine (Invitrogen) supplemented with 5% FBS (Atlanta biologics), 10 μg/mL transferrin (Invitrogen), and $3x10^{-8}$ M sodium selenite (Sigma-Aldrich) at 3,250 cells/$cm^2$. Cells were cultured at 37°C in 5% CO2 and fed every 2-3 days until 90% confluent.

After trypsinization, ATDC5 cells were seeded at $5x10^4$ cells/$cm^2$ or $5x10^5$ cells/$cm^2$ on the decellularized cartilage microcarriers through overnight incubation at a high cell density (500,000 cells/mL) in ATDC5 growth media in 50 mL conical tubes with 5 mL of agarose to provide a flat bottom for microcarriers to settle without clumping. After overnight incubation, the media was collected after to determine seeding efficiency with a hemocytometer by counting unattached cells. The microcarriers were then transferred to 6-well super-low attachment plates (Nunclon™Sphera™, ThermoFisher Scientific) and cultured on a rotary orbital shaker at 60 RPM for up to 7 days and samples were collected at Days 1, 4, and 7 for Live/Dead staining and histological analysis.

### *3.2.4 Human Chondrocyte Isolation*

Human cartilage was ethically obtained from distal end of adult femurs of diabetic patients (n=4) undergoing above knee amputations at Emory University Hospital (IRB No.

00051432). Briefly, articular cartilage was dissected and care was taken to exclude any areas of osteoarthritis. Cartilage was then cut into 2 mm x 2 mm pieces and sequentially digested with 1 mg/mL pronase (30 min) and 1mg/mL collagenase type 2 (overnight, ~15 hours) at 37°C with slow agitation. The digested cartilage was filtered through a 70 μm mesh, and any pieces larger than the mesh were resuspended in fresh 1 mg/mL collagenase type II and digested for an additional night (~15 hours). Isolated primary chondrocytes were washed in growth media consisting of DMEM/F-12, 10% fetal bovine serum, 50μg/mL L-ascorbic acid 2-phosphate, and penicillin-streptomycin-amphoteracin B (100 U/mL, 100 U/mL, and .25 μg/mL). Chondrocytes were frozen in 80% media, 10% FBS, 10% DMSO until microcarrier seeding except for a small portion from each donor that were seeded immediately on TCPS for endotoxin testing with the HEK-Blue LPS Detection Kit. Any vials from donors that tested positive for endotoxin were immediately disposed of (1 donor/4 donors total for a final n=3). Monolayer cultures on tissue culture treated polystyrene (plated) were used as a control for comparison with microcarrier culture and cells were seeded at $1x10^4$ cells/$cm^2$ in growth media and media changes were performed every 2-3 days. A total of 5 wells were also seeded in glass tissue culture plates $1x10^4$ cells/$cm^2$ for live/dead staining and confocal microscopy.

### *3.2.5 Chondrocyte Expansion on Microcarriers*

The decellularized cartilage microcarriers (DCμCs) from the 180-250 micron sieve and Cultispher®-G microcarriers (CGμCs) were rehydrated in chondrocyte growth media for 30 minutes before cell loading. Primary human chondrocytes pooled from 3 donors were then seeded at $1x10^4$ cells/$cm^2$, mixed with gentle pipetting with a wide-bore pipette, and then split in 12-well Nunclon™Sphera™ suspension plates. The monolayer and

suspension microcarrier culture plates were placed in the same incubator at 37°C and 5% $CO_2$. The microcarrier cell suspension was incubated under static conditions at 250,000 cells/mL overnight, after which time the microcarriers were again mixed with gentle pipetting, allowed to settle, and then media was removed with any unattached cells. The microcarriers were supplemented with 1 mL/well of chondrocyte growth media and placed on a rotary orbital shaker at 80 RPM for the duration of the experiment. Media changes were performed every 3-4 days and samples were collected at days 1, 7, and 14 to assess viability, proliferation, and ECM deposition.

### *3.2.6 Live/Dead staining*

Samples from each group were collected at days 1, 3, 7, 11, and 14 to assess viability via Live/Dead staining. Microcarriers were pipetted using a wide bore 1000µL pipette, allowed to settle, and rinsed twice with DPBS. Glass-plated samples were aspirated and washed with DPBS before staining with 8µM calcein-AM and 8 µM ethidium homodimer-1 for one hour at 4ºC according to the protocol of Live/Dead™ Viability/Cytotoxicity Kit (Thermo Fisher) and imaged with a Zeiss 700B Laser Scanning Confocal Microscope.

### *3.2.7 Histological and Immunofluorescent Staining*

Histological samples were fixed in 10% neutral buffered formalin, embedded in 1.5% agarose hydrogel, manually processed for histology, and embedded in paraffin. Samples were sectioned (5µm) for routine histology with hematoxylin and eosin (H&E) and safranin O/fast green (Saf O) staining. For immunofluorescent staining of collagen I and II, slides were deparaffinized and antigen retrieval was performed in 10mM sodium

citrate pH 6.0 at 60ºC overnight in a water bath. After blocking with 4% normal serum, samples were incubated with primary antibodies (Col2A1 mouse monoclonal antibody [1:200 SC-52658, Santa Cruz Biotechnology] and Col1 rabbit polyclonal [1:100 ab34710, Abcam]) overnight (~15 hours), washed in .05% Tween PBS (2x, 2 min), and then incubated with secondary antibodies for one hour (555 goat anti-mouse [1:200 4409S, Cell Signaling Technology] and AF488 goat anti-rabbit [1:200 4412, Cell Signaling Technology] in 4% normal serum) before washing 2x in .05% Tween PBS, rinsing once in water, and then mounting in SlowFade™ Gold Antifade Mountant with DAPI (Thermo Fisher) and imaging.

### *3.2.8 Molecular Analysis*

mRNA levels for signaling molecules and matrix proteins were measured in chondrocytes cultured on the various carriers to determine phenotypic stability. On Days 1, 7, and 14, samples were washed in DPBS, collected in lysis buffer (Quiagen), and frozen at -80ºC. At the conclusion of the experiment, RNA and DNA were extracted using QIAzol, QIAshredders, DNeasy spin columns, and RNeasy MiniElute columns according to the manufacturer's instructions (Quiagen). Briefly, samples were shredded in QIAshredders, run through DNeasy spin columns, and then the run through from the DNA columns was washed and run through the RNeasy spin columns to collect both RNA and DNA from each sample following Quiagen instructions for each. DNA was quantified with PicoGreen® analysis. RNA was quantified with Nanodrop (Thermo Scientific) and 270 ng RNA was reverse transcribed to cDNA (RNA to cDNA Conversion Kit 4387406, Thermo Scientific). Real-time quantitative polymerase chain reaction (PCR) was performed with gene-specific primers using the Fluidigm Biomark System using recommended TaqMan®

Assay Primer/Probe Sets (Thermo Fisher Scientific). Levels of mRNA were measured for SRY (sex determining region Y)-box 9 (Sox9), aggrecan (Acan), cartilage oligomeric matrix protein (Comp), type-I collagen alpha 1 (Col1), type-II collagen alpha 1 (Col2), runt-related transcription factor 2 (Runx2), osteopontin (Opn/Spp1), type-X collagen (Col10), fibromodulin (Fmod), matrix metallopeptidase 13 (MMP-13), and insulin-like growth factor 1 (Igf-1). All genes are presented as $2^{-\Delta\Delta C_T}$ with ribosomal protein S18 (Rps18) as the housekeeping gene and normalized to day 0 chondrocytes as the control [190].

### *3.2.9 Statistical Analysis*

All data are reported as mean ± standard deviation, with a minimum of N=4 independent samples for each experimental group. Statistical significance was determined using one-way or two-way ANOVA, followed by Tukey's post hoc analysis (GraphPad® Prism 7.0); $p<0.05$ was considered statistically significant. Otherwise Student's t-tests were performed with $\alpha=0.05$ also using GraphPad® Prism 7.0 where appropriate. Gene expression tests for normality, principal component analysis, heat map generation, and cluster analysis was performed in JMP Genomics with SAS® analytics.

## 3.3 Results

### *3.3.1 Cartilage Decellularization*

Native cartilage had many visible cellular nuclei while the decellularized cartilage showed no cells and lacunae remained vacant after decellularization (Figure 1 A&B). No residual DNA was visible by gel electrophoresis after decellularization and less than 2

percent of the original DNA content was detected by the PicoGreen assay (<.4 ng of DNA/mg dry weight) (Figure 1 C&D). Glycosaminoglycan content was almost completely removed by the decellularization process based upon Safranin O staining (Figure 1 E).

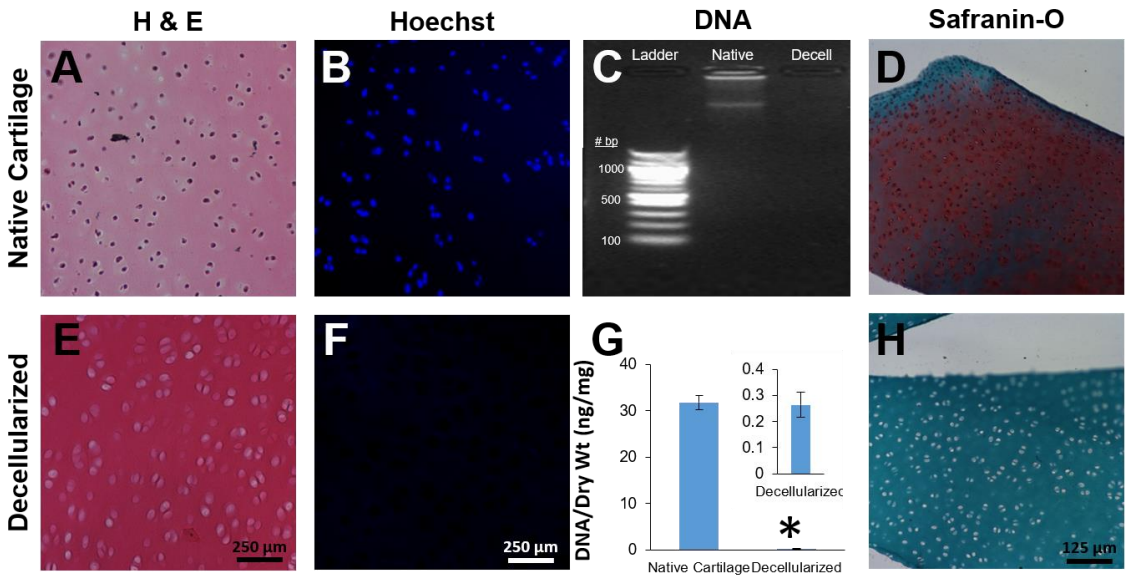


**Figure 1. Effective Decellularization of Porcine Articular Cartilage.** Decellularization of porcine cartilage was verified via lack of visible nuclei after hematoxylin & eosin (H&E) (A&E) & Hoechst staining (B&F), lack of visible DNA after gel electrophoresis (C), and <2% of DNA remaining when quantified via PicoGreen® assay (G) (*p<0.05 vs Native Cartilage using Student's t-test). Safranin-O staining shows decellularization also removes glycosaminoglycans (H).

### *3.3.2 Cartilage Microcarrier Characterization*

The dry weight of cartilage samples was recorded during each step of fabrication to determine microcarrier yield efficiency. Almost half of the staring mass of cartilage was lost due to decellularization (~49% of initial mass), whereas subsequent milling and sieving resulted in relatively little loss, 9% and 2% respectively. The remaining 40% of the initial mass was decellularized cartilage microcarriers; 15% of which in the 20-180 micron sieve,

16% in the 180-250 micron sieve, and 9% between the 250-400 micron sieves (Figure 2 A). Size analysis was performed on DC and CG microcarriers using microscopy and image analysis with ImageJ. Hydrated CG µCs had a diameter around 250 microns while the 180-250 sieved DC µCs were closer to 400 microns (Figure 2 B). The CG carriers were more spherical with an aspect ratio around 1.2 compared to 1.5 aspect ratio for DC µCs (Figure 2 C&D).

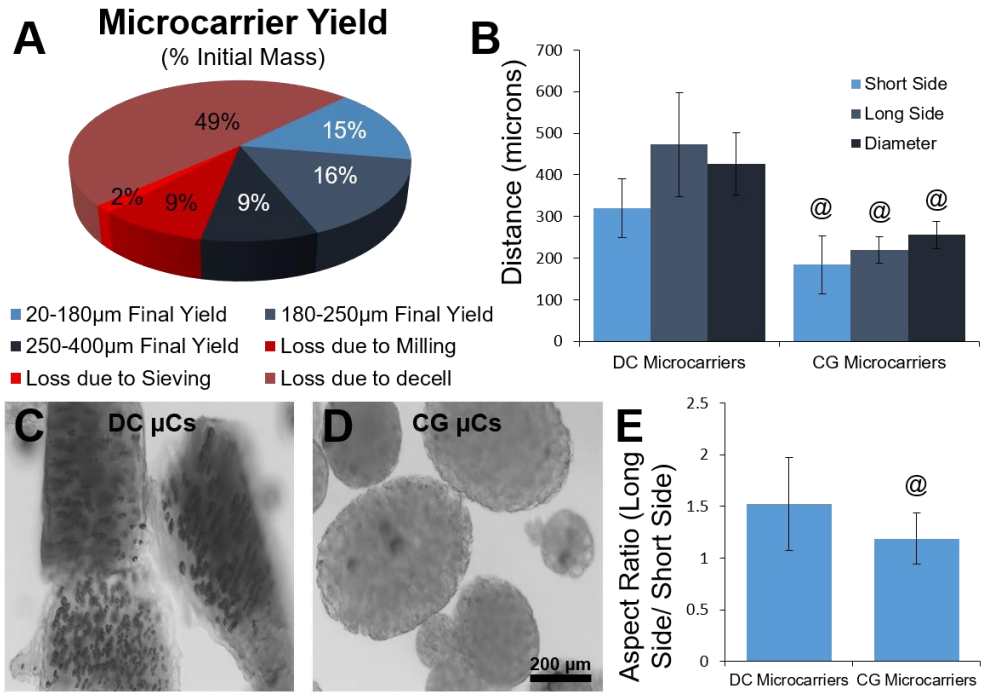


**Figure 2. Characterization of Microcarriers.** The final yield of the 180-250 and 250-400 micron sieved DC-µCs was 15% and 16% of the initial weight of the cartilage pieces respectively and the majority of loss during processing was due to decellularization (A). The 180-250 micron sieved DC-µCs were larger in comparison to commercially available CG-µCs with hydrated diameters around 400 and 250 microns respectively based on ImageJ® analysis of the longest side, shortest side, and average diameters across µCs (n=105 and 97, respectively). Statistical significance was determined using ANOVA with post-hoc Tukey correction (@$p<0.05$ vs DC µCs) (B). DC-µCs and CG-µCs both varied in size with some clumping even in the absence of cells (C). The CG µCs were rounder than the DC µCs, resulting in an aspect ratio closer to 1 (@$p<0.05$ vs DC µCs using Student's t-test) (D). All results graphed as mean±SD.

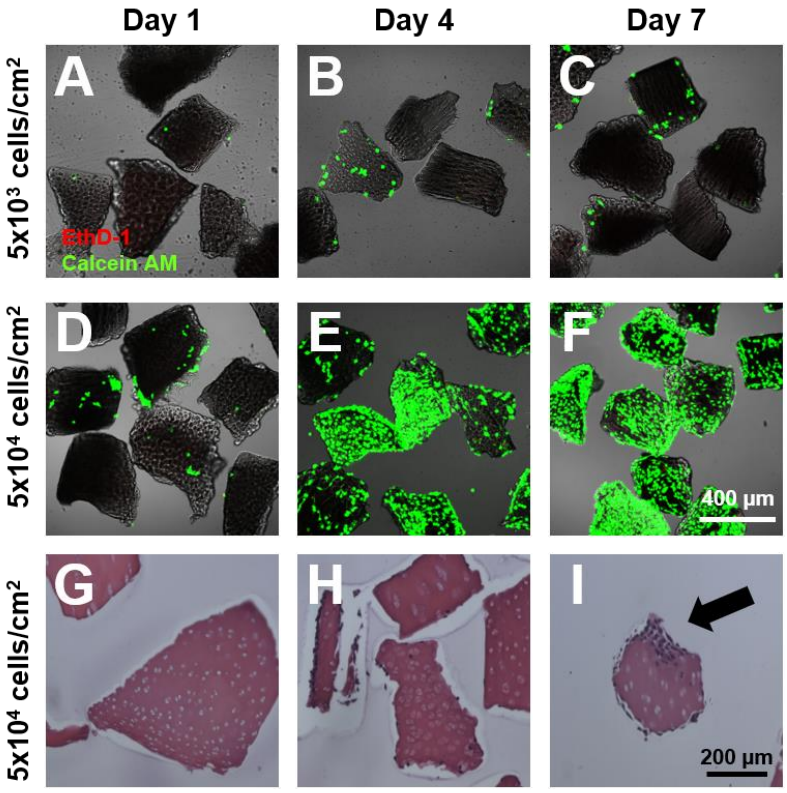


**Figure 3. Chondrogenic ATDC5 cells attach to and proliferate on decellularized cartilage microcarriers and maintain a high viability over 7 days of culture.** The chondrogenic mouse teratocarcinoma ATDC5 cell line maintained a high viability and proliferated up to 7 days at both seeding densities although $5x10^3$ cells/cm$^2$ resulted in patchy seeding with some microcarriers still empty on Day 7 whereas $5x10^4$ cells/cm$^2$ seeding resulted in near confluence at 7 days on some DC µCs (A-F). The cells proliferated on the surfaces/edges of the DC µCs, as seen by positive nuclei staining with H&E along the borders of the sectioned µCs (I).

### *3.3.3 Microcarrier Seeding with ATDC5 Cells*

Initial cell seeding experiments were performed with ATDC5 cells, a chondrogenic mouse teratocarcinoma cell line. The size analyses were used to approximate microcarrier surface area and ATDC5 cells were seeded at $5x10^3$ or $5x10^4$ cells/cm$^2$. Both densities achieved >70% loading efficiency, and proliferated over the 7-day culture period while maintaining high viability (**Figure 3** A). Although the cells seeded at $5x10^4$ cells/cm$^2$ were more evenly distributed after seeding on day 1, confluence was varied and inconsistent

over some μC surfaces after just 7 days. As expected, the cells did not infiltrate into the interiors of the DC μCs over the 7-day culture period and proliferated primarily on the surface/edges of the decellularized microcarriers (**Figure 3** B). Consequently, human chondrocytes were seeded at an intermediate density of $1x10^4$ cells/$cm^2$ for subsequent studies since ATDC5 cells proliferate faster than chondrocytes but the lower density of $5x10^3$ had less consistent seeding [189].

### *3.3.4 Human Chondrocyte Expansion*

Primary chondrocytes proliferated on all surfaces (DC μCs, CG μCs, and TCPS) over the 14-day culture period and maintained a high viability as determined by live/dead confocal imaging (**Figure 4** A-D). Chondrocytes exhibited increased attachment to the DC microcarriers than the CG microcarriers or TCPS based on Day 1 DNA content (**Figure 4** C). Cell proliferation on all three of the surfaces led to progressive increases at day 7 and day 14. Both DC and CG microcarrier groups yielded higher expansion than plated groups on days 7 and 14 and CG carriers had significantly more DNA than DC carriers at Day 14 (**Figure 4** C). Positive safranin O staining of human chondrocytes on the surface of the DC μCs at 14 days indicated glycosaminoglycan presence (**Figure 5** A, indicated by black arrow). CG chondrocyte constructs maintained high levels of collagen I over the culture and DC μCs had small amounts of collagen I localized to the lacunae and carrier surface. Chondrocytes cultured on CG carriers expressed little to no collagen II at any of the observed time points while DC carriers maintained collagen II similar to native cartilage (**Figure 5** B).

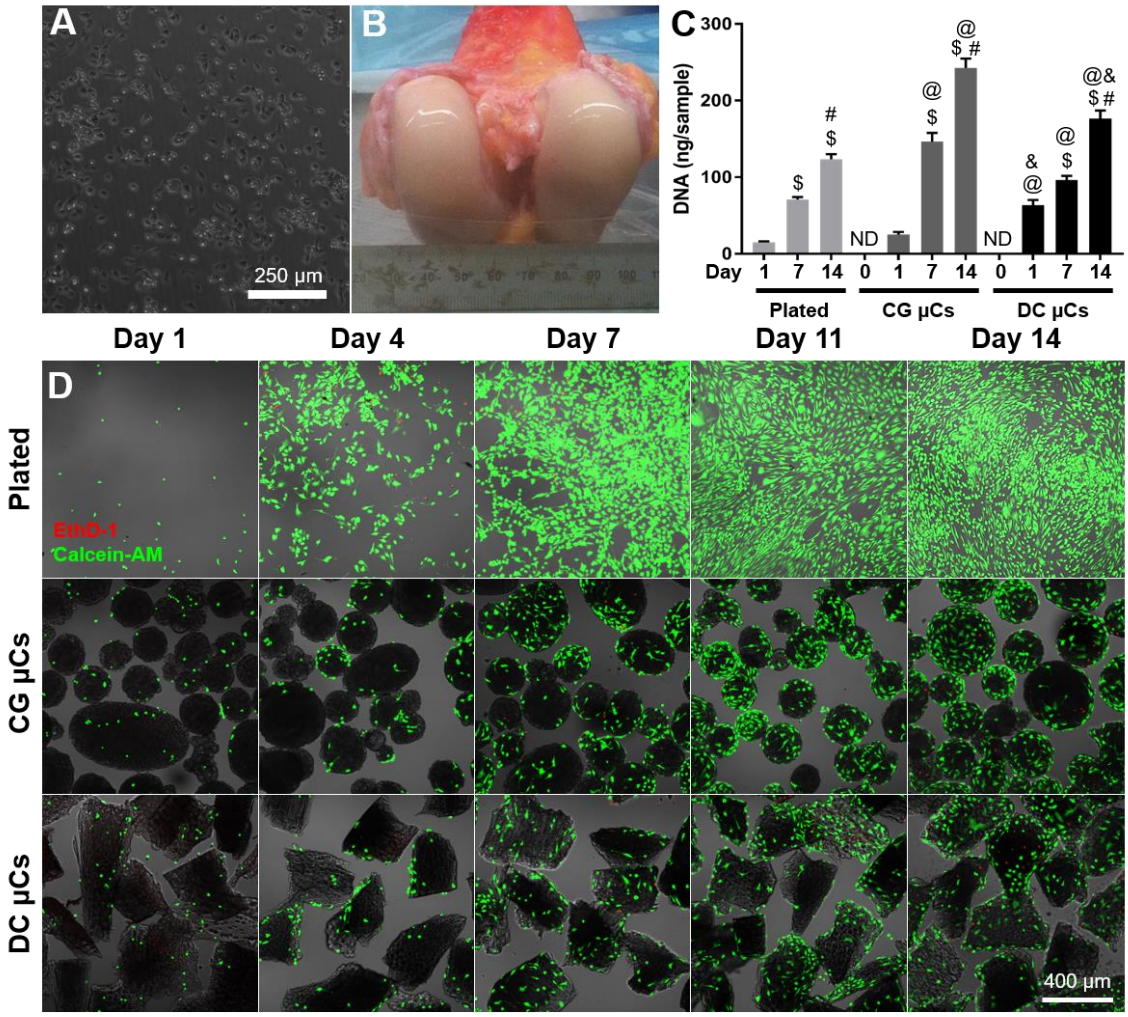


**Figure 4. Primary human chondrocytes attach to and proliferate on ECM microcarriers over 14 days**. Primary human chondrocytes (A) isolated from the femurs (B) of diabetic patients were plated or seeded on gelatin Cultispher®-G Microcarriers (CG µCs) or decellularized cartilage microcarriers (DC µCs) at $1x10^4$ cells/$cm^2$. Chondrocytes attached to DC µCs better than either of the other surfaces based on DNA content with PicoGreen® Assay after overnight seeding (C). Chondrocytes proliferated faster in suspension µC culture than plated culture, and fastest on the CG µCs over 14 days (C). Results are graphed as mean±SD and statistical significance was determined with 2-way ANOVA with post-hoc Tukey correction ($ vs Day 1 with same substrate, # vs day 7 same substrate, @ vs plated at same time point, & vs CG µCs at same time point) (C). Confocal imaging results after Live/Dead staining indicate cells maintain high viability while proliferating over all three surfaces (D).

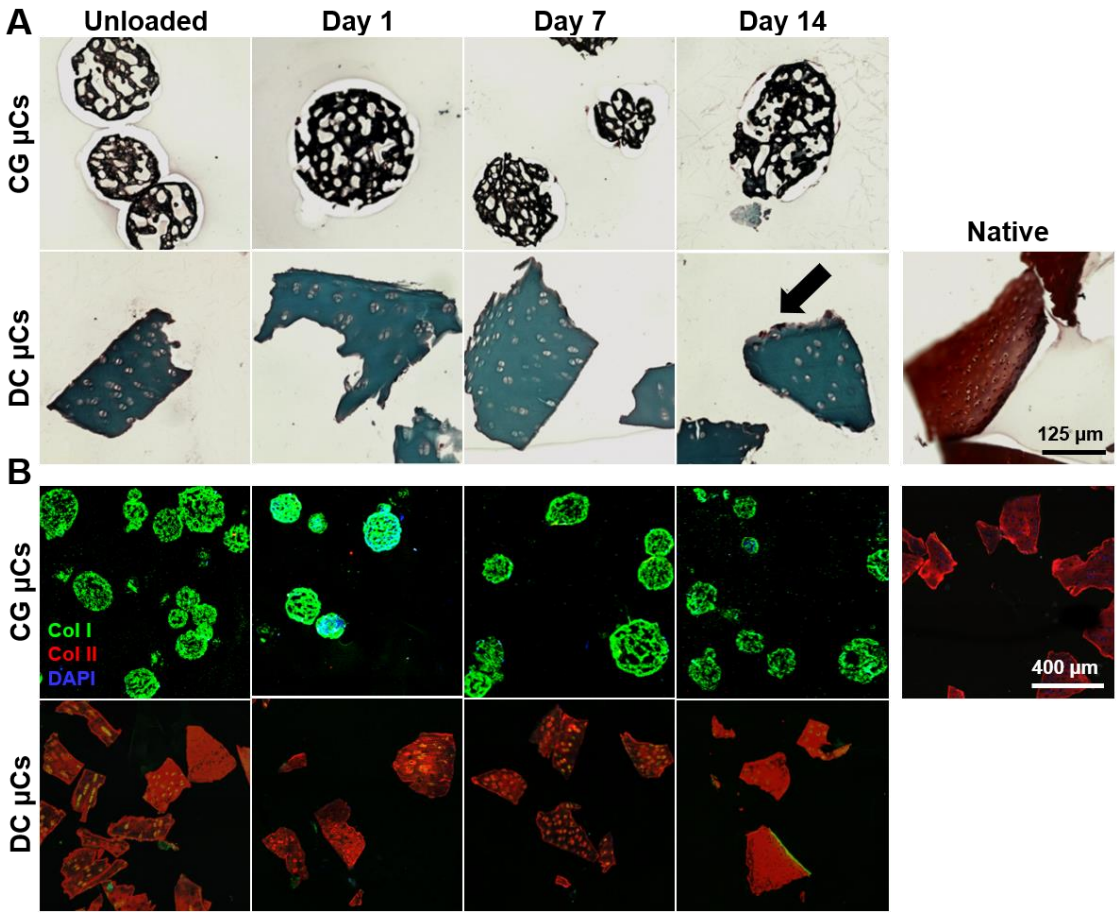


**Figure 5. DC µCs support chondrocyte GAG retention and retain collagen type II structure.** Primary human chondrocytes expanded on DC µCs stained positively for glycosaminoglycans with Safranin O staining up to 14 days, as indicated by the black arrow (A). Immunofluorescent staining of collagens type I and II indicate CG µCs had little to no collagen type II over the 14 days of culture and retained their collagen I while DC µCs retained their collagen type II structure over 14 days similar to native cartilage (B).

### *3.3.5 Gene Expression Analysis*

Chondrogenic gene expression increased on both mirocarriers in comparison to plated monolayers. More specifically, chondrogenic transcription factor, SOX9, expression was higher in chondrocytes on the DC carriers at day 1 and increased on the CG carriers at day 7. SOX9 decreased on all surfaces at day 14, although DC carriers had higher SOX9 than plated chondrocytes (**Figure 6** A). Aggrecan expression increased at day 7 for chondrocytes on all three surfaces, but was greater on the DC µCs at days 7 and 14 (**Figure**

**6** B). Cartilage oligomeric matrix protein (COMP) increased on both microcarriers at 7 days, but was highest in the CG-cultured chondrocytes at day 7 (**Figure 6** C). Collagen I expression increased on day 7 for the plated and CG μC chondrocytes, but was not significantly different from day 1 on day 7 for DC μC chondrocytes and was not statistically different on day 14 on any of the surfaces (**Figure 6** D). Collagen II expression increased on all surfaces at day 7 in comparison to day 1, and to a higher extent for both microcarrier groups (**Figure 6** E). Col II expression decreased on both carriers on day 14 compared to day 7 (**Figure 6** E). The ratio of collagen type II to type I was higher on both carriers at day 1 than the plated carriers but decreased on all surfaces at days 7 and 14 (**Figure 6** F). Osteoblastic transcription factor, runt-related transcription factor 2, Runx2, increased on all surfaces at day 14 compared to day 1, but also increased on the CG carriers on day 7 (**Figure 6** G). Bone sialoprotein, or osteopontin, expression increased for chondrocytes cultured on both carriers in comparison to plated chondrocytes, but decreased on days 7 and 14 (**Figure 6** H). Collagen X expression decreased on all surfaces on days 7 and 14 in comparison to day 1 (**Figure 6** I). Fibromodulin expression increased on both carriers at day 7 (**Figure 6** J). DC μC culture resulted in increased MMP-13 expression in comparison to plated and CG cultured chondrocytes (**Figure 6** K). Insulin-like growth factor 1 expression increased on day 14 in comparison to days 1 and 7 for all groups **Figure 6** L).

Principal component analysis (PCA) of the gene expression data resulted in clustering of fresh day 0 chondrocytes (yellow marker) with all day 1 samples (light pink, green, and blue markers) and day 7 chondrocytes (green marker) were clustered very

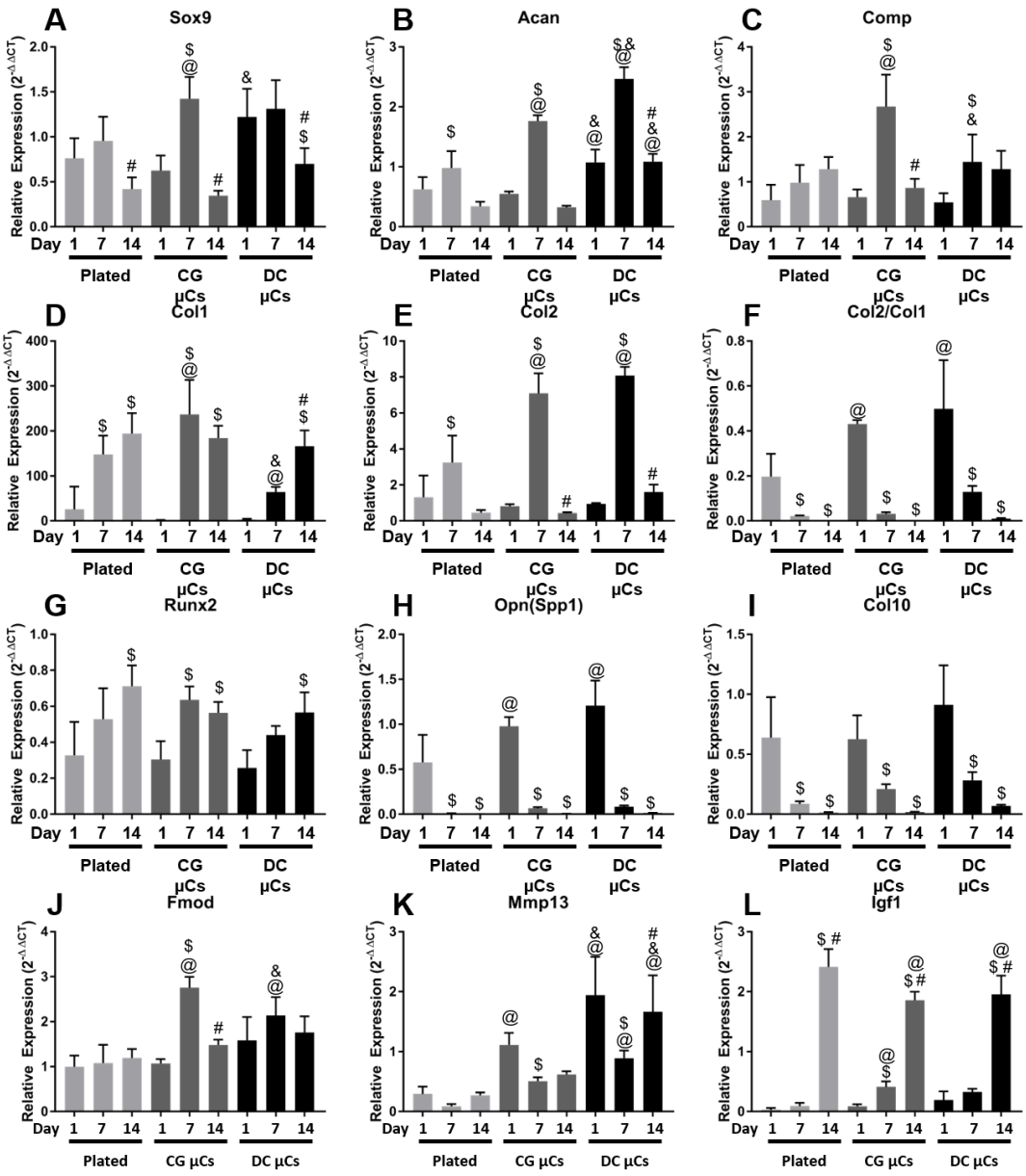


**Figure 6. qRT-PCR gene expression of plated chondrocytes in comparison to CG and DC µC culture.** PCR of chondrocytes using Fluidigm Biomark System with TaqMan® Primers for SRY (sex determining region Y)-box 9 (Sox9), aggrecan (Acan), cartilage oligomeric matrix protein (Comp), type-I and type-II collagen alpha 1 (Col1, Col2), the ratio of Col2/Col1, runt-related transcription factor 2 (Runx2), osteopontin (Opn/Spp1), type-X collagen (Col10), fibromodulin (Fmod), matrix metallopeptidase 13 (MMP-13), and insulin-like growth factor 1 (Igf-1). All genes are presented as $2^{-\Delta\Delta C_T}$ with housekeeping gene Rps18 and normalized to day 0 chondrocytes (relative expression=1). Data is graphed as mean±SD. 2-way ANOVA with Tukey correction ($ vs Day 1 same substrate, # vs day 7 same substrate, @ vs plated at same time, & vs CG µCs at same time).

closely along principal component 1, which accounted for 95% of the sample variability (**Figure 7**). All other day 7 samples clustered closer to the day 14 samples on the other end of PC1, apart from one day 14 DC µC sample (forest green marker, **Figure 7**). PC2 captured variability between day 7 plated cultures from days 1 and 14, but did not distinguish differences in de-differentiation and captured less than 5% of the variability (**Figure 7**).

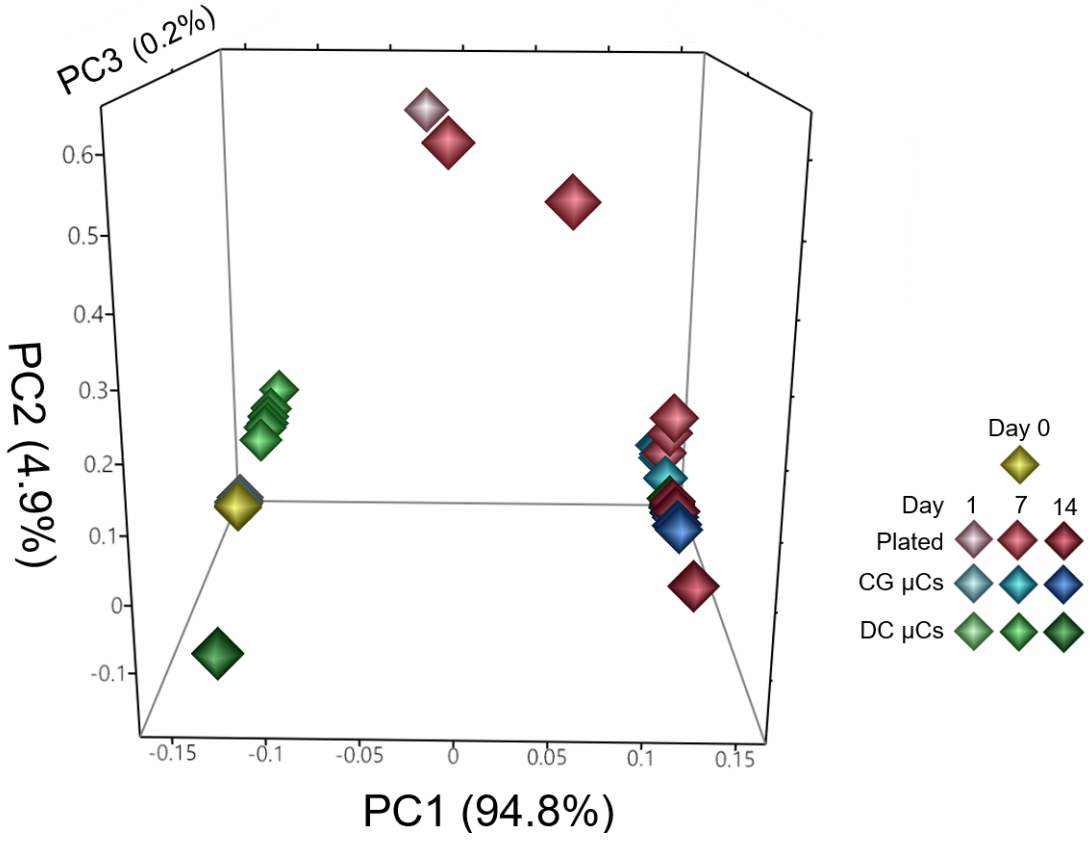


**Figure 7. Day 7 DC µCs expanded chondrocytes cluster near day 0 and day 1 chondrocytes based on principal component analysis of gene expression data.** The first through third principal components from a principal component analysis of PCR gene expression data from all 12 genes of interest were compared for chondrocytes cultured on all three substrates. Principal component 1 (PC1) captured 94.8% of the variability while components 2 and 3 captured only 4.9% and .2% respectively. All day 1 samples clustered with day 0 chondrocytes (bright yellow marker) on all three PCs. All day 14 samples clustered together along PC1 along with day 7 plated samples and most day 7 CG µC

samples. Day 7 DC μC samples clustered with day 0 and 1 samples along PC1, but all but one of the day 14 DC μC samples clustered with the other de-differentiated day 14 samples.

## 3.4 Discussion

In this study, the ability of decellularized cartilage microcarriers to support chondrocyte expansion *ex vivo* was investigated. Cartilage microcarriers were effectively decellularized, retaining <2% of their original DNA content while retaining endogenous collagen II. Microcarrier culture enhanced chondrocyte proliferation over 14 days in comparison to traditional plated culture and DC μCs supported greater chondrocyte attachment. Microcarrier culture enhanced expression of chondrogenic genes, such as Sox9, aggrecan, collagen type II, and increased fibromodulin and MMP-13. Collagen I, runx2, and Igf-1 increased over time for all chondrocyte cultures, while collagen type X, osteopontin, and the ratio of collagen II to collagen I decreased. DC μC culture enhanced aggrecan and MMP-13 expression and reduced collagen I after 7 days in comparison to CG μCs. Moreover, PCA of gene expression results clustered day 7 DC μCs chondrocyte expression with that of day 0 chondrocytes while CG μCs and plated cultures at day 7 were more similar to other dedifferentiated day 14 samples. Overall, this study illustrates that decellularized cartilage microparticles retain native extracellular matrix molecules and support chondrocyte expansion with less de-differentiation for up to 7-days *ex vivo*.

Conventional chondrocyte expansion protocols for ACI typically involve culture on tissue-culture polystyrene and enzymatic harvest of the cells before implantation or seeding onto a biomaterial scaffold, such as collagen I/III [179], chondroitin-sulfate Panagopoulos, 2012 #395}, hyaluronic acid [181], PLA/PGA/PDO [182], or an agarose-

alginate hydrogel [183]. While the use of implantable scaffolds reduces the number of cells required to fill the defect site, potentially reducing donor site morbidity and expansion time and costs, the inability of chondrocytes to proliferate in these scaffolds necessitates prior expansion. The lack of a scaffold that accurately mimics the cartilage microenvironment may also limit therapeutic efficacy, since type-I collagen is present in scar tissue and fibrocartilage and is associated with a dedifferentiated chondrogenic phenotype.

Previous studies have focused separately on the expansion of chondrocytes on either microcarriers or decellularized tissue, but both have their drawbacks. Current microcarrier platforms do not provide the same biochemical milieu of native cartilage ECM, and decellularized cartilage sheets failed when implanted *in vivo* due to their limited integration with chondral defects and low cellularity [107, 109, 191, 192]. By combining microcarrier expansion and decellularized cartilage tissue in this study, we created a novel microcarrier platform that promoted chondrogenic expansion and could serve as a delivery vehicle for cartilage cell-based therapies to treat chondral defects.

Type II collagen (col 2) is one of the most prominent collagens in cartilage ECM, making up 90 - 95% of the collagen in the ECM and providing major structural support in combination with proteoglycans [193]. Immunofluorescent staining of col2 revealed retention of the collagen II in DC μCs when compared to native cartilage, but a lack of col2 in CG μC cultures (**Figure 5** B). Col2 expression in human chondrocytes increased at day 7 for all culture substrates and retained levels similar to freshly isolated chondrocytes over the 14 days of culture on the DC μCs (**Figure 6** E). Col1, which is associated with a more de-differentiated phenotype of fibrocartilage, increased in the plated and CG μC groups at

days 7 and 14, but was less in DC μC groups after 7 days and not different than day 1 expression (**Figure 6** D).

Proteoglycans account for 10-15% of articular cartilage in wet weight and the most prevalent in cartilage is aggrecan [193]. DC μC culture promoted similar aggrecan expression to that of freshly isolated chondrocytes and was further increased at day 7. The chondrogenic transcription factor, Sox9, was increased on DC μCs at day 1 in comparison to CG μC culture, and was increased in CG μC groups in comparison to plated chondrocytes on day 7. Cartilage oligomeric matrix protein increased for CG μCs compared to plated groups at day 7, but not DC μCs.

While dedifferentiation is commonly thought to be reflected by the relative changes of collagen types II and I, dedifferentiation can also involve changes in the expression of chondrogenic and osteogenic factors, along with ECM components and matrix metalloproteinase. Many previous studies lack freshly isolated chondrocyte controls and compare changes in gene expression over passages 2 through 4, after which point dedifferentiation may already be critical. Our study demonstrates that significant changes occur over the first passage, and that changes are dependent on the culture surface and duration. For example, some osteogenic factors increased (ie. Runx2) over the culture duration while others decreased (Opn and Col10) over the 14-day culture period.

The complex nature of these phenotypic changes lends itself well to principal component analysis where the differences between day 0 chondrocytes and plated day 14 chondrocytes are easily distinguishable. Day 7 DC μC cultured chondrocytes clustered with all day 0 and day 1 groups while the plated day 7 samples clustered with all other day

14 samples on principal component 1, which accounted for 94.8% of the sample variance. Day 7 CG μC cultured chondrocytes had more variability on PC1, but most of the samples clustered with other de-differentiated day 14 samples. Our findings suggest that principal component analysis may provide a more thorough understanding of phenotypic changes that occur during dedifferentiation.

## 3.5 Conclusions

This study demonstrates that decellularized cartilage microcarriers can be efficiently fabricated with nearly complete DNA removal while retaining their native collagen II structure, and that they can be used to expand human chondrocytes *ex vivo* to aid in retention of a chondrogenic phenotype. Decellularized cartilage microcarriers offer a versatile expansion platform for chondrocytes, as microcarrier constructs can be directly implanted into a tissue defect site, providing a physiologically relevant extracellular matrix while requiring fewer cells and eliminating the need for expansion on polystyrene and subsequent enzymatic cell harvesting. Consequently, decellularized cartilage microcarriers may be useful for direct *in vivo* tissue regeneration therapies such as MACI.

## 3.6 Acknowledgements

This work was supported by National Institutes of Health Grant R21 AI109499. OB was funded by a Graduate Research Fellowship from the National Science Foundation. EEM and AS received the President's Undergraduate Research Award of Georgia Institute of Technology. The authors would like to thank Giuliana E. Salazar-Noratto and Dalia Arafat Gulick for their assistance collecting and analyzing Fluidigm data, and Andrew Shaw for his assistance with confocal microscopy imaging.

# CHAPTER 4. CHARACTERIZING THE EFFECT OF CULTURE PARAMETERS ON MSC IMMUNOMODULATION OF OA

## 4.1 Introduction

Originally thought to be a disease specific to cartilage degeneration, osteoarthritis is now considered an inflammatory disease of the entire joint and multiple inflammatory mediators have been shown to play a pivotal role in the initiation and persistence of osteoarthritis (OA). In fact, synovial inflammation precedes detectable structural changes and is an indicator of future medial cartilage loss [19-22]. Healthy synovium is normally two to three layers thick and lacks inflammatory cells, but the onset of inflammation is marked with hyperplasia of the lining cells and infiltration of macrophages, T and B cells [23], mast cells [24], and natural killer cells [25]. OA chondrocytes express an array of cytokines, chemokines, alarmins, damage-associated molecular pattern molecules, and adipokines that act as paracrine factors and initiate cartilage degradation locally, but also reach the synovium to increase cytokine production by synovial macrophages and fibroblasts, which promote inflammation and further enhance cartilage damage [18].

Although non-steroidal anti-inflammatory drugs (NSAIDs) are often administered for pain management in OA, they inhibit proteoglycan secretion and are not disease modifying or recommended for cartilage cell therapies [53]. Inflammation is a complex biological process involving many molecules and signaling pathways, thus current drug treatment regimens for immune diseases targeting a single molecule or pathway are often ineffective and insufficient to suppress the chronic inflammation involved in osteoarthritis

due to inherent compensatory pro-inflammatory pathways, causing patient success to vary greatly [54]. The inherent immunomodulatory capabilities of mesenchymal stem cells (MSCs) offer a potent alternative to conventional drug treatment regimens due to their ability to regulate multiple signaling pathways and cell types of innate and adaptive immunity.

MSC immunomodulation is highly regulated by the inflammatory state of their microenvironment, and inflammatory cytokines tumor necrosis factor alpha (TNF-α) and interleukin 1 beta (IL-1β) (both of which are upregulated in OA) have also been shown to activate MSC expression of immunomodulatory factors such as PGE2, IDO, and HGF [133-135]. MSC-secreted immunomodulatory paracrine factors can affect multiple cell types, inhibit inflammatory cytokine secretion, promote anti-inflammatory M2 macrophages and tolerogenic dendritic cell phenotypes [122-124], regulate antigen presentation [125, 126], and modulate the balance of B and T cell phenotypes and proliferation [127-129] [130-132].

Interestingly, 3D aggregation of MSCs also enhances immunomodulatory paracrine factor secretion, including VEGF, FGF-2, HGF, EGF, SDF-1, BMP2, TSG-6, PGE-2, and angiogenin in comparison to monolayer culture [149-154]. The McDevitt lab has previously developed a 3-D MSC spheroid culture platform that both enhances the immunomodulatory factor secretion and the suppression of macrophage TNFα production compared to adherent MSC monolayers [155].

Consistent positive patient responses in clinical trials involving MSC therapies have not been clearly demonstrated and has largely been attributed to inconsistent number

of MSCs at the sites of inflammation [194, 195]. Spheroid delivery of MSCs improves cell retention and survival, yielding better engraftment and treatment in cardiac and skeletal muscle models, colitis models, as well as bone defects [139, 145-148]. Additionally, discrepancies in processing, culture conditions, passage number, and donor characteristics have all contributed to variability in transplanted cell populations for clinical studies [196]. While the exact mechanisms of the environmental regulation of MSC immunomodulation are not yet fully understood, it is clear that biochemical and physical culture parameters play important roles. Understanding the specific effects of culture conditions regulating MSC immunomodulatory activity may provide new insights into components of the microenvironment that can be modulated to enhance success of MSC-based therapies for OA.

Therefore, the objective of this study was to determine the roles of MSC culture condition and format on MSC paracrine activity and modulation of OA both *in vitro* and *in vivo*. Human MSCs from multiple donors and sources were cultured as adherent monolayers (single cells) or 3D aggregates (spheroids) under rotary and static culture and the effect of culture format and media composition on MSC secretome was analyzed. The ability of MSCs to modulate the inflammatory microenvironment of activated synoviocytes was characterized *in vitro*. Furthermore, the effect of MSC culture format on MSC retention and modulation of OA progression was evaluated in a rat medial meniscal transection model of OA. The results of this study demonstrate that culture format and conditions modulate MSC paracrine secretion and immunomodulation in a dose dependent, and donor dependent manner and provide a translatable approach to pre-condition MSCs to enhance their modulation of OA-associated inflammation.

## 4.2 Materials and Methods

### *4.2.1 Cell Culture and Expansion*

Human bone marrow-derived MSCs were obtained from the Texas A&M College of Medicine Institute for Regenerative Medicine and expanded according to established protocols [197]. Approximately $1x10^6$ cryopreserved MSCs were seeded onto a 15-cm tissue culture dish in 20 mL MSC growth medium (MSCGM, Minimal Essential Medium Alpha (MEMα, VWR, Radnor, PA) supplemented with 16.5% fetal bovine serum (FBS, Atlanta Biologicals, Atlanta, GA), 2mM L-glutamine (Corning cellgro, Manassas, VA), 100 U/mL penicillin, 100 µg/mL streptomycin, .25 µg/mL amphotericin (Corning cellgro)). After overnight incubation, adherent MSCs were washed with phosphate-buffered saline (PBS, Invitrogen, Carlsbad, CA) and detached from the plate using 0.25% trypsin and 1 mM EDTA in Hanks' Balanced Salt Solution (Corning cellgro). Dissociated cells were counted using a hemocytometer and plated onto 15-cm tissue culture dishes at a density of 60 cells/$cm^2$ in 20 mL MSCGM per dish. Media was completely exchanged every 3 days until cells reached approximately 70% confluence. Cells were trypsinized, counted, and either re-plated for monolayer expansion cultures or used for experiments at passage 4. MSCs from Texas A&M College of Medicine Institute for Regenerative Medicine were used for evaluation of MSC injectability and the pilot MMT animal model described below.

Human bone marrow-derived MSCs from three male donors were also obtained from RoosterBio Inc. (Frederick, MD) and expanded according to the manufacturer's protocols. Briefly, $10^7$ cryopreserved MSCs were plated in twelve T225 flasks in 45 mL of RoosterBio High Performance Media and incubated at 37°C for 7 days in a humidified 5%

CO2 incubator. Media was exchanged after 4 days of culture. Cultures were passaged at 80% confluency by washing with 10 mL PBS followed by incubation with 10 mL of 0.25% trypsin at 37ºC. An equal volume of RoosterBio High Performance Media was added to quench trypsin activity. Dissociated cells were then collected and centrifuged at 200xg. Cells were all frozen to similar passage doubling levels as recommended by the manufacturer (PDL 13±1.5). Cells were frozen in CryoStor CS5 cell cryopreservation media (STEMCELL Technologies, Vancouver, BC, Canada) prior to expansion for experiments. MSCs were expanded for one passages from frozen stocks by plating $1x10^6$ cells in 45mL MSCGM in T-175 tissue culture treated flasks. Media was exchanged every three days and cells were passaged at 80% confluency. MSCs from RoosterBio Inc. were used in immunomodulatory factor quantification, co-culture and transwell studies, and animal experiments described below. MSC phenotype up to PDL 18 in each donor was verified by flow cytometry for MSC markers CD90, CD73, and CD105 and compared to negative and isotype controls.

### *4.2.2 Spheroid Formation and Culture*

Forced-aggregation of single cell suspensions of MSCs was used to generate MSC spheroids. Spheroids were formed overnight in 400 μm agarose microwells for a high throughput method of generating homogenous cell aggregates [198]. Briefly, 600,000 MSCs pooled from three donors at similar population doubling levels (±1.5 PDL) were added to 24-well microwell inserts containing approximately 1,200 wells and centrifuged at 200xg for 5 min to force aggregation of spheroids with approximately 500 cells per aggregate. After 18h in the microwells, spheroids were removed and transferred to suspension culture in 100 mm bacteriological grade Petri dishes at 600,000 cells per plate.

Spheroids were cultured in suspension on a rotary orbital shaker for up to 4 days at 65 RPM. Additionally, adherent MSC controls from the same donors and PDL were plated in 24-well tissue culture treated polystyrene plates at a density of ~1300 cells/cm$^2$. MSC spheroids and adherent controls were cultured in MSCGM. After 4 days of culture, MSCs and conditioned media were collected for cell counting (Countess II Automated Cell Counter, Thermo Fisher Scientific, Waltham, MA), immunomodulatory factor quantification, viability assays, and treatment in a rat model of OA.

### *4.2.3 Assessing the Effect of Confluence & Rotary Culture on hMSC Secretome*

hMSCs from the same three RoosterBio donors described previously were pooled to compare the effect of rotary culture on monolayer hMSCs and compared to spheroid culture at the previous "normal" density of 1,300 cells/cm$^2$ in 24-well plates. Additionally, because hMSCs in spheroid culture are inhibited by the contact of surrounding cells, monolayer single cells were also plated at ten times higher seeding density (13,000 cells/cm$^2$) in order to reach confluence in the first 24-36 hours of culture (Figure 13). Spheroids cultured on the rotary orbital shaker as described previously were used as controls for comparison.

### *4.2.4 Influence of Media Composition on MSC Proliferation and Secretome*

Media comparisons of MSC secretome as single cells and spheroids were performed in MSCGM described previously and a defined, xeno-free serum-free culture medium, MSC NutriStem® XF medium with PLTMax ® human platelet lysate (Biological Industries, Cromwell, CT). For comparison of expansion, hMSCs from one RoosterBio donor (Lot 00141) were seeded at 2,222 cells/cm$^2$ in T-75 flasks in 15mL of MSCGM

containing FBS or PLTMax containing human platelet lysate (PL). Media was replenished after 4 days of culture and cells were harvested at day 5. Conditioned media was collected and frozen as described previously and cells were trypsinized in .05% Trypsin-EDTA and cell count and size were quantified. hMSC secretome was then compared in single cells and spheroid culture following that expansion. Conditioned media was collected as described previously after 4 days of culture of single cells (plated at the normal density of 1,300 cells/cm$^2$ under static conditions) and spheroids.

### *4.2.5 Cell Number and Immunomodulatory Factor Quantification*

MSCs cultured as monolayers or spheroids were cultured for 4 days in MSCGM and evaluated for total cell number and immunomodulatory factor secretion. The number of starting cells, final population, and cell size were quantified for each culture condition using Countess II Automated Cell Counter (Thermo Fisher) according to the manufacturer's protocol. Collected spheroids were trypsinized (0.25% trypsin, Corning) for 5 minutes at 37°C and gently triturated with a 27G needle to form a single cell suspension to determine cell count for each sample. Conditioned media was collected and inflammatory cytokines were quantified using MILLIPLEX MAP Human Cytokine/Chemokine Magnetic Bead Panel – Immunology Multiplex Assay (EMD Millipore). Conditioned media was diluted 1:4 in MSCGM as our optimization has shown that this concentration is in the center of a linear range of signal vs cytokine concentration. Samples were then analyzed according to the kit protocol and normalized to the standard provided with the kit after subtracting background of MSCGM media alone. Only cytokines that had over 50% of samples in the detectable limit were reported. All samples were read out on a MAGPIX instrument (Luminex).

### *4.2.6 Synoviocyte Culture and Expansion*

Because the synovium is a major site of gross and microscopic changes that occur early in disease progression, an *in vitro* model of activated synoviocytes was used to model OA-associated inflammation [26]. Human fibroblast-like synoviocytes from three separate donors were purchased and cultured to passage 3 in proprietary Synoviocyte Growth Media (SGM) according to manufacturer's instructions (Cell Applications, Inc, San Diego, CA). After expansion, synoviocytes were frozen in CryoStor® CS5 freezing media prior to experiments. After overnight recovery in SGM, synoviocytes were trypsinized, counted, and pooled from all three donors in equal amounts and seeded in a 96-well plate in SGM at 2500 cells/well (~8,300 cells/$cm^2$). After 24 hours in SGM, synoviocytes were activated for 24 hours in one of the following medium.

### *4.2.7 Synoviocyte Activation*

Multiple activation protocols were initially compared based on variation in prior literature. Activation was performed in either SGM or MSCGM in preparation for co-culture studies with MSCs. Lipopolysaccharide (LPS)-induced synoviocyte activation was compared at a low, medium, and high dose of .1, 1, and 50 μg/mL in accordance with variances reported in prior synoviocyte studies [197-200]. Synoviocyte activation with human interleukin-1β (IL-1β) and tumor necrosis factor α (TNF-α) was also compared at .05, .5, and 5 ng/mL. SGM or MSCGM without cytokines was added to control unactivated wells for comparison. Activation medium was removed and fresh SGM or MSCGM was added after 24 hours. After four days, medium and cells were collected to quantify synoviocyte proliferation and inflammatory cytokine secretion via MILLIPLEX MAP

Human Cytokine/Chemokine Magnetic Bead Panel – Immunology Multiplex Assay (EMD Millipore).

### *4.2.8 Synoviocyte and MSC Dosing Study*

To compare suppression of synoviocyte activation by adherent and spheroid MSCs, varying ratios of MSCs to synoviocytes were compared. Human fibroblast-like synoviocytes were plated in SGM overnight, activated in 5 ng/mL IL-1β and TNF-α in MSCGM for 24 hours as described previously. After 24 hours, activation media was removed and MSCs from individual RoosterBio donors or pooled from 3 donors as single cells or spheroids were added directly to the 96-well plate (co-culture) or separated with a 5.0μm-pore-size transwell insert (Corning®, Corning, NY, USA) at ratios of 1:3, 1:9, or 1:27 synoviocytes to MSCs. Conditioned media collected from monolayer single cells or spheroids cultures after 4 days and was compared to direct co-culture and transwell cultures. Single cells and spheroid MSCs alone were also cultured at the same densities to serve as controls for comparison for secretome analyses. Media was removed and immediately frozen after 4 days of culture and cells were collected for cell counting as described previously.

### *4.2.9 MSC Spheroid Viability and Injectability*

An *in vitro* experiment was performed to test the effects of incubation time and injection through a syringe needle on cell morphology and viability. Human MSCs (Texas A&M) from two donors were first characterized and expanded to P3 and then frozen until use. After thawing, MSCs from both donors were plated overnight (recovery) and then pooled together before expanding for seven to ten days. To produce spheroids, hMSCs

were added to 24-well micro-well inserts, centrifuged to form aggregates (500 cells/spheroid), and incubated overnight. The following morning, hMSCs (single cells or spheroids) were loaded into 1mL syringes in MEMα (Lonza) at a density of $1x10^6$ cells/50µL (the amount delivered per animal) with 150µL/syringe and incubated for up to 4 hours at 4ºC to simulate the time required to perform subsequent intra-articular injections of all animals if groups were randomized. MSCs were then injected through a 27 gauge needle into glass bottom plates and viability and morphology were evaluated using Live/Dead® viability assay (calcien-AM/Ethidium Homodimer-1 (EtD-1)) (n=3).

*4.2.10 MMT Animal Model and BLI Tracking*

A preliminary pilot study was performed to compare intra-articular injection of MSCs as single cells or as spheroids in the rat MMT model of OA. Human MSCs (Texas A & M) were pooled from two donors and lentivirally labeled for GFP/luciferase expression and then expanded for approximately 10 days before the MMT surgery. The Georgia Tech IACUC approved all animal studies (Protocol #A15019). Weight matched Lewis rats (275-300g) were acclimated for one week and then underwent sham or MMT in the left leg (n=3). Briefly, the animals were anesthetized with isoflurane, and the skin over the medial aspect of the left femoro-tibial joint was shaved and aseptically prepared. The medial collateral ligament (MCL) was exposed by blunt dissection and transected to reflect the meniscus toward the femur. The joint space was visualized, and a full thickness cut was made through the meniscus at its narrowest point. The skin was closed with 4.0 Vicryl sutures and then stapled using wound clips. hMSCs were intra-articularly injected 24 hours after MMT surgery (Day 1) in 40 mg/mL luciferin in MEMα using a 27-gauge needle. Bioluminescence intensity (BLI) was conducted on each animal at 1, 3, 7, 14, and

21 days using an IVIS® spectrum *in vivo* imaging system to track the hMSCs. Rats were anesthetized using isofluorane and 50µL luciferin (40 mg/mL in MEMα) was injected intra-articularly. Animals were positioned with the anterior side facing up and scanned at 5, 10, 15, and 20 minutes post-luciferin injection (auto-exposure; 1.5cm subject height). BLI images were evaluated by selecting an elliptical region of interest (ROI) over the knee of the animal's left leg using Living Image® Software Version 3.2 (Caliper Life Sciences). BLI counts were normalized first by exposure time and ROI area and then to the corresponding day 1 value for each sample. All animals were euthanized at 3 weeks with $CO_2$.

### *4.2.11 µ-CT Analysis*

Animals were sacrificed after 21 days and joints were dissected, formalin fixed for 3 days, and then scanned using a Scanco µCT 40 at 45 kVp, 177µA, 200 ms integration time, and a voxel size of 16 µm following equilibration in 30% Hexabrix™ 320 contrast agent (Covidien, Hazelwood, MO) in PBS without calcium and magnesium at 38°C for 30 minutes. The EPIC-µCT images were reconstructed sagittally and coronally, manually contoured, and analyzed at suitable thresholding levels to separate the cartilage from bone and background. Scanco evaluation software was used to calculate cartilage attenuation, volume, and thickness for the medial third of the medial plateau. To quantify cartilage fibrillation, scanned sections of the medial tibial plateaus were exported as TIFF files, and a MATLAB® (MathWorks, Natica, MA) program was used to measure the cartilage surface roughness defined as the root-mean-square of differences between the representative and polynomial fit surfaces of the cartilage [201]. Osteophyte volume was determined with the rotated coronal images by manually contouring the medial-proximal

edge of the medial tibial plateau using the Scanco evaluation software and thresholds were used to separate osteophyte bone from cartilage and background (Figure 15 E). For focal lesion analysis, lesions were defined as cartilage defects extending to the subchondral surface. The lesion areas were manually contoured to create appropriate VOIs and within the VOI the cartilage volume was subtracted from the total volume to give lesion volume (Figure 15 F).

### *4.2.12 Histological Analysis*

Following μ-CT, tibias of both surgerized legs and contralateral controls were dehydrated and routinely processed, transected sagittally along the load-bearing plane, and paraffin-embedded via vacuum infiltration with both load-bearing faces exposed for sectioning (n=6). Sagittal sections were cut at 5 μm thickness in strips of 12 (representing a total thickness of 120 microns) with 4 sections mounted to each slide. Sections were stained for sGAGs with a 0.5% Safranin-O (Saf-O) solution and a 0.2% aqueous solution of FastGreen as a counter-stain. Sections representing the most damage were imaged for each sample at 4x magnification with a Zeis LSM microscope and Mosaix color brighfield tile imaging.

### *4.2.13 Partial Least Squares Regression Modeling*

PLSR modeling was conducted in MATLAB using the partial least squares algorithm by Cleiton Nunes available on the Mathworks File Exchange. Bio-Plex cytokine sample data was pre-normalized to appropriate control media also incubated for 4 days as discussed above. All secretome data was z-scored for heatmap representation, and then directly inputted to the algorithm. For each PLSR analysis, an orthogonal rotation in the

LV1-LV2 plane was used to choose a new LV1 that better separated cell phenotype/Y-variable. LV1 and LV2 scores were then output in MATLAB for statistical comparisons with multi-way ANOVAs in JMP Genomics Pro as previously described [202].

#### *4.2.14 Statistics*

All data are reported as mean ± standard deviation and were analyzed using multi-way ANOVAs with Bonferroni Correction with $\alpha=0.05$ in JMP Genomics Pro with SAS® analytics (SAS, Cary, NC). Otherwise, t-test and one-way ANOVAs with Bonferroni post-hoc tests $\alpha=0.05$ were performed using GraphPad Prism® (GraphPad Software, Inc. 7.03, La Jolla, CA) whenever appropriate.

## 4.3 Results

### *4.3.1 Spheroid Culture Enhances Immunomodulatory Cytokine Secretion*

To determine the impact of spheroid culture on the secretion of immunomodulatory factors, conditioned media was collected after four days of culture and analyzed from MSC pooled from 3 commercial donors (RoosterBio) using MILLIPLEX MAP Human Cytokine/Chemokine Magnetic Bead Panel – Immunology Multiplex Assay. When cultured as spheroids, MSCs secreted greater amounts of nearly all detectable cytokines in the array, with significant increases in G-CSF, Fractalkine, IFN-ɣ, IL-6, IL-7, GRO, MCP-3, IL-8, IP-10, MCP-1, PDGF-AA, IL-1RA, MIP-1a, and VEGF (Figure 8).

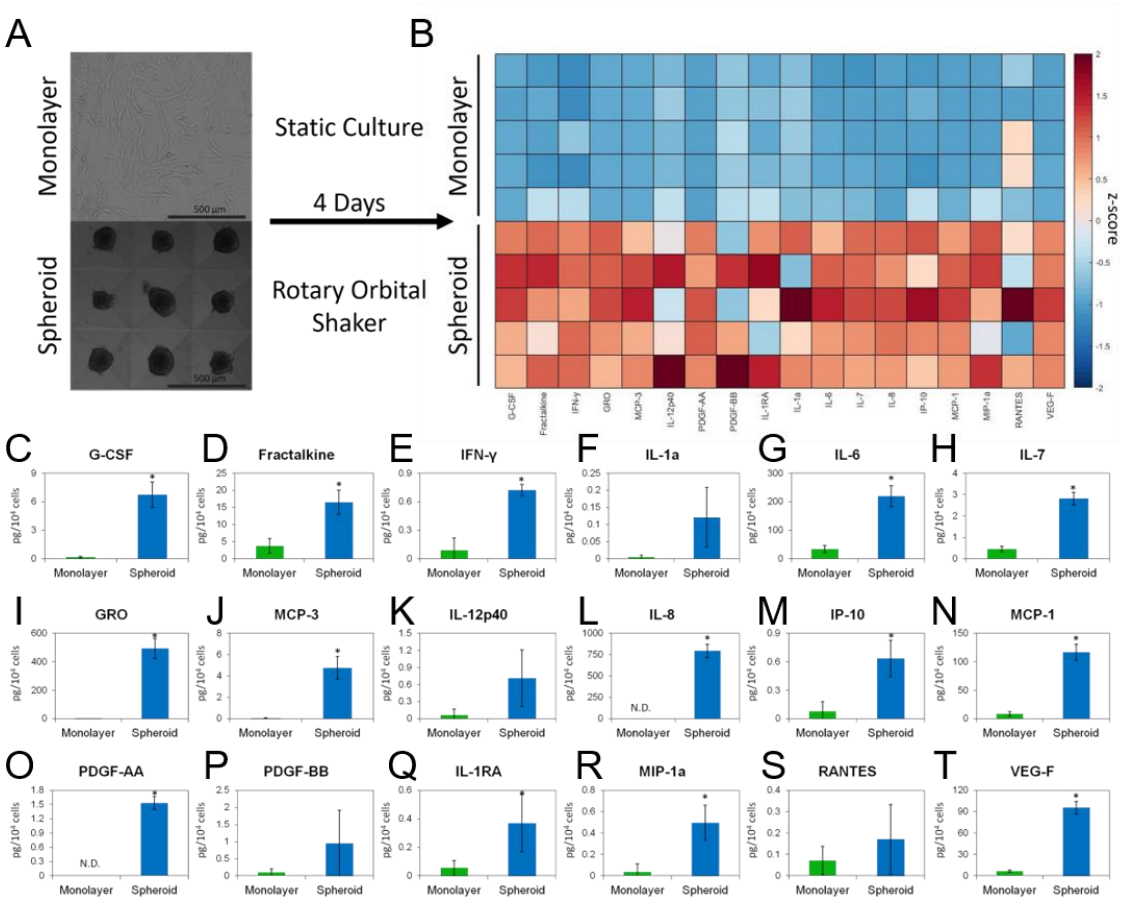


**Figure 8. Spheroid culture format enhances hMSCs immunomodulatory cytokine production.** Human MSC were pooled from 3 commercial donors. After overnight formation, spheroids were cultured 4 days on rotary orbital shaker and media was collected and analyzed using a Milliplex® Human Cytokine/Chemokine Magnetic Bead Panel Kit and compared to static monolayer cultures. * α=0.05 vs monolayer single cells with Bonferroni Student's t-test (n=5). Graphed as mean ± SD.

### *4.3.2 Assessing Donor Variability*

Donor variability in hMSC secretome was assessed in three male donor lots from RoosterBio. In order to control for some changes in expansion rates between donors, rather than using cells from the same passage, cells were expanded to the same passage doubling level (±1.5). All donors maintained high purity over the culture up to PDL 18 as evidenced by >97% positive staining for CD73, 90, and 105 (Figure 9). Spheroids from all three

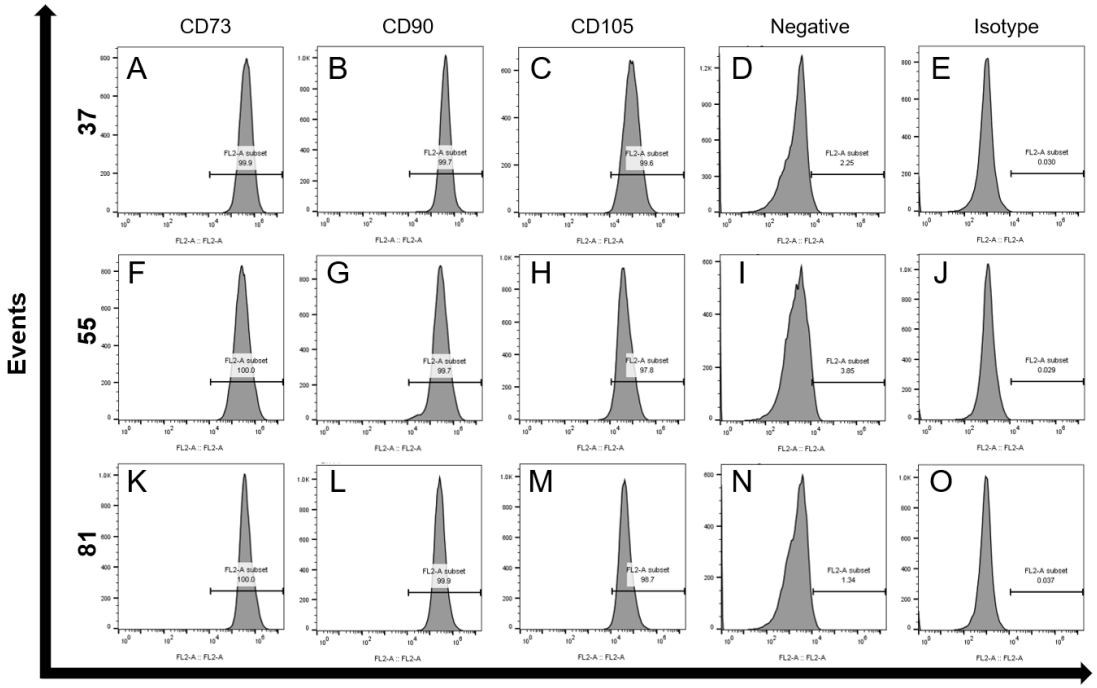


**Figure 9. hMSCs maintain their phenotype up to passage doubling level (PDL) 18.** hMSCs expanded from three male donor lots 37, 55, and 81 maintain their phenotype with greater than 97% positive for MSC markers CD73, CD90, CD105, and less than 4% positive in negative and isotype controls) up to PDL 18 ± 1).

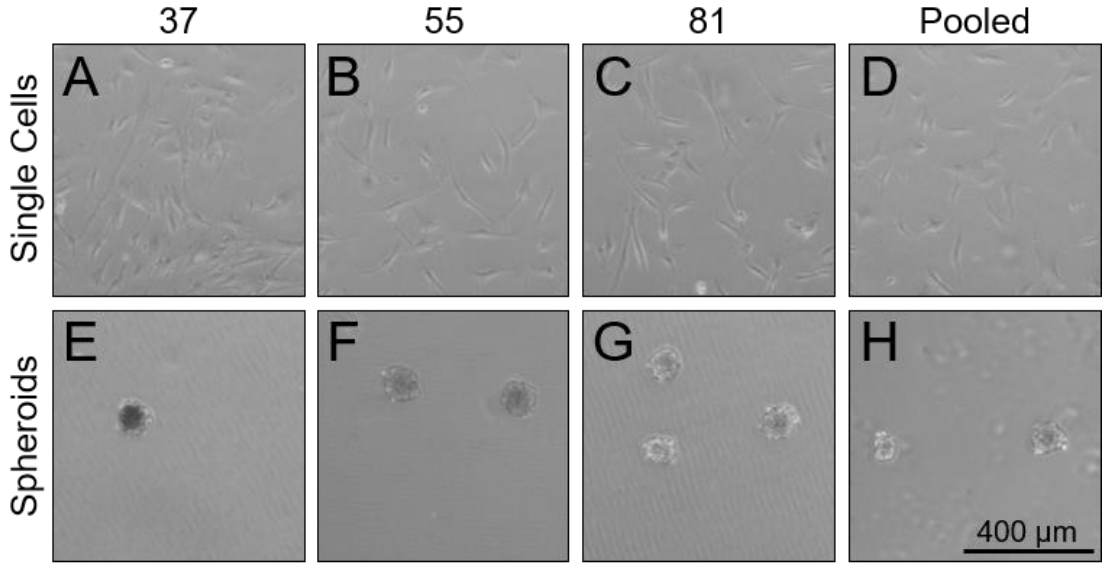


**Figure 10. hMSCs from 3 donors (37, 55, & 81) maintain their morphology in both monolayer single cell and spheroid culture over 4 days.**

donor lines maintained their morphology over the 4 days of culture at which time the conditioned media was collected and secretomes were compared for single cell and spheroid cultures (Figure 10). PLSDA analysis of z-scored secreted cytokines normalized to cell count exhibited separation between rotary and static culture on LV1 while LV2 separated spheroid donors (Figure 11). Most cytokines were upregulated in spheroid rotary culture, but not in spheroids that plated down under static culture (Figure 12). Donor variability was more evident in spheroid culture format than monolayer single cells, although not significantly in different in LV2 scores (adjusted p-value of 0.053) (Figure 12). Graphs of individual cytokine concentrations normalized to cell count show spheroid culture enhanced secretion of most quantified cytokines including IL-8, IL-7, IFN-ɣ, GRO, G-CSF, Fractalkine, VEGF, IP-10, IL-1a, MCP-3, PDGF-AA, and MCP-1. There were no significant differences between different donors cultured as single cells, but spheroid culture had significantly different donor variability in IL-8, GRO, IP-10, MCP-3, PDGF-AA, and MCP-1. Spheroids pooled from all three donors cultured statically on tissue culture polystyrene behaved more similarly to pooled plated single cells and were only significantly different in MCP-1. Plated spheroids had reduced cytokines in comparison to the pooled spheroids cultured on rotary for multiple cytokines including IL-7, IL-8, IL-6, GRO, G-CSF, Fractalkine, MCP-3, and MCP-1. Altogether, rotary culture of MSC spheroids increases secretion of immunomodulatory cytokines in comparison to single cells and is dependent on rotary culture. Additionally, rotary spheroid culture amplifies differences due to donor source that were not evident in static single cell cultures.

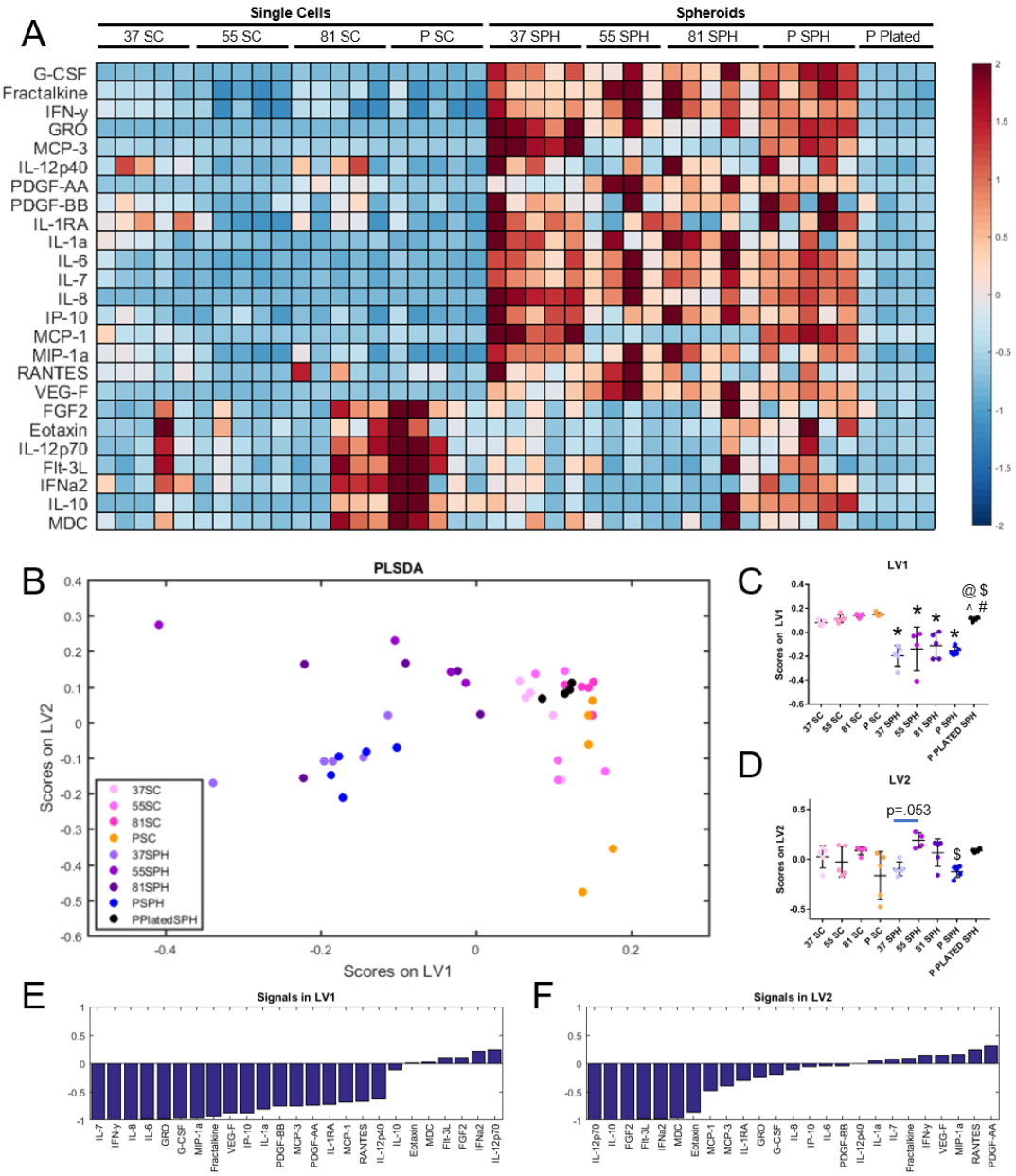


**Figure 11. hMSC secretome is increased in spheroid rotary culture, but not plated spheroids, and donor variability in secretome is more evident in spheroid culture than monolayer.** hMSCs from 3 donors (lot #37, 55, and 81) were cultured or pooled (P) during monolayer or spheroid culture under rotary and static conditions. Conditioned media was collected after 4 days and immunomodulatory cytokines were quantified with using Milliplex® Human Cytokine/Chemokine Magnetic Bead Panel Kit. Heatmaps of the z-scored data indicates relative cytokines levels (A). PLSDA analysis (B) of z-scored secreted cytokines exhibited separation of rotary and static culture on LV1 (C) while LV2 varied among donors (D). LV signal plots detail which cytokines are weighted in the latent variables in the PLSDA separation (E&F). Significant differences between groups are based on multi-way ANOVA with Bonferroni correction and α=0.05. *vs SCs same donor; # vs 37, $ vs 55, @ vs 81 same culture format, and ^ vs P SPH.

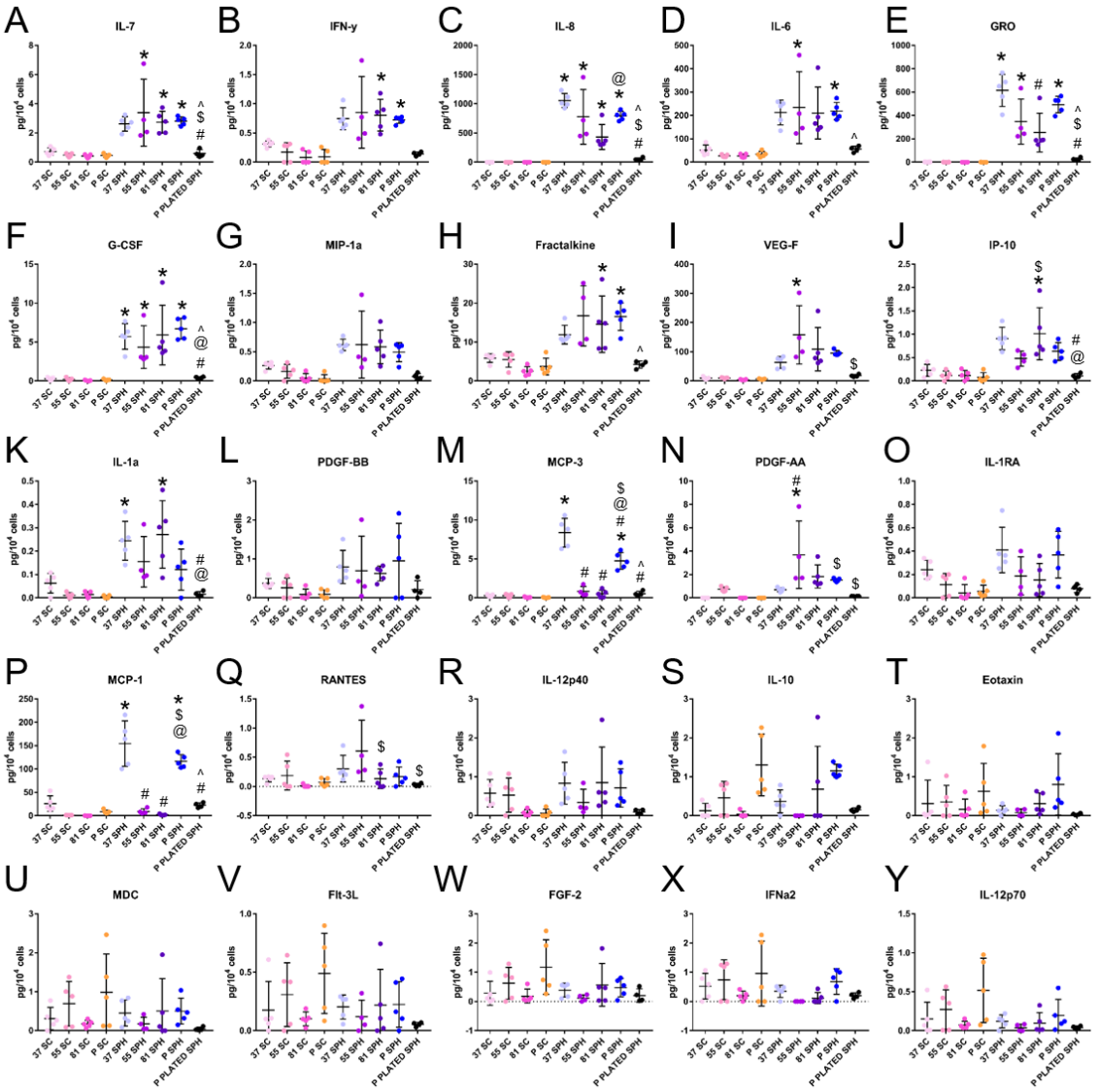


**Figure 12. Rotary spheroid culture enhances hMSC secretion of immunomodulatory factors not evident in static spheroid culture and donor variability is more evident in spheroid culture than single cells.** Commercial hMSCs from RoosterBio from 3 male donors (lots 37, 55, and 81) were cultured separately or pooled (P) under static monolayer single cell (SC) culture or 3D aggregate (SPH) rotary culture or allowed to plate down under static culture (P Plated SPH). Conditioned media was collected after 4 days and immunomodulatory cytokines were quantified using Milliplex® Human Cytokine/ Chemokine Magnetic Bead Panel Kit. Most cytokines were upregulated in spheroid rotary culture, but not in plated spheroids and donor variability was more evident in spheroid culture format than monolayer single cells. Significant differences between groups are based on multi-way ANOVA with Bonferroni correction and $\alpha$=0.05. *vs SCs same donor; # vs 37, $ vs 55, @ vs 81 same culture format, and ^ vs P SPH.

### *4.3.3 Effect of Confluence and Rotary Culture on MSC Secretome*

Since the enhancement of spheroid culture was dependent on rotary culture, an additional experiment was performed on hMSCs pooled from the same three donors to compare the effect of rotary culture on monolayer hMSCs cultured as single cells and compared to spheroid culture. Additionally, because hMSCs in spheroid culture are inhibited by the contact of surrounding cells, monolayer single cells were also plated at ten times higher seeding density (approximately 70% confluence) in order to reach confluence in the first 24 hours of culture (Figure 13). Conditioned media was collected from rotary and static cultures of single cells (normal density and 10x density) and spheroids after 4 days. The single cells plated at 10x density were confluent by day 2 of culture and all single cell cultures had a much higher concentration of cells per mL of culture media and rotary culture had no effect on cell proliferation at the normal seeding density (Figure 13). PLSDA analysis of z-scored secreted cytokines exhibited separation of spheroid and single cell culture on LV1 while LV2 showed some separation of normal static culture from all other cultures of MSCs (Figure 14). Surprisingly, confluence in the 10x higher density groups did not increase the secretome of MSC single cells in comparison to normal density and there were no significant differences in any of the cytokines between single cells cultured in rotary or static or at higher densities (Figure 15). Rotary spheroid culture, on the other hand, continued to increase MSC secretion of multiple cytokines including IL-7, FGF-2, MCP-3, VEG-F, MCP-1, GRO, IL-8, IL-10, IFN-ɣ, MDC, G-CSF, PDGF-AA, Fractalkine, and IFN-α2 (Figure 15).

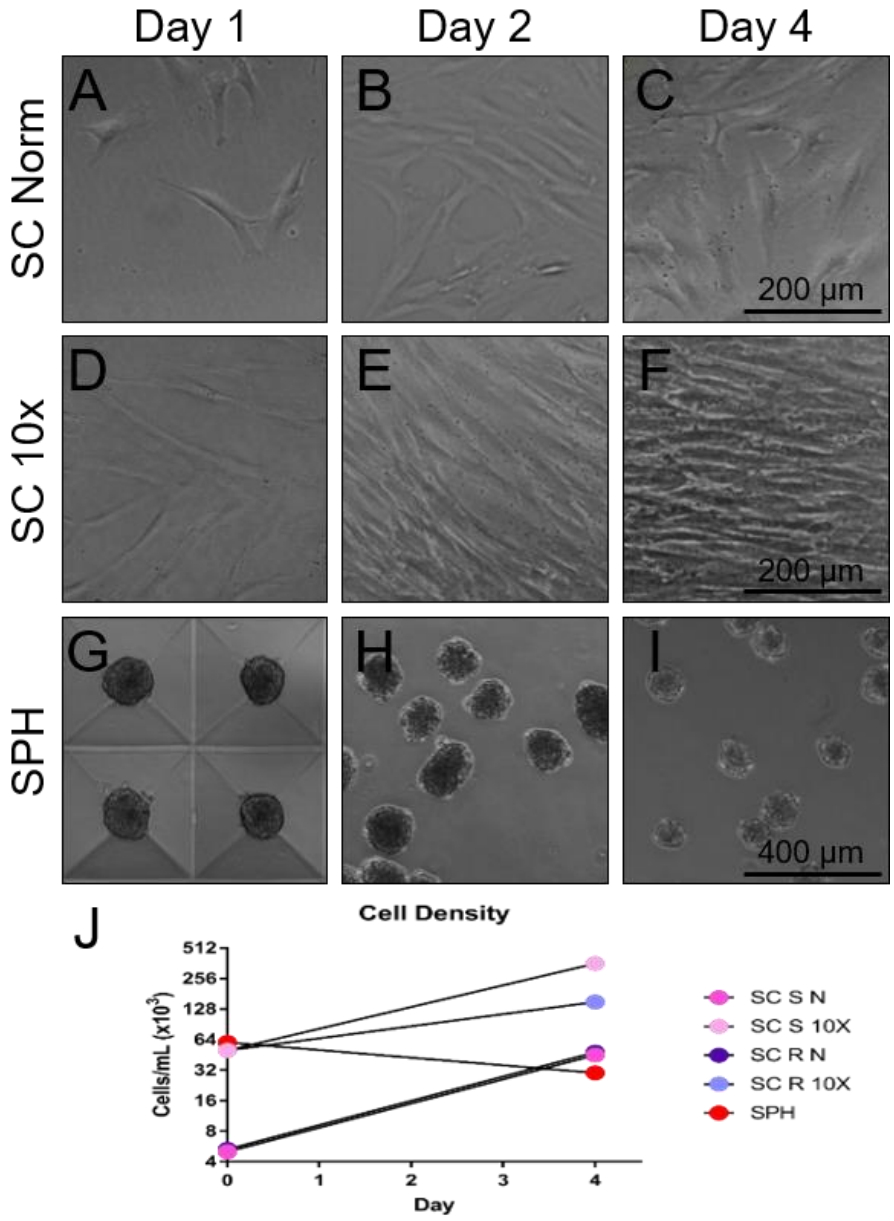


**Figure 13. hMSC single cells plated at ten times higher cell density reach confluence between 24 and 36 hours.** hMSC single cells were plated 10x higher cell density and culture statically or on a rotary orbital shaker for 4 days. Cell counts for single cells and spheroids were quantified after 4 days when conditioned media was collected and all single cells had a higher cell concentration per mL of conditioned media than spheroid culture.

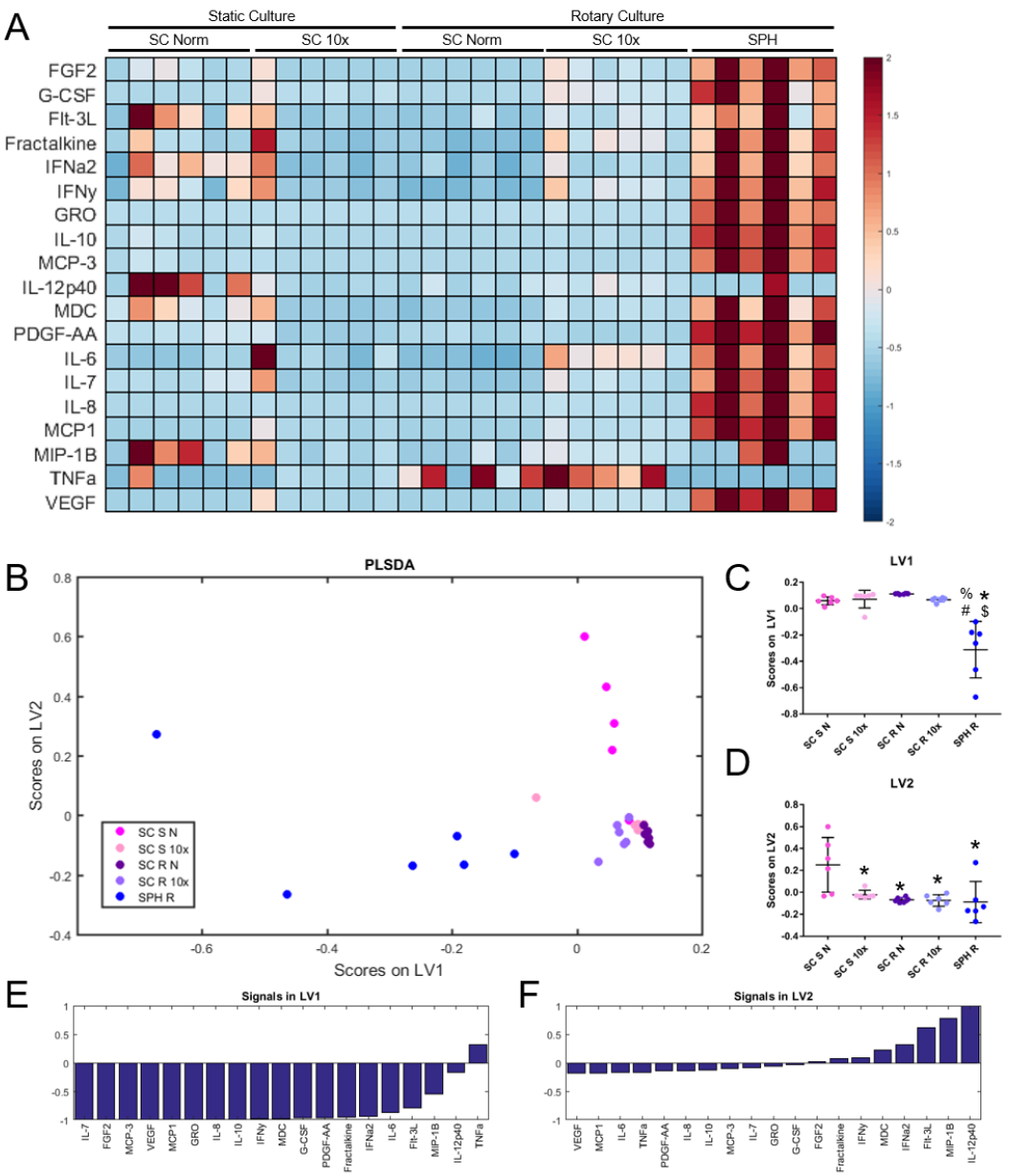


**Figure 14. Seeding density and rotary culture have little effect on hMSC single cell secretome in comparison to hMSC spheroid culture.** hMSC single cells were plated 10x higher cell density (10x) and the normal density (N) and cultured statically (S) or on a rotary (R) orbital shaker for 4 days. Cytokines in the conditioned media were quantified with a Milliplex® Human Cytokine/Chemokine Magnetic Bead Panel Kit. Heatmaps of the z-scored data indicates relative cytokines levels (A). PLSDA analysis (B) of z-scored secreted cytokines exhibited separation of spheroid and single cell culture on LV1 (C) while LV2 showed some separation of normal static culture from all other cultures (D). LV signal plots detail which cytokines are weighted in the latent variables in the PLSDA separation (E&F). Significant differences between groups are based on multi-way ANOVA with Bonferroni and $\alpha$=0.05. *vs SC S N. # vs SC S 10x, $ vs SC R N, % vs SC R 10x.

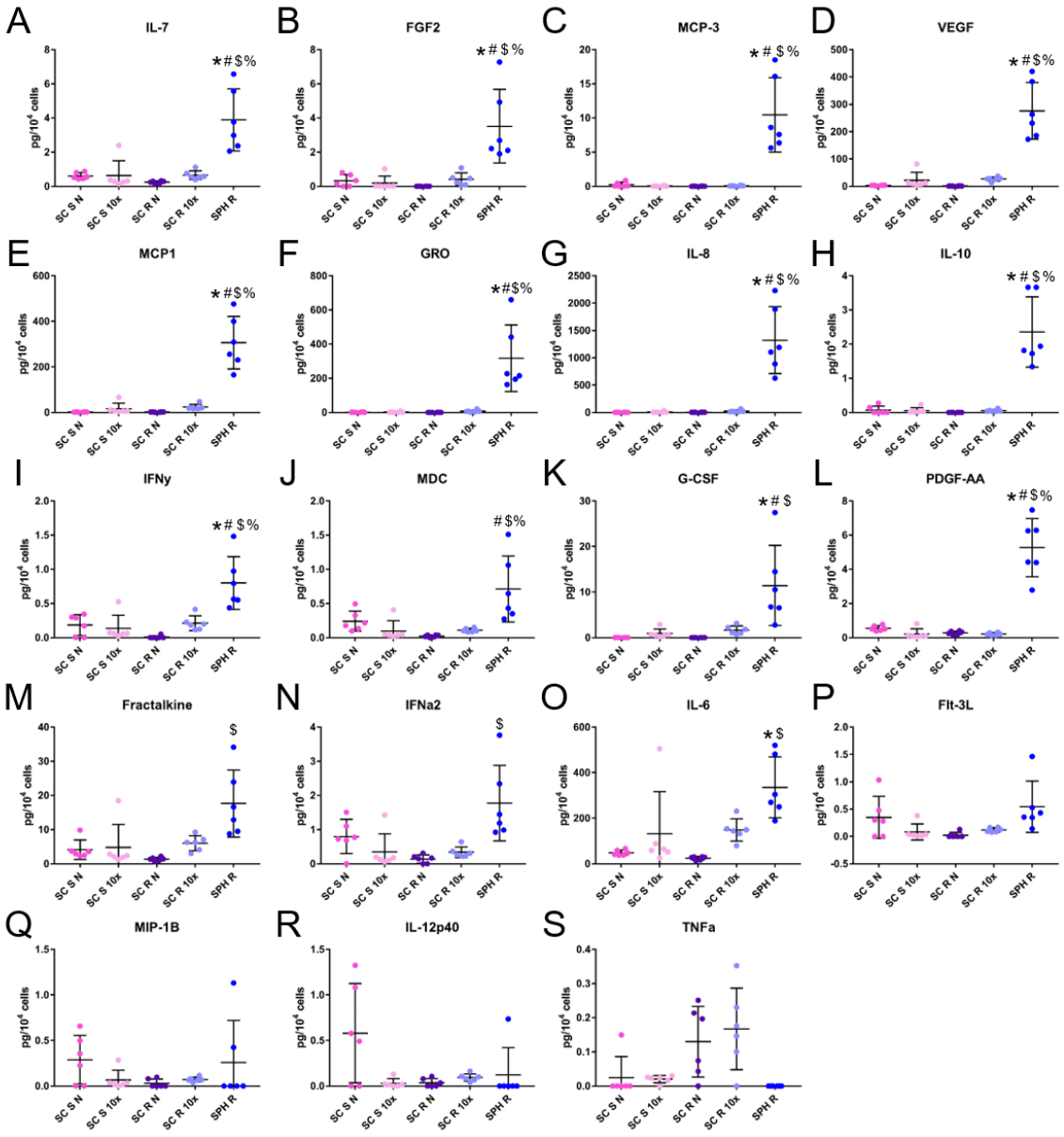


**Figure 15. Seeding density and rotary culture have little effect on hMSC single cell secretome in comparison to hMSC spheroid culture**. hMSC single cells were plated 10x higher cell density (10x) and the normal density (N) and cultured statically (S) or on a rotary (R) orbital shaker for 4 days. Cytokines in the conditioned media were quantified with a Milliplex® Human Cytokine/Chemokine Magnetic Bead Panel Kit. Only spheroid culture enhanced MSC secretion of immunomodulatory factors. Significant differences between groups are based on multi-way ANOVA with Bonferroni correction and $\alpha$=0.05. *vs SC S N. # vs SC S 10x, $ vs SC R N, % vs SC R 10x.

### *4.3.4 Quantifying the Effect of Culture Media on MSC Proliferation and Secretion*

Multiple culture medias and formulations are commonly used for hMSC culture, but the most recent culture methodologies often utilize defined, xeno-free medias in preparation for transplantation. Therefore, we compared the more traditional MSC growth media containing FBS (MSCGM) to a commercially available xeno-free media containing human platelet lysate (PLTmax). After 5 days of expansion at the same seeding density, cells cultured in the PL containing media were smaller in size and expanded faster compared to MSCGM containing FBS (Figure 16)**.**

After expansion in each media type, MSCs were harvested and either replated as single cells or used to form spheroids as described previously. The single cells and spheroids were both formed and cultured in the two medias to assess the effect of media composition on MSC secretome. PLSDA analysis of z-scored secreted cytokines exhibited separation of media types on LV1 while LV2 showed separation of single cells and spheroids (Figure 17). There were no significant differences between media types in single cell cultures, but spheroid culture was significantly different between the media types in LV1 scores (Figure 17). Spheroid culture in FBS increased GRO, VEG-F, MDC, IL-8, Flt-3L, IL-6, and Fractalkine but not in spheroids cultures in PL media (Figure 18). Spheroid culture in PL media significantly increased IL-4 compared to all other culture groups (Figure 18). Altogether, spheroid culture in FBS containing media enhances secretion of most quantified immunomodulatory cytokines and variations due to media composition are more evident in spheroid format.

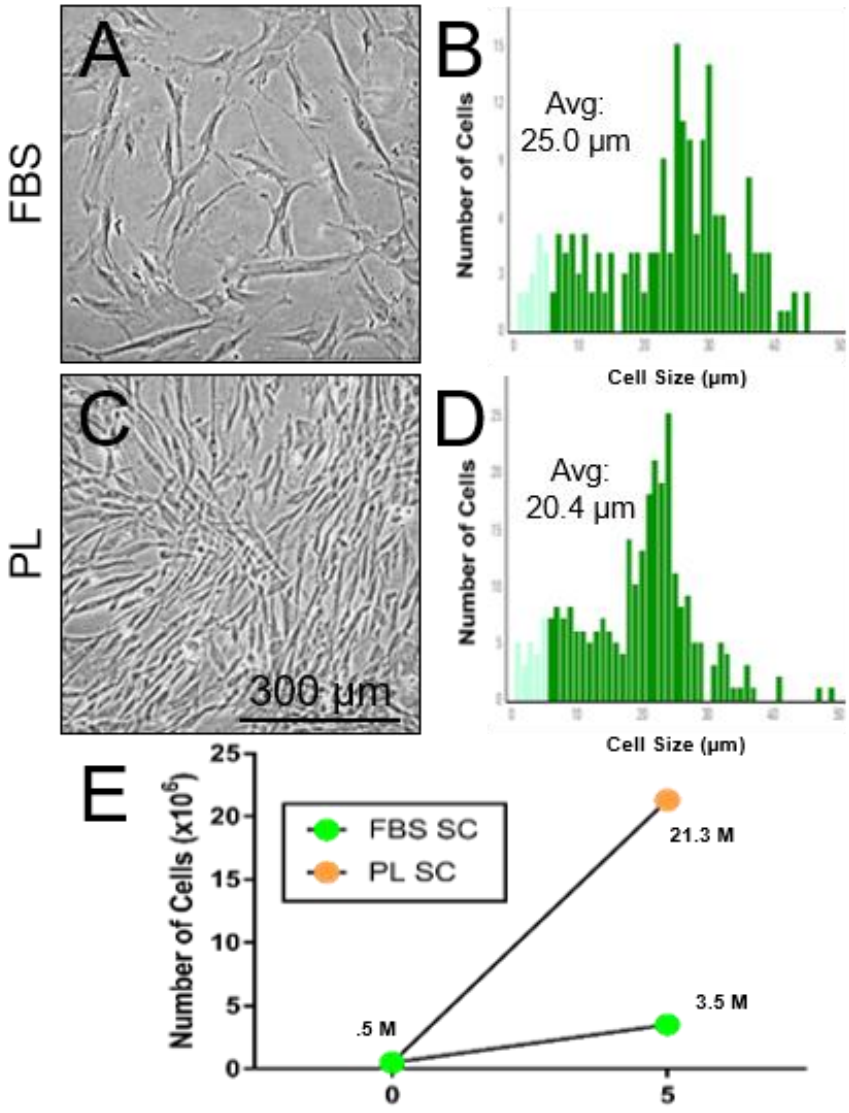


**Figure 16. hMSCs proliferate faster and are smaller in size in platelet lysate containing PLTmax media compared to MSC growth media containing FBS.** hMSCs were expanded in FBS containing MSCGM (A) or a defined, xeno-free media containing human platelet lysate (B). After 5 days of expansion at the same seeding density, cells cultured in the PL containing media were smaller in size (B vs D) and expanded faster (E) compared to MSCGM containing FBS.

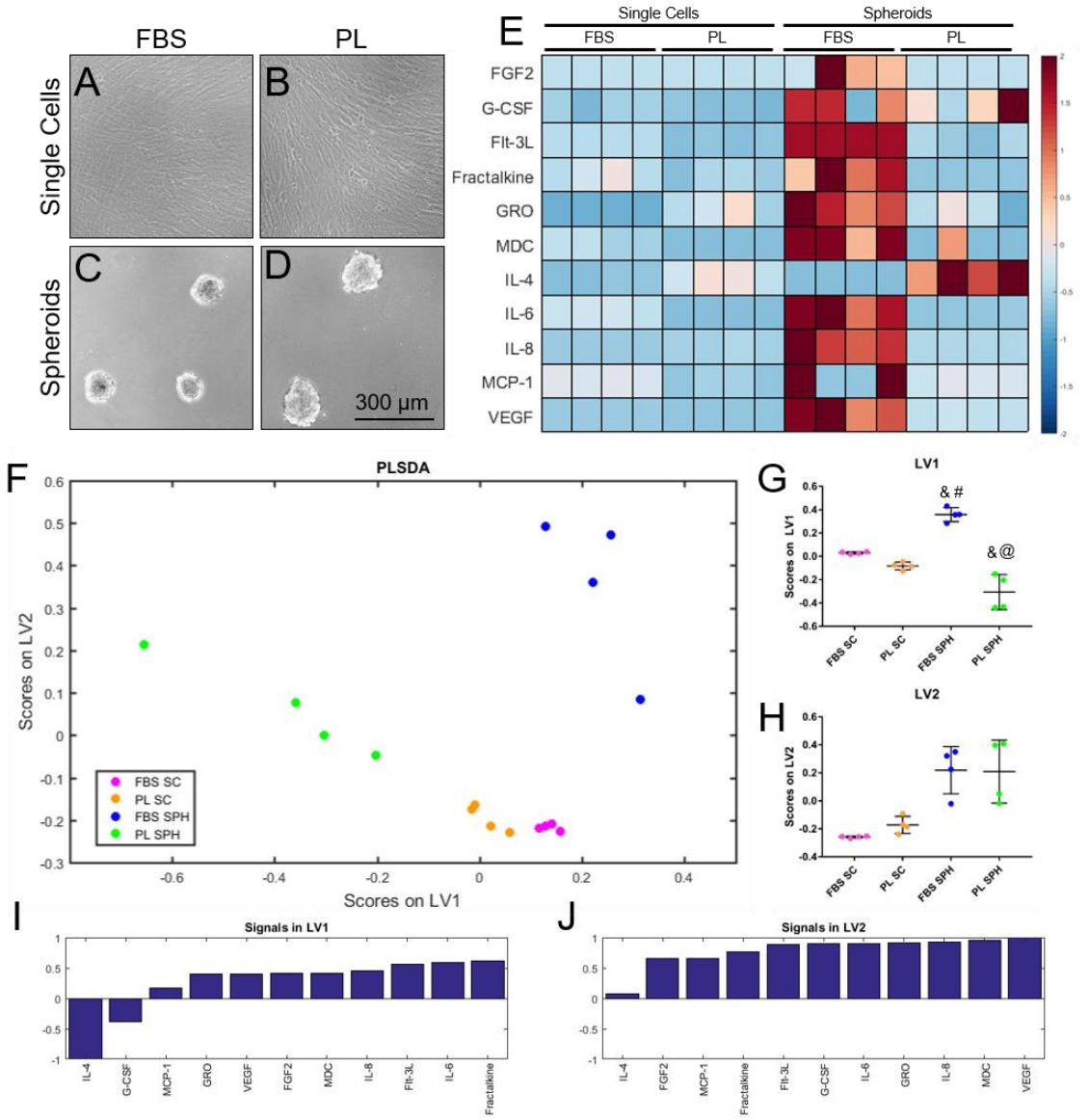


**Figure 17. Spheroid culture enhances the effect media composition has on MSC secretome.** hMSCs were expanded in FBS containing MSCGM or PL containing xeno-free media, passaged, and then cultured as single cells (A & B) or spheroids (C & D) for 4 days. Cytokines in the conditioned media were quantified with a Milliplex® Human Cytokine/Chemokine Magnetic Bead Panel Kit. Heatmaps of the z-scored data indicates relative cytokines levels (E). PLSDA analysis (F) of z-scored secreted cytokines exhibited separation of media types on LV1 (G) while LV2 showed separation of single cells and spheroids (H). LV signal plots detail which cytokines are weighted in the latent variables in the PLSDA separation (E&F). There were no significant differences in media type in single cell culture, but differences in media were significant between spheroid cultures for LV1 scores. Significant differences between groups are based on multi-way ANOVA with Bonferroni and $\alpha$=0.05. *vs FBS SC, # vs PL SC, & @ vs FBS SPH.

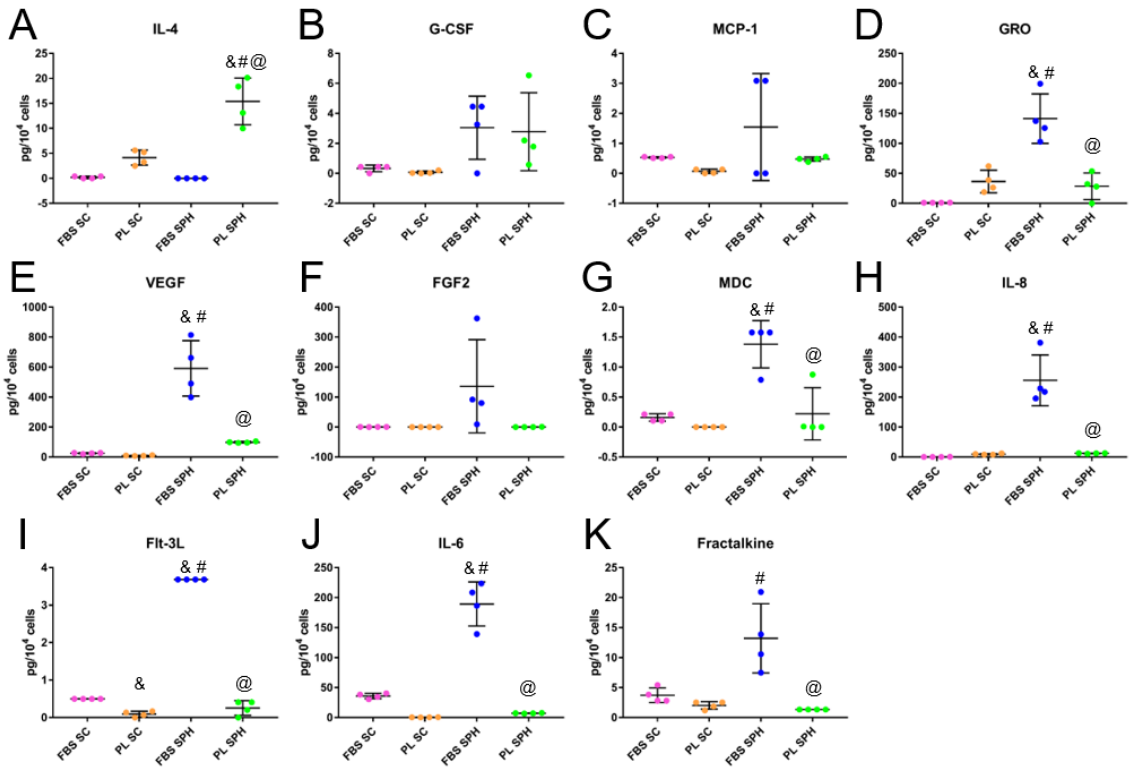


**Figure 18. The effect of media composition on MSC secretome is more pronounced in spheroid cultures and FBS cultured MSC spheroids have increased immunomodulatory secretion in comparison to PL cultured spheroids except for IL-4.** hMSCs were expanded in FBS containing MSCGM or PL containing xeno-free media, passaged, and then cultured as single cells (A & B) or spheroids (C & D) for 4 days. Cytokines in the conditioned media were quantified with a Milliplex® Human Cytokine/Chemokine Magnetic Bead Panel Kit. There were no significant differences in media type in single cell culture, but differences in media were significant between spheroid cultures. FBS media had higher concentrations for all detectable cytokines except for IL-4 which was significantly higher in PL spheroid cultures. Significant differences between groups are based on multi-way ANOVA with Bonferroni and $\alpha$=0.05. *vs FBS SC, # vs PL SC, & @ vs FBS SPH.

### *4.3.5 Validation of In Vitro Model of OA with Activated Synoviocytes*

Multiple groups have tested potential OA therapies in vitro using activated synoviocytes, but culture methodologies, techniques, and parameters for synoviocyte activation vary widely among groups [197-200]. In order to validate an *in vitro* model for OA-associated inflammation, changes in the inflammatory milieu secreted by activated

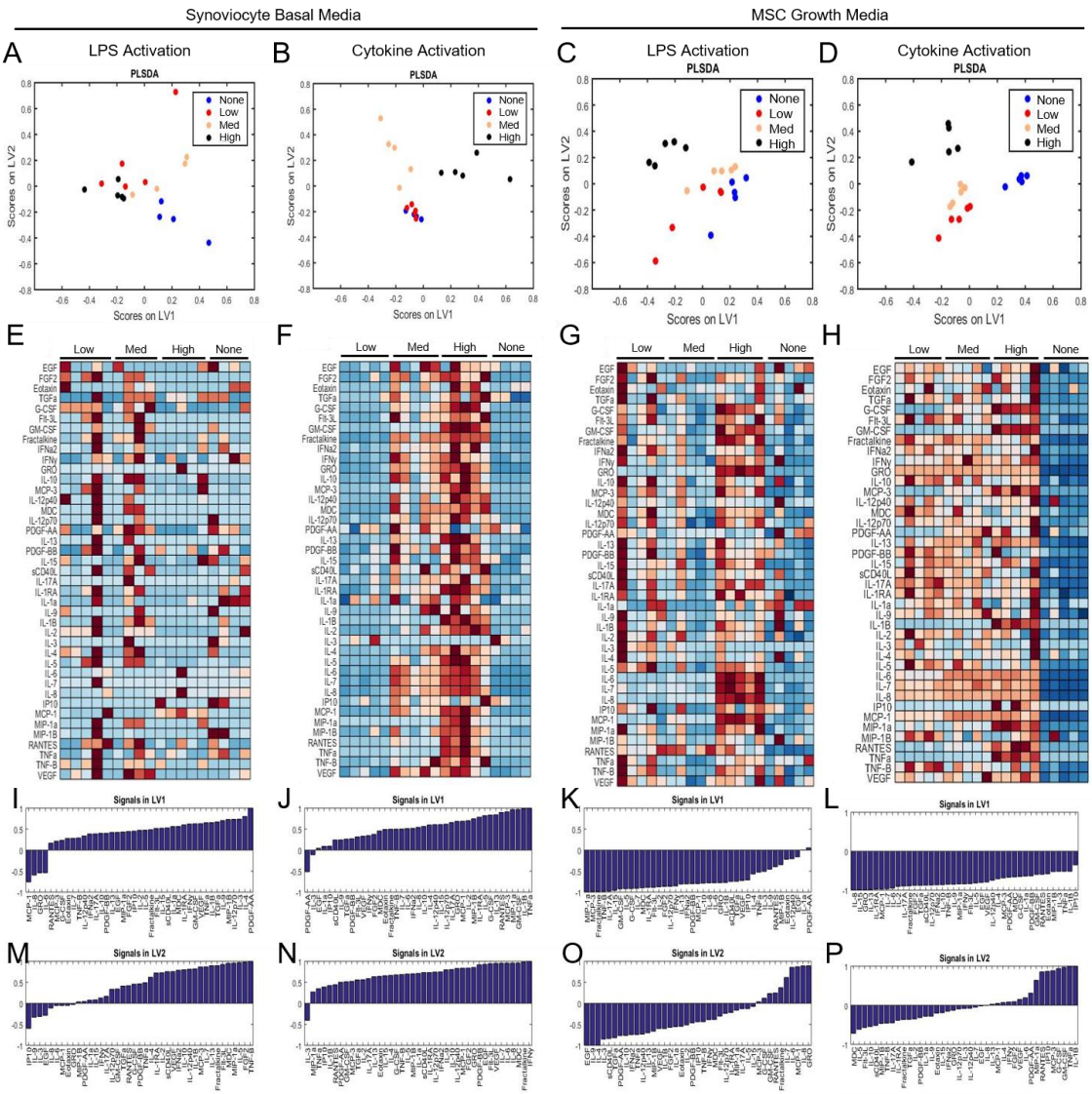


**Figure 19. Comparison of Synoviocyte Activation Protocols for In Vitro Model of OA.** Human synoviocytes cultured in synoviocyte growth medium (SGM) or MSC growth medium (MSCGM) were activated with a low, medium, and high dose of LPS (.1, 1, and 50 µg/mL) or a combination of cytokines TNF-α and IL-1β (.05, .5, and 5 ng/mL). 24 hours after activation, media was changed to fresh MSCGM and conditioned media from the activated synoviocytes was characterized after 4 days using Milliplex® Human Cytokine/Chemokine Magnetic Bead Panel Kit. PLSDA analysis of z-scored secreted cytokines was used to visualize separation between doses and unactivated cytokines (A-D). Heatmaps of the z-scored data also indicate which cytokines exhibited a dose-dependent response to activation (E-H) and LV signal plots detail which latent variables (cytokines) are involved in the PLSDA separation (I-P). Cytokine activation in MSCGM (D) exhibited the clearest separation between unactivated and activated synoviocytes in LV1 with clear dose-dependent responses to activations in LV2.

synoviocytes was compared in both a proprietary synoviocyte growth medium (SGM) and MSCGM. A 24-hour activation at low, medium, and high doses of LPS or TNF-α and IL-1β was compared after 4 additional days in fresh MSCGM without activation cytokines. PLSDA analysis of z-scored secreted cytokines revealed the clearest separation between unactivated and activated synoviocytes (on the LV1 axis) and a dose dependent response (on the LV2 axis) when synoviocytes were activated with a combination of TNF-α and IL-1β (Figure 19 D). Heatmaps of the z-scored data indicate a dose-dependent response to activation, particularly for the cytokines weighted most highly in LV2 (Figure 19 H).

### *4.3.6 Co-culture and Transwell Culture of Activated Synoviocytes & MSCs*

To compare suppression of synoviocyte activation by adherent and spheroid MSCs, varying ratios of MSCs to synoviocytes were compared. Human fibroblast-like synoviocytes were activated for 24-hours in 5 ng/mL IL-1β and TNF-α in MSCGM as described previously. After 24 hours, activation media was removed and MSCs pooled from 3 donors as single cells or spheroids were added directly to the 96-well plate (co-culture) or separated with a 5.0μm-pore-size transwell insert at ratios of 1:3, 1:9, or 1:27 synoviocytes to MSCs. Conditioned media collected from monolayer single cells or spheroids culture after 4 days was compared from direct and transwell cultures. PLSDA analysis of z-scored secreted cytokines shows separation of unactivated and activated synoviocytes on LV1 while LV2 showed separation of MSC concentration as single cells and spheroids (Figure 20). Synoviocyte activation increased GRO, IFN-ɣ, Eotaxin, IL-8, MIP-1a, IL-12p70, IL-12p40, IL-7, RANTES, TNF-α, IL-10, and IL-1β in comparison to unactivated synoviocytes (Figure 21). Most of these cytokines did not decease with MSC SC or SPH co-culture or conditioned media, although MIP-1a, IL-12p70, and IL-12p40

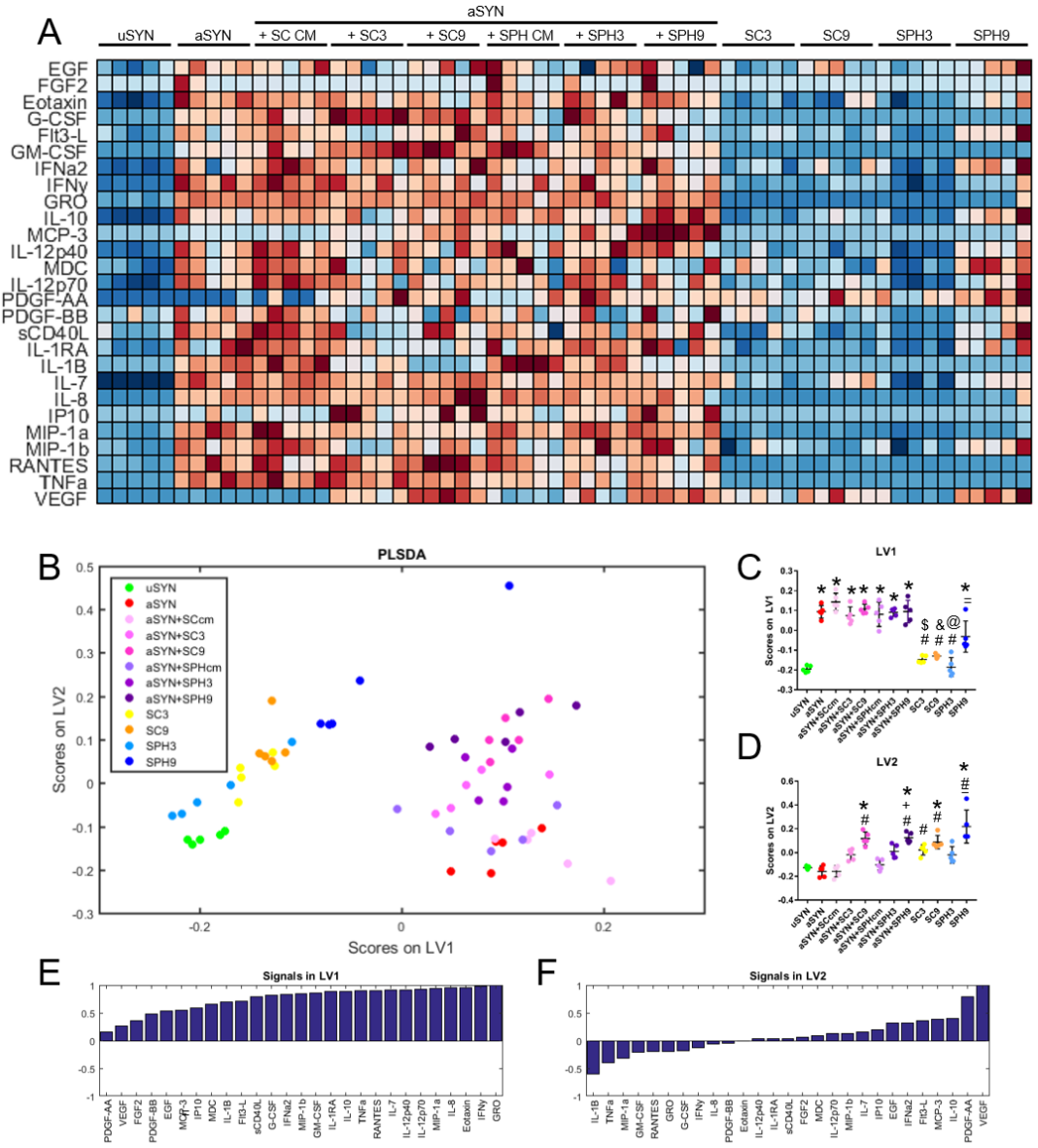


**Figure 20. Co-culture of Activated Synoviocytes, MSC Single Cells, and Spheroids.** hMSC single cells and spheroids pooled from 3 donors were co-cultured at ratios of 3:1 and 9:1 with activated synoviocytes or with conditioned media treated synoviocytes for 4 days. Cytokines in the conditioned media were quantified with a Milliplex® Human Cytokine/Chemokine Magnetic Bead Panel Kit. Heatmaps of the z-scored data indicates relative cytokines levels (A). PLSDA analysis (B) of z-scored secreted cytokines shows separation of unactivated and activated synoviocytes on LV1 (C) while LV2 showed separation of MSC concentration as single cells and spheroids (D). LV signal plots detail which cytokines are weighted in the latent variables in the PLSDA separation (E&F). Significant differences between groups are based on multi-way ANOVA with Bonferroni and $\alpha$=0.05. * vs uSYN, # vs aSYN, + vs cond med same format, $ vs 3:1 same format, & vs SC same dose, @ vs SPH same dose, % vs SC3, X vs SC9, = vs SPH3.

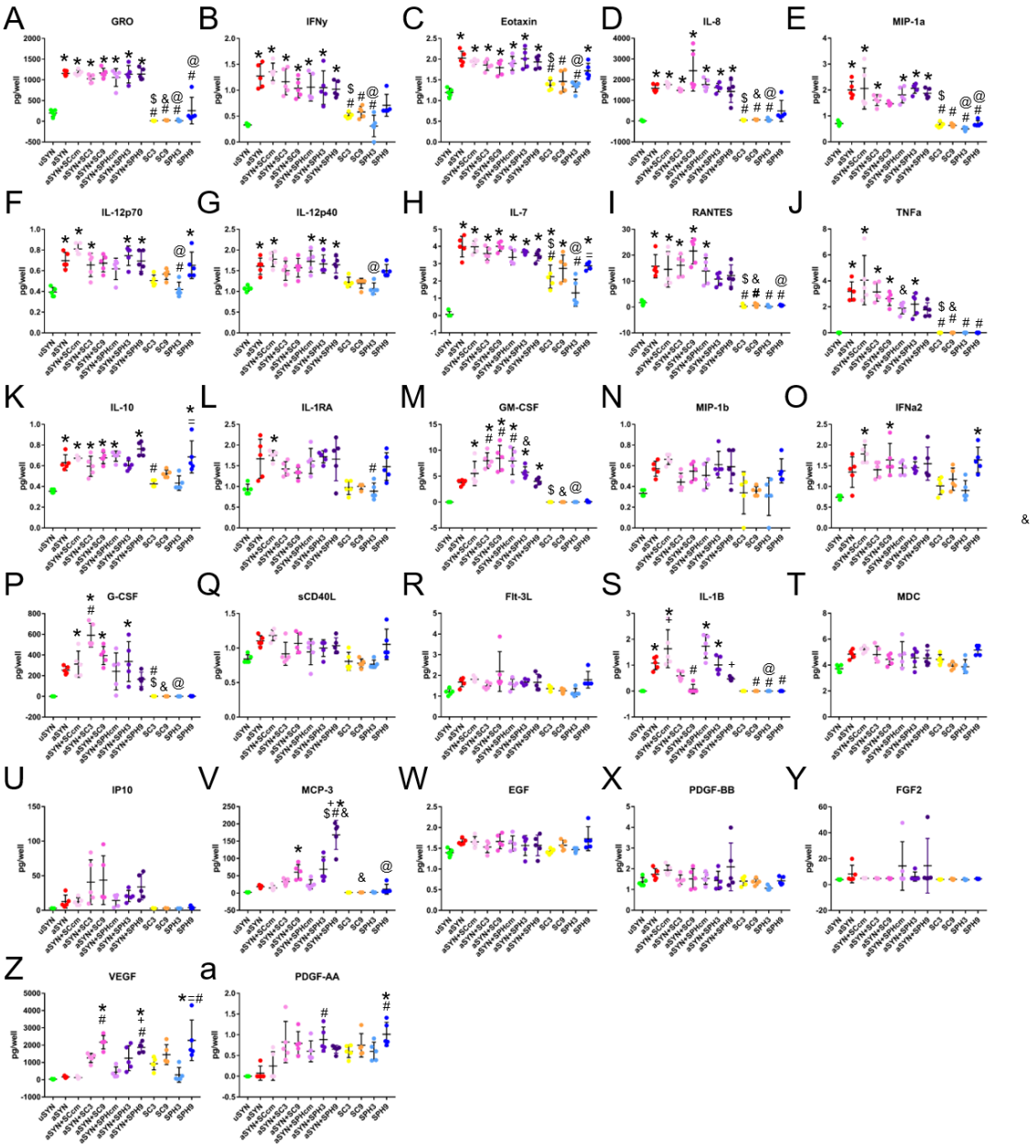


**Figure 21. Secretome of Activated Synoviocytes, MSC Single Cells, and Spheroid Co-culture.** hMSC single cells and spheroids pooled from 3 donors were co-cultured at ratios of 3:1 and 9:1 with activated synoviocytes or with conditioned media treated synoviocytes for 4 days. Cytokines in the conditioned media were quantified with a Milliplex® Human Cytokine/Chemokine Magnetic Bead Panel Kit. Significant differences between groups are based on multi-way ANOVA with Bonferroni and $\alpha$=0.05. * vs uSYN, # vs aSYN, + vs cond med same format, $ vs 3:1 same format, & vs SC same dose, @ vs SPH same dose, % vs SC3, X vs SC9, = vs SPH3.

were not significantly different from activated or unactivated co-cultures and were between the two concentrations in aSYN:9SC co-cultures (Figure 21). IL-1β was significantly decreased in aSYN:9SC co-cultures and aSYN:3SC and aSYN:9SPH were between aSYN and uSYN values and not significantly different from either (Figure 21). MSC culture increased secretion of VEGF with or without the presence of aSYN. Co-culture of MSCs and aSYN stimulated secretion of G-CSF in both single cells and spheroids, GM-CSF in single cells and spheroid conditioned media, and MCP-3 in spheroid cultures (Figure 21). Altogether, co-culture of MSCs with activated synoviocytes was only able to significantly reduce activation-induced IL-1β production and did not affect most other cytokines upregulated by activation. There were some effects that required both aSYN and MSC co-culture as single cells and spheroids to elucidate a change in cytokine concentrations. Surprisingly, MSC spheroid co-culture did not have many significant changes and actually induced fewer changes in activated synoviocyte co-culture than MSCs as single cells.

Transwell cultures of MSCs with aSYN at 3:1, 9:1, and 27:1 were also performed to determine if any effects from co-cultures were due to direct contact or soluble factor secretion. Unactivated and activated synoviocytes were separated along LV1 of the PLSDA plot and surprisingly, 9:1 and 27:1 SC:aSYN transwell cultures and 27:1 SPH:aSYN cultures resulted in significantly lower LV1 scores than aSYN alone (Figure 22). 9:1 and 27:1 SC:aSYN and 27:1 SPH:aSYN transwell cultures resulted in decreased IL-1β and the 27:1 SC:aSYN resulted in less IFN-ɣ and IL-12p70 that was not statically significant from aSYN or uSYN (Figure 23). Interestingly, 3:1 and 9:1 MSC:aSYN cultures all increased IL-12p40 concentrations, but not the 27:1 MSC:aSYN groups

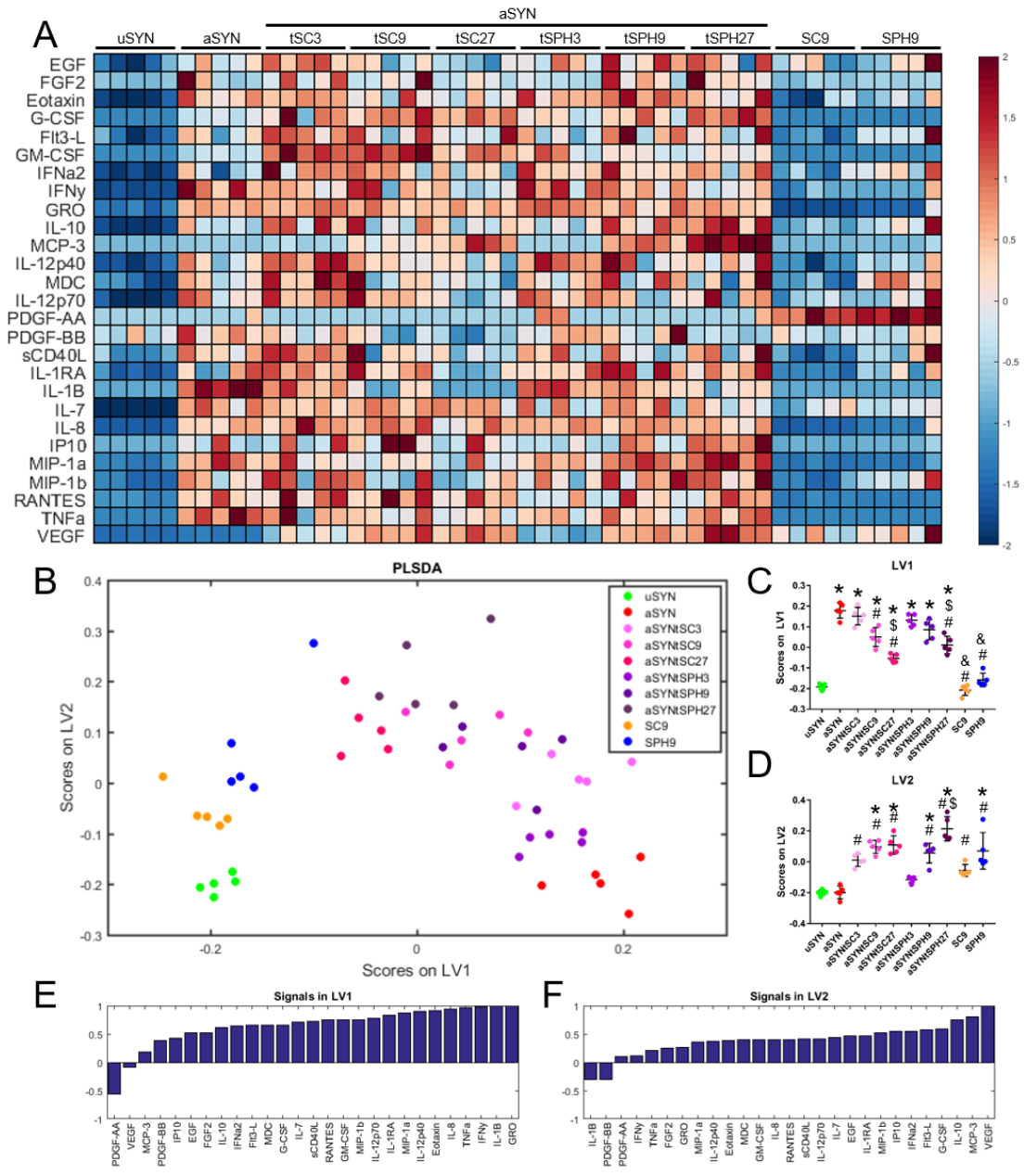


**Figure 22. Transwell Culture of Activated Synoviocytes, MSC Single Cells, and Spheroids**. hMSC single cells and spheroids were cultured in transwells with activated synoviocytes at ratios of 3:1, 9:1 , or 27:1 for 4 days. Cytokines in the conditioned media were quantified with a Milliplex® Human Cytokine Magnetic Bead Panel Kit. Heatmaps of z-scored data indicates relative cytokines levels (A). PLSDA analysis (B) of z-scored secreted cytokines shows separation of unactivated and activated synoviocytes on LV1 (C) while LV2 showed separation of MSC concentration (D). LV signal plots detail which cytokines are weighted in the latent variables in the PLSDA separation (E&F). Multi-way ANOVA with Bonferroni and α=0.05. * vs uSYN, # vs aSYN, $ vs 3:1 same format, ! vs 9:1 same format, & vs SC same dose, @ vs SPH same dose, % vs SC9.

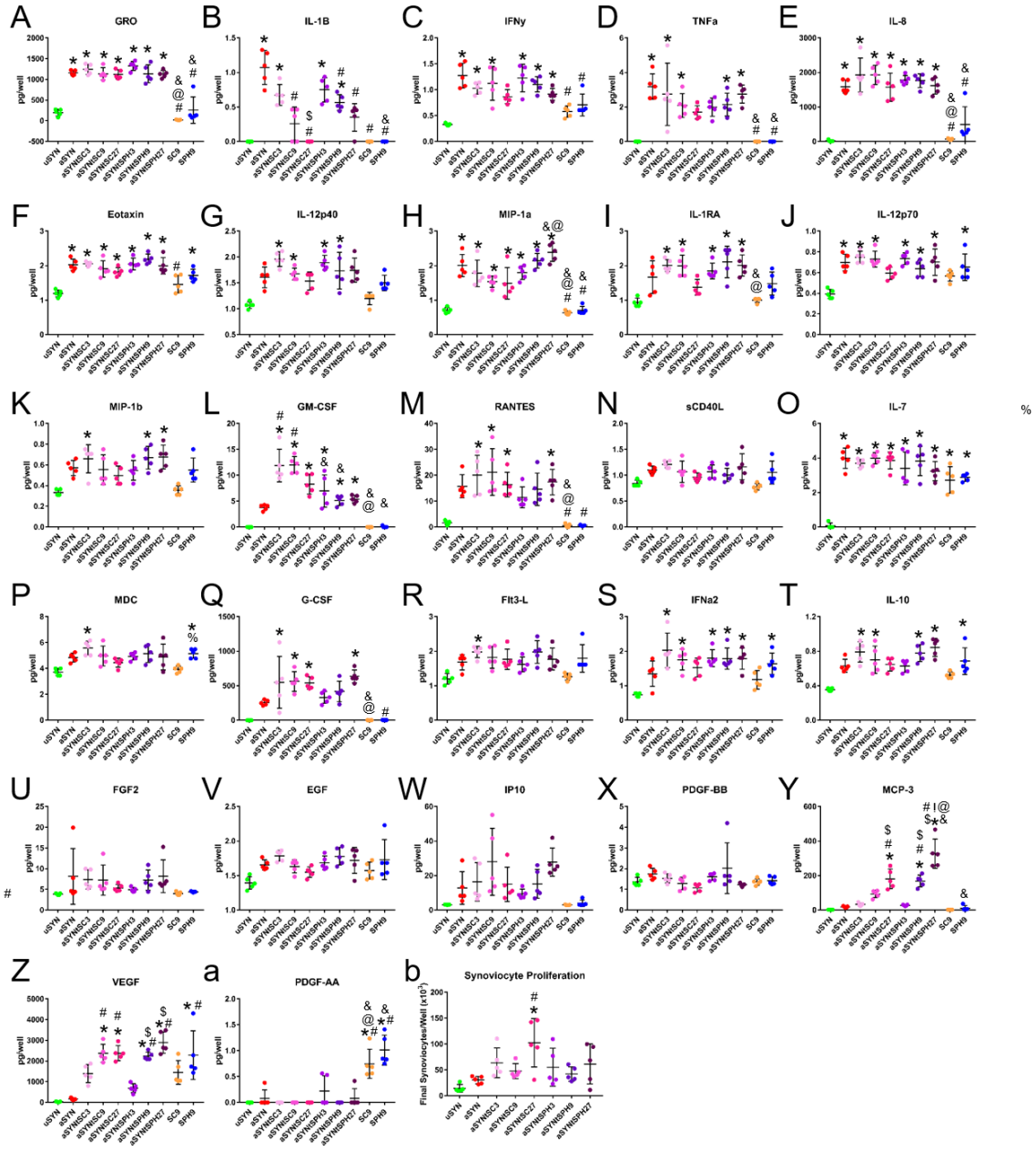


**Figure 23. Secretome of Transwell Culture of Activated Synoviocytes and MSC Single Cell and Spheroids.** hMSC single cells and spheroids were cultured in transwells with activated synoviocytes at ratios of 3:1, 9:1 , or 27:1 for 4 days. Cytokines in the conditioned media were quantified with a Milliplex® Human Cytokine Magnetic Bead Panel Kit. Only IL-1β was significantly reduced to levels similar to uSYN in aSYN:MSC transwell cultures and many other cytokines were no longer significantly different from aSYN. aSYN proliferation also increased in 27:1 SC:aSYN cultures (b). Multi-way ANOVA with Bonferroni and α=0.05. * vs uSYN, # vs aSYN, $ vs 3:1 same format, ! vs 9:1 same format, & vs SC same dose, @ vs SPH same dose, % vs SC9.

(Figure 23). MSC groups increased IFN-α2, IL-10, MCP-3, and VEG-F (Figure 23). MSCs also increased GM-CSF, RANTES, and G-CSF, but to a significantly less extent in SPH groups (Figure 23). Transwell culture at 27:1 SC:aSYN also increased synoviocyte proliferation in comparison to activated and unactivated synoviocytes alone, but co-cultures at other cell concentrations had no significant differences (Figure 23).

In order to understand the variance between the co-culture and transwell systems at the same aSYN:MSC ratios, a one-way ANOVA of co-culture and transwell studies was performed. The ANOVA showed that only responses to IL-1RA and PDGF-AA were significantly different, although the transwell culture did show more differences within multiple individual cytokines (Figure 24). IL-1RA had a large weight in LV1 scoring for both PLSDA models while the co-culture PLSDA model had little dependence on PDGF-AA and the transwell model had high dependence on PDGF-AA concentrations. Altogether, culture of MSCs as single cells and spheroids with activated synoviocytes was unable to change many cytokines involved in activation, but there was a dose dependent response to some cytokines in which SCs co-culture and transwell resulted in less activation than SPH cultures at the same concentrations.

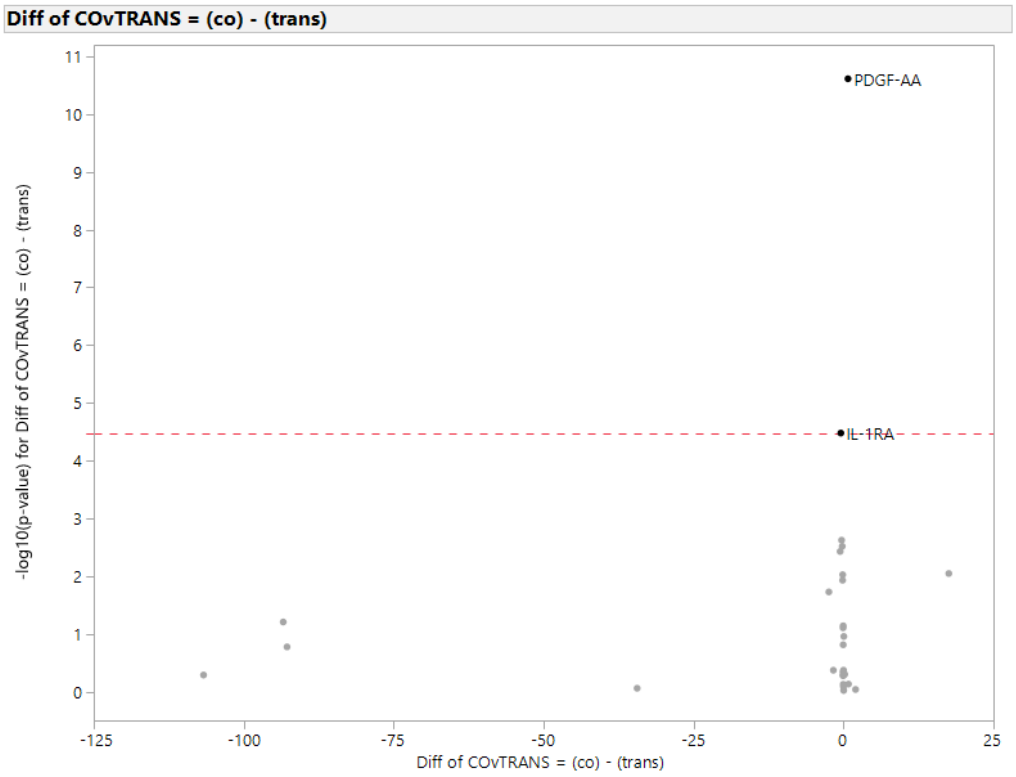


**Figure 24. Transwell and co-culture are only significantly different for IL-1RA and PDGF-AA cytokine concentrations.** Volcano plot for one-way analysis of variance (ANOVA) between co-culture and transwell aSYN:MSC studies with the same ratios (1:3 and 1:9) show only IL-1RA and PDGF-AA are significantly different between co-culture and transwell format.

### *4.3.7 Assessing Injectability of MSC Single Cells and Spheroids*

A preliminary in vitro experiment was performed to test the effects of incubation time and injection on cell morphology and viability. Spheroids and single cells at $1x10^6$ cells/50µL MEMα (the amount delivered per animal) were loaded into syringes at 150µL/syringe. Spheroid morphology and viability was maintained after injection through the 27 gauge needle and four hours of incubation, but the single cells had some clumping and cells in the centers of those clusters were often dead after incubation (Figure 25). Based on these results, syringes were prepared immediately before injection and order of injection was sorted by treatment group to minimize incubation time.

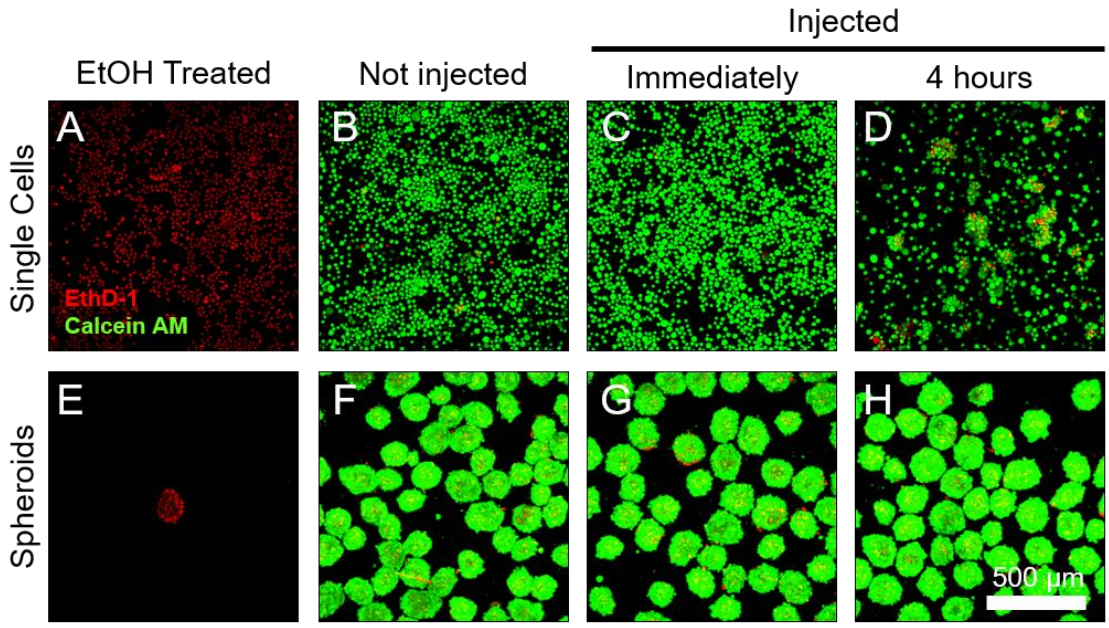


**Figure 25. hMSC single cells & spheroids (n=3) maintain viability after injection up to 4h after syringe preparation.** $1x10^6$ hMSCs in 50µL of MEMα (Lonza) were incubated at 4ºC for 4 h and injected through a 27G needle into a glass bottom plate to assess viability & morphology. Spheroids maintained their morphology over 4 hours with relatively little clumping (D), but single cells had more clumps after 4 hours of incubation (D).

### *4.3.8 hMSCs Remain in the MMT Joint Less Than 1 Week*

To determine if spheroid formation can enhance MSC retention and homing in the joint space, human MSCs lenti-virally labeled for GFP/luciferase expression were intra-articularly injected one day after MMT surgery and tracked with IVIS imaging with injections of luciferin on days 1, 3, and 7. The BLI signal decreased to around 60% of the initial signal by day 3 and less than 1% of the signal was evident after 1 week (Figure 26). There were no significant differences between MSCs delivered as single cells and spheroids.

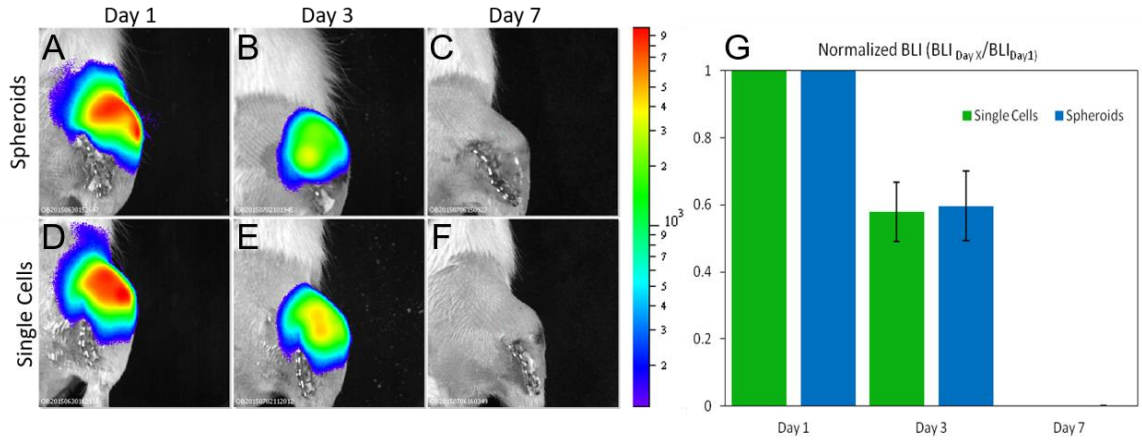


**Figure 26. hMSC single cells & spheroids (n=3) remain in the MMT joint for less than 1 week.** In both single cell and spheroid groups, lenti-virally labeled hMSCs had normalized bioluminescent signals that decreased ~40% in the first 48 hours following injection, with <1% of the cells remaining after 7 days. One-way ANOVA showed no significant differences between single cell and spheroid groups.

### *4.3.9 MSCs Reduce OA Progression in the OA Model*

MSCs spheroids and single cells pooled from 3 donors were injected one day after medial meniscal transections in the rat MMT model to determine the efficacy of MSC spheroids in treating OA. Saggital sections representing the area of largest lesion or damage for each sample showed little differences in the healthy, smooth surfaces of the sham animals and those treated with single cells following MMT (Figure 27). Cartilage thickness maps of the entire tibial plateau shows that the MMT alone group has more damage and MSC treatment with single cells and spheroids seems to attenuate that progression (Figure 28 A). There are some lesions and abrasions in the spheroid treated group, but qualitatively appear to be less extensive and smaller than the MMT only group. Surface roughness corresponding to cartilage surface fibrillation was significantly increased in MMT samples but not MSC treated groups (Figure 28 D). There were no significant changes in cartilage

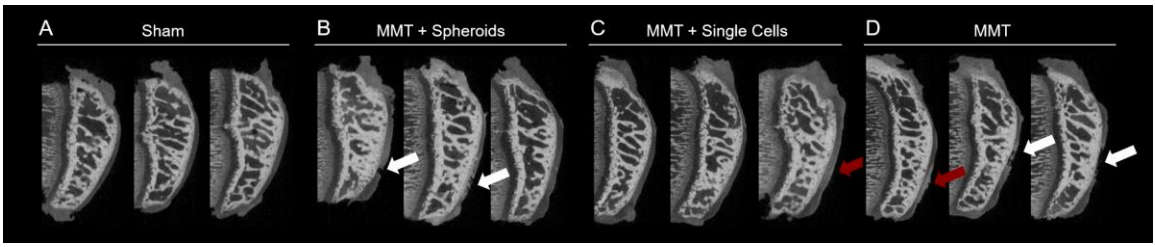


**Figure 27. Representative image of EPIC-μCT images isolating erosion and lesions.** Animals were harvested 21 days after sham (A) or MMT (D) surgery treated with spheroids (B) or single cells (C) on day 1. Lesions (white arrows) and erosions (red arrow) were observed in all MMT groups, although animals that underwent MMT alone appeared to have the most damage.

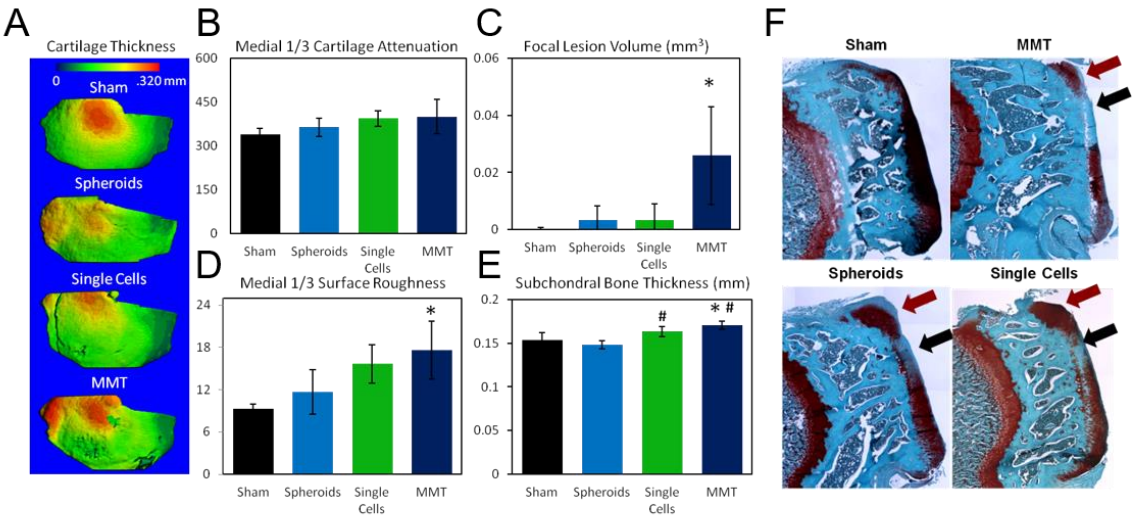


| | Sham | Spheroids | Single Cells | MMT |
|---|---|---|---|---|
| Lesions | 0/3 | 2/3 | 0/3 | 5/6 |
| Osteophytes | 0/3 | 1/3 | 1/3 | 3/6 |

**Figure 28. hMSC single cells & spheroids reduce OA progression in the rat MMT model of OA.** There was fibrillation and thinning of the medial third of the tibial cartilage (A) and an increase in cartilage lesion volume (C), surface roughness (D), and subchondral bone thickness (E) 21 days after MMT surgery, but treatment with MSCs delivered as single cells or spheroids reduced lesion volume (C) and surface roughness (D) to levels similar to animals that underwent sham surgery. Treatment with spheroids had less subchondral bone thickening than single cells (E). All animals that underwent MMT surgery had cartilage thickening (red arrow) and some GAG depletion as evidenced by lack of Safranin O staining (black arrow) on the tibial plateau, but hMSC treatment with single cells or spheroids reduced GAG depletion and lesion volume (F). There were also fewer osteophytes formed in hMSCS treated animals. Statistical significance based on ANOVA with Bonferroni Correction *$p<0.05$ vs Sham, #$p<0.05$ vs Spheroid.

attenuation (Figure 28 B). Treatment with spheroids had less subchondral bone thickening than single cells (Figure 28 E). All animals that underwent MMT surgery had cartilage thickening (red arrow) and some GAG depletion as evidenced by lack of Safranin O staining (black arrow) on the tibial plateau, but hMSC treatment with single cells or spheroids reduced GAG depletion and lesion volume (Figure 28 F). There were also fewer osteophytes formed in hMSCS treated animals (Figure 28).

## 4.4 Discussion

MSCs are the most commonly used cell type in clinical trials for various applications. Despite promising in vitro and in vivo pre-clinical data, however, there have been numerous failures of MSC trials to demonstrate efficacy in several therapeutic applications. Limited consistency in clinical outcomes utilizing MSCs therapies is often attributed to lack of sufficient cell number and variation due to donors and culture methodologies. Our results demonstrate that 3D aggregation of MSCs increases endogenous immunomodulatory factor secretion that is more sensitive to donor variability, culture format, and media composition in comparison to traditionally cultured single cells. No changes in MSC secretome were detectable in multiple MSC donors cultured as single cells, but spheroid culture differentially enhanced the paracrine profiles of the same donors elucidating more variation in donor secretome and potential therapeutic functionality. Therefore, spheroid culture that mimics the cell-cell and cell-matrix interactions and 3D nature of the endogenous MSC niche may be a better predictor of cellular responses and efficacy upon transplantation.

Expansion and culture in a defined, xeno-free media containing platelet lysate resulted in faster expansion and smaller cells than FBS containing growth media, but resulted in reduced immunomodulatory secretion in spheroid format. This media-dependent response for MSC aggregates is consistent with previous findings [155]. Thus, medias optimized for MSC growth may not be the best suited for culture for therapies that are dependent on the immunomodulatory capacity of MSCs.

Increased cell-contact dependent Notch signaling and intercellular adhesions such as E-cadherin have previously been implicated in the enhancement of paracrine activity of MSC aggregates [139, 203, 204]. Surprisingly, increasing cellular contact of single cells in monolayer by altering their seeding density and time to confluence resulted in reduced paracrine activity in comparison to single cells seeded at a lower density. Additionally, rotary altering the hydrodynamic environment through rotary orbital culture plated cells also reduced single cell paracrine activity. Thus, although the mechanisms responsible for increased paracrine activity of MSCs cultured as spheroids still need to be elucidated, aggregation is a simple, yet effective means to not only enhance immunomodulatory cytokine production, but also sensitivity to culture conditions.

The increase in the secretory profile in spheroid culture in comparison to monolayer culture is consistent with previous findings [149-154]. Furthermore, culturing MSCs in an inflammatory environment that models OA-inflammation can modulate the MSC secretome. Surprisingly, spheroid culture format did not improve the suppression of activated synoviocytes in comparison to single cells. A previous study by our group has shown that a greater number of MSC as spheroids is required to suppress T-cell proliferation in CD3/CD28 activated PBMCs when MSCs were aggregated and that MSC

immunomodulation of T-cell proliferation was partially contact mediated. Alternatively, comparisons of our transwell and co-culture models demonstrate no contact-dependence on MSC modulation of activated synoviocytes and transwell culture enhanced therapeutic response. An alternative hypothesis is that since MSC modulation of their secretome is dependent upon the environment and inflammation enhances their immunomodulatory response, spheroid culture may alter the inflammatory milieu exposed to the cell surface. Another study on hMSC aggregates in hanging drops resulted in a time-dependent increase in the number of apoptotic cells, and cellular stress signaling via NFκB and caspase was required for PGE2 production and reduction in macrophage inflammation by hMSC spheroids [154]. A more thorough understanding of cytokine production in spheroid culture, particularly in spatially different locations (surface vs interior) correlating the secretome and cellular environment may provide better insight into the mechanisms of MSC immunomodulation and elucidate ways to better engineer beneficial therapeutic outcomes. A computational modeling strategy developed to investigate heterogeneous regulation of transcriptional and endogenously secreted factors in embryoid body (EB) morphogenesis may also be useful in determining the spatiotemporal modulation of MSC paracrine activity in spheroid cultures [205].

Previous studies have shown that spheroid delivery of MSCs *in vivo* has also improved cell retention and survival, yielding better engraftment and treatment in cardiac and skeletal muscle models, colitis models, as well as bone defects [139, 145-148]. Surprisingly, this study demonstrated no significant differences in MSC retention with spheroid delivery and all MSCs decreased to 60% after 48 hours with less than 1% remaining after 7 days. Unlike most of these tissues, the knee joint space is considered

immunoprivileged as clinical evidence of tissue rejection is rare [206], but the joint space does have rapid clearance of small molecules and clearance is increased with disease severity [207, 208]. Our findings of rapid clearance within the first were similar to those of other studies of MSCs delivered as single cells delivered to ACL (anterior cruciate ligament)- transected rat knees [209].

The ultimate objective of this study was to quantitatively assess the efficacy of MSC spheroids as a disease modifying intervention for osteoarthritis. Using the post-traumatic rat medial meniscal transection (MMT) model of OA, single injections of MSCs as single cells and spheroids were compared to MMT and sham MCL transected knees 21 days after surgery. EPIC-μCT image analysis showed MSCs delivered as single cells or spheroids reduced lesion volume and surface roughness to levels similar to animals that underwent sham surgery. Surface fibrillation and erosion, as measured by surface roughness, are some of the hallmarks of OA progression and are one of the earliest indicators detectable via μ-CT analysis. Treatment with spheroids had less subchondral bone thickening than single cells. All animals that underwent MMT surgery had cartilage thickening and some GAG depletion on the tibial plateau, but hMSC treatment with single cells or spheroids reduced GAG depletion and lesion volume. There were also fewer osteophytes formed in hMSCS treated animals although changes were not significantly different between treatments.

Reduction of OA progression with MSCs as single cells is consistent with previous studies of MSCs delivered to rat models of OA [210, 211]. Other studies suggest the relatively short treatment window and residence time of injected cells may be insufficient to modulate OA progression, particularly if allowed to progress to later stages [209].

Weekly intra-articular injections of MSCs in ACL-transected rat knees resulted in significantly reduced OA progression and attenuated synovitis compared to control limbs at 8 and 12 weeks, but there were no significant differences in single injection or weekly injections at their earliest time point of 4 weeks.

The MSC-synoviocytes co-culture and transwell studies were a better predictor for the observed in vivo response than analyzing the secretome of MSC single cells and spheroids alone. While the spheroid format may enhance MSC paracrine secretion in vitro, functional assays with relevant cell types may aid in predicting efficacy of MSC therapies upon transplantation.

## 4.5 Conclusion

OA is a complex disease involving inflammation of multiple tissues and involvement of multiple signaling pathways. MSCs offer a promising approach for cell-based immunomodulation of OA due to their ability to modulate multiple cell populations. Because MSC therapies have yielded variable results, developing robust culture conditions to enhance MSC paracrine productivity may improve therapeutic outcomes. Our results suggest that environmental parameters, including spheroid culture, media composition, and donor source can modulate the secretion of anti-inflammatory molecules by MSCs. Spheroid culture can elucidate variances due to alterations in the microenvironment, media formulation, and donors that may be masked in monolayer culture. Both MSCs delivered as single cells and spheroids resulted in improvements in early stage OA progression in a rat model, and further studies are needed to elucidate the effect of delivery format as a potential disease modifying OA therapy.

# CHAPTER 5. INVESTIGATING THE EFFECT OF AMNION ON MSC IMMUNOMODULATION

## 5.1 Introduction

Osteoarthritis (OA) is the leading cause of disability in the US and involves cartilage degradation and chronic inflammation in the entire joint. In fact, inflammation precedes detectable structural changes and is an indicator of future medial cartilage loss [19-22]. Thus, therapeutic strategies targeting OA-associated inflammation are likely essential in developing a disease modifying therapy. Current treatment options focus on symptomatic management via pain relievers or surgical intervention; both with clear limitations [212]. Non-steroidal anti-inflammatory drugs (NSAIDs) are commonly used to treat OA-associated pain, but have strong side-effect including gastro-intestinal complications and negatively effecting chondrocyte proteoglycan synthesis [53, 213]. Clinical trials have tested a number of potential disease modifying OA drugs (DMOADs), including matrix-metalloproteinase inhibitors (MMPis), cytokine blockers, inhibitors of inducible nitric oxide synthase (iNOS), and doxycycline; however, none have shown a clear therapeutic benefit to date [214]. Current drug treatment regimens for immune diseases targeting a single molecule or pathway are often ineffective and insufficient to suppress the chronic inflammation involved in osteoarthritis due to the inherent compensatory pro-inflammatory pathways and multiple cell-types involved [18, 26, 27]. OA remains a pervasive and burdensome condition with limited effective clinical options.

MSCs secrete multiple immunomodulatory cytokines and can modulate multiple cell types involved in both innate and adaptive immunity, making them an attractive therapeutic option for OA. MSC immunomodulation is highly dependent on the local cytokine milieu and the efficacy of MSC therapies is dependent on the microenvironment upon implantation [215]. Although high concentrations of inflammatory cytokines are involved in acute injuries, chronic cases generally exhibit lower levels of inflammatory cytokines. In fact, the relatively low concentration of inflammatory cytokines in OA in comparison to rheumatoid arthritis is responsible for the initial misconception that it was not an inflammatory disease [40].

3D aggregation of MSCs enhances immunomodulatory paracrine factor secretion and improves retention and therapeutic outcome in cardiac and skeletal muscle models, colitis models, as well as bone defects in comparison to single cells [139, 145-148]. MSCs can be pre-conditioned with inflammatory cytokines before implantation to amplify their secretory profile and IFN-γ pre-treated MSCs have exhibited improved resolution of inflammation in models of colitis [246] and graft-versus-host disease [247] compared to non-treated MSCs. Despite the enhancement of MSC immunomodulation, the transient effects of pre-treatment may limit the potential of MSCs to modulate immune responses for more than a few days, particularly in environments that do not expose the cells to high concentrations of IFN-γ [156]. The McDevitt lab has shown that incorporation of IFN-γ-loaded heparin microparticles into MSC spheroids sustained immunomodulatory paracrine production and increased the polarization of co-cultured macrophages to a less inflammatory M2 phenotype [156]. Strategies involving treating chronic inflammation with any pro-inflammatory cytokines are often met with apprehension however, since

altering the natural ebb and flow of pro- and anti-inflammatory cytokine may result in further inflammation with sustained stimulation.

Alternatively, the multiple factors eluted from dehydrated amnion can also modulate stem cell paracrine activity and proliferation [164]. The amniotic membrane is the innermost layer of the placenta and exhibits immunosuppressant and anti-inflammatory activity that protects the fetus and ensures acceptance by the mother's immune system. Micronized dehydrated human amnion/chorion membrane has been shown to be non-immunogenic [158, 159]; contains a number of beneficial growth factors, including platelet derived growth factor (PDGF), fibroblast growth factor (FGF), and transforming growth factor beta (TGF-β) [160, 161]; and improves maintenance of chondrocyte phenotype [162, 163]. Previous work in the Guldberg lab has demonstrated that a single intra-articular injection of micronized amnion attenuates osteoarthritis development in the medial meniscal transection (MMT) rat model of OA [166].

To address the transient effects of pre-treatment, we hypothesized that ECM-based presentation of cytokines within spheroidal MSC aggregates may provide a means of locally concentrating and sustaining presentation of bioactive cytokines capable of potentiating MSC immunomodulatory activity. Previous work from our group has demonstrated the use of microparticles to deliver growth factors and small molecules throughout stem cell aggregates [248–251]. This study will investigate the effect of amnion particles on MSC trophic factor production and immunomodulatory activity both in vitro and in vivo.

The working hypothesis for this aim is that co-delivering MSCs and amnion will have a synergistic effect on suppressing inflammation and decreasing OA progression. The effect of amnion incorporation and co-culture on MSC spheroid secretome was quantified in direct (co-culture) vs indirect (transwell) systems to evaluate cross-talk between MSCs and the amnion matrix. Modulation of the inflammatory microenvironment with the combinatorial approach was also characterized *in vitro* in co-cultures with activated synoviocytes. Furthermore, the OA progression after combinatorial treatments with amnion and MSCs was evaluated in a rat medial meniscal transection model of joint degeneration. The results of this study demonstrate that engineering the biochemical and physical components of MSC constructs can modulate MSC paracrine secretion and immunomodulation which can be tailored to better treat OA.

## 5.2 Materials and Methods

### *5.2.1 Preparation of Amnion*

Amnion was prepared using the proprietary PURION® process and AmnioFix Injectable was used for all the studies (MiMedx Group, Inc. Marietta, GA). To account for donor to donor variations, five different batches of each formulation, each from a different donor, were pooled before use by aseptically mixing equal weights in the dry powder form and thoroughly mixing the pooled donors on a rotisserie for 30 minutes. Dried, pooled amnion particles were stored at 4ºC and the same batch of pooled amnion was used for all subsequent studies.

### *5.2.2 Fluorescent Tagging of Amnion to Evaluate Spheroid Incorporation*

Pooled amnion suspended at 1mg/mL in 50mM sodium bicarbonate buffer and VivoTag® 680XL (Perkin Elmer, Inc, Waltham, MA, USA) suspended at 10mg/ml in dimethyl sulfoxide were added to the amnion suspensions at a ratio of 1 mg dye to 20 mg amnion. The suspensions were mixed for an hour at room temperature then centrifuged and washed two times in saline to remove excess dye. The tagged amnion was then suspended in MSC growth media at 80 mg/mL in preparation for spheroid incorporation.

### *5.2.3 Cell Culture and Expansion*

Human bone marrow-derived MSCs from three male donors were obtained from RoosterBio Inc. (Frederick, MD) and expanded according to the manufacturer's protocols. Briefly, $10^7$ cryopreserved MSCs were plated in twelve T225 flasks in 45 mL of RoosterBio High Performance Media and incubated at 37°C for 7 days in a humidified 5% CO2 incubator. Media was exchanged after 4 days of culture. Cultures were passaged at 80% confluence by washing with 10 mL PBS and then incubated with 10 mL of 0.25% trypsin at 37ºC. An equal volume of RoosterBio High Performance Media was added to quench trypsin activity. Dissociated cells were then collected and centrifuged at 200xg. Cells were all frozen to similar passage doubling levels (PDL 13±1.5) in CryoStor CS5 cell cryopreservation media (STEMCELL Technologies, Vancouver, BC, Canada) prior to expansion for experiments. MSCs were expanded for one passages from frozen stocks by plating $1x10^6$cells in 45mL MSCGM in T-175 tissue culture treated flasks. Media was exchanged every three days and cells were passaged at 80% confluence.

### *5.2.4 Spheroid Formation and Culture*

Forced-aggregation of single cell suspensions of MSCs was used to generate MSC spheroids. Spheroids were formed overnight in 400μm agarose microwells for a high throughput method of generating homogenous cell aggregates [198]. Briefly, 600,000 MSCs pooled from three donors at similar population doubling levels were added to 24-well microwell inserts containing approximately 1,200 wells and centrifuged at 200xg for 5 min to force aggregation of spheroids with approximately 500 cells per aggregate. For in vitro studies, amnion was incorporated into spheroids by adding 2.4, .8. and .26 mg/well of amnion rehydrated in MSCGM to each insert. After 18h in the microwells, spheroids were removed and transferred to 96-well tissue culture treated plates with or without activated synoviocytes at ratio of 1:9 synoviocytes to MSCs. After 4 days of culture, MSCs and conditioned media were collected for cell counting (Countess II Automated Cell Counter, Thermo Fisher Scientific, Waltham, MA). Only .26 mg/well of amnion was incorporated into MSC spheroids for subsequent co-culture and in vivo studies and syringes were prepared immediately upon spheroid extraction from microwell inserts.

### *5.2.5 Synoviocyte Culture and Expansion*

Activated synoviocytes were used as an in vitro model of OA-associated inflammation since the synovium is a major site of gross and microscopic changes that occur early in disease progression [26]. Human fibroblast-like synoviocytes from three male donors were purchased and cultured to passage 3 in proprietary Synoviocyte Growth Media (SGM) according to manufacturer's instructions (Cell Applications, Inc, San Diego, CA). After expansion, synoviocytes were frozen in CryoStor® CS5 freezing media prior to experiments. After overnight recovery in SGM, synoviocytes were trypsinized, counted, and pooled from all three donors in equal amounts and seeded in a 96-well plate in SGM

at 2500 cells/well (~8,300 cells/cm$^2$). After 24 hours in SGM, synoviocytes were activated for 24 hours in 5 ng/mL human interleukin-1β (IL-1β) and 5 ng/mL tumor necrosis factor α (TNF-α) in MSCGM. MSCGM without cytokines was added as a control for unactivated synoviocytes. Activation medium was removed and fresh MSCGM was added after 24 hours along with MSC and/or amnion. Spheroids and amnion were added directly to the synoviocytes in 96-well plates (co-culture) or separated with a 5.0μm-pore-size transwell insert (Corning®, Corning, NY, USA) at ratios of 1:9 synoviocytes to MSCs. Spheroid MSCs and amnion alone were also cultured at the same densities to serve as controls for comparison for secretome analyses. After four days of co-culture, conditioned medium was immediately frozen at -80°C and cells were counted using Countess II Automated Cell Counter (Thermo Fisher) according to the manufacturer's protocol.

### *5.2.6 Immunomodulatory Factor Quantification*

Conditioned media was collected and inflammatory cytokines were quantified using MILLIPLEX MAP Human Cytokine/Chemokine Magnetic Bead Panel – Immunology Multiplex Assay (EMD Millipore). Conditioned media was diluted 1:2 in MSCGM and samples were analyzed according to the kit protocol and normalized to the standard provided with the kit after subtracting background of MSCGM media. All samples were read out on a MAGPIX instrument (Luminex).

### *5.2.7 MMT Animal Model and BLI Tracking*

Intra-articular injections of MSC spheroids with and without amnion were compared in the rat medial meniscal transection (MMT) model of OA. The Georgia Tech IACUC approved all animal studies (Protocol #A15019). Weight matched Lewis rats (250-

300g) underwent sham or MMT in the left leg as described previously [168]. Briefly, the animals were anesthetized with isoflurane, and the skin over the medial aspect of the left femoro-tibial joint was shaved and aseptically prepared. The medial collateral ligament (MCL) was exposed by blunt dissection and transected to reflect the meniscus toward the femur. The joint space was visualized, and a full thickness cut was made through the meniscus at its narrowest point. The skin was closed with 4.0 Vicryl sutures and then stapled using wound clips. hMSC spheroids and/or amnion was intra-articularly injected 24 hours after MMT surgery (Day 1) using an insulin syringe with 1 million MSCs and/or .5mg of amnion (AmnioFix Injectable, MiMedx Group, Inc. Marietta, GA) suspended in 50µL MEMα. All animals were euthanized at 3 weeks with $CO_2$ and legs were harvested for cryohistology or micro-CT and paraffin histology. Whole joints were fixed in sucrose and frozen for cryo histology (n=3) or dissected, formalin fixed for 4 days, decalcified with Immunocal® (StatLab, McKinney, TX ) for 7 days, and then scanned for micro-CT before histological analysis.

### *5.2.8 EPIC µ-CT Analysis of Articular Cartilage*

Decalcified tibias were incubated in Conray® contrast agent (Guerbet Group, Villepinte, France) for 24 hours at 37ºC. Legs were scanned using a Scanco µCT 40 at 45 kVp, 177µA, 200 ms integration time, and a voxel size of 16 µm. The EPIC-µCT images were reconstructed sagittally and coronally, manually contoured, and analyzed at suitable thresholding levels to separate the cartilage from bone and background. Scanco evaluation software was used to calculate cartilage attenuation, volume, and thickness for the medial plateau. To quantify cartilage fibrillation, scanned sections of the medial tibial plateaus were exported as TIFF files, and a MATLAB® (MathWorks, Natica, MA) program was

used to measure the cartilage surface roughness, defined as the root-mean-square of differences between the representative and polynomial fit surfaces of the cartilage [201]. For focal lesion analysis, lesions were defined as cartilage defects extending through at least 50% of the cartilage thickness along the subchondral surface. The lesion areas were manually contoured to create appropriate VOIs and within the VOI the cartilage volume was subtracted from the total volume to give lesion volume.

### *5.2.9 Histological Staining*

Following μ-CT, tibias of both surgerized legs and contralateral controls were dehydrated, routinely processed, and transected sagittally along the load-bearing plane. Samples were paraffin-embedded via vacuum infiltration with both load-bearing faces exposed for sectioning (n=6). Sagittal sections were cut at 5 μm thickness in strips of 12 (representing a total thickness of 120 microns) with 4 sections mounted to each slide. Slides were stained with toluidine blue and the sample representing the most significant cartilage damage was imaged at 4x magnification for automated histological scoring.

For whole joint histology, surgerized legs and contralateral controls (n=3) fixed in sucrose were cryoembedded with OCT freezing medium. Care was taken to preserve the synovium, meniscus and femoro-meniscal connective tissue. Joints were sagittally sectioned from the posterior joint surface to the load-bearing surface consistent with the paraffin embedded samples and recommended OARSI scoring methodologies. 10-micron sections were collected (CryoStar NX70 Cryostat, Thermo Fisher Scientific, Waltham, MA). Cryotape was used to preserve and transfer samples during sectioning and sectioned samples remained frozen at -80°C until staining. Samples were stained in toluidine blue

and slides with the most significant cartilage damage were imaged at 4x magnification consistent with paraffin embedded samples. Care was taken to include the synovial lining in images of the entire joint capsule for automated histological scoring.

### *5.2.10 Automated Histological Scoring*

Prior to grading, the histological images were all rotated so that the medial side was on the right and randomized to blind the grader. A semi-automated graphic user interface (GUI) for the evaluation of knee OA in rodents was previously developed and characterized by collaborators at the University of Florida [216]. Specifically, a MATLAB® GUI was designed for image analysis of toluidine blue stained rat knees using the OsteoArthritis Society International (OARSI) histopathology initiative's recommendations for histological assessments of osteoarthritis in the rat [172]. The user was prompted to select areas of measurement for (1) the entire medial plateau, (2) the area of total cartilage damage, (3) areas with significant (>50%) cartilage damage, (4) a contour of any existing lesions, (5) a contour of the cartilage-bone interface, (6) subchondral bone thickness on the medial and lateral sides of the medial plateau, (7) osteophyte thickness, and (8) the synovial lining thickness on the medial side. From these inputs and a pixel to micron conversion, the GUI function measures the degeneration widths of total and significant degeneration, osteophyte size, subchondral bone thickening, lesion width and depth, joint capsule thickness, and systematically calculates cartilage degeneration scores along the lateral, central, and medial thirds of the medial plateau. The synovial lining thickness was only quantified in cryo-embedded samples and is not necessary for the other automated measurements for scoring.

### *5.2.11 Partial Least Squares Modelling*

PLSR modelling was conducted in MATLAB using the partial least squares algorithm by Cleiton Nunes available on the Mathworks File Exchange. Bio-Plex cytokine sample data was pre-normalized to control media. All secretome data was z-scored for heatmap representation, and then directly inputted to the algorithm. For each PLSR analysis, an orthogonal rotation in the LV1-LV2 plane was used to choose a new LV1 that better separated cell phenotype/Y-variable consistent with previous studies [202]. LV1 and LV2 scores were then output in MATLAB for statistical comparisons with multi-way ANOVAs in JMP Genomics Pro.

### *5.2.12 Statistical Analysis*

All data are reported as mean ± standard deviation and were analyzed using multi-way analysis of variance (ANOVA) with Bonferroni Correction for post-hoc analysis with $\alpha=0.05$ in JMP Genomics Pro with SAS® analytics (SAS, Cary, NC). Otherwise, t-test and one-way ANOVAs with Bonferroni Correction with $p<0.05$ or $\alpha=0.05$ were performed in GraphPad Prism® (GraphPad Software, Inc. 7.03, La Jolla, CA) whenever appropriate.

## 5.3 Results

### *5.3.1 Amnion Incorporation in MSC Spheroids*

To establish optimal amnion-loading conditions within MSC spheroids, we first incorporated amnion at multiple doses. Previous studies investigating MSC delivery to the MMT model have used $10^6$ cells per injection in a volume of 50µL saline. Additionally, the Guldberg lab has previously delivered 50µL of saline or 80mg/mL of amnion in saline

according to the product insert, for a total of 4mg/animal. Therefore, a ratio of 4mg amnion to $10^6$ cells was investigated as the highest dose, corresponding to 2.4mg and $.6x10^6$ cells/insert. Three and nine-fold lower doses of amnion to MSCs were also investigated with .8 and .26 mg of amnion per insert with $.6x10^6$ MSCs. Both the 2.4 and .8 mg/inserts yielded large, heterogenous clumps of MSCs and amnion that led to clumping and difficult injections through a 27-gauge needle. The .8 mg/insert dose of amnion allowed for consistent incorporation and spheroid formation (Figure 29).

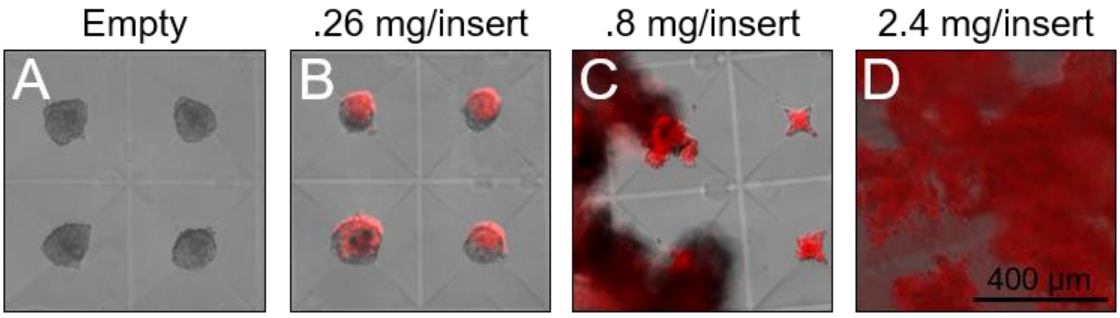


**Figure 29. Amnion Incorporation within hMSC Spheroids.** Tagged amnion was added to dissociated MSCs from adherent cultures and thoroughly mixed before forced aggregation to entrap particles within microwells. Amnion was incorporated at .26, .8, and 2.4 mg/insert with 600,000 human MSCs. After overnight incubation, the .26mg/insert (B) yielded spheroids similar in size and structure to those with hMSCs alone (A) while higher doses yielded heterogenous clumping and inconsistent incorporation (C&D).

### *5.3.2 Culture with Amnion Modulates the MSC Spheroid Secretome*

In order to determine if amnion and hMSCs have synergistic effects, amnion was cultured in direct and indirect contact with spheroids and the secretory profile was quantified. All wells had the same amount of MSCs or amnion in the same volume of media and MSCs and amnion were separated by a transwell (AtSPH), co-cultured by adding both to the wells (SPH+AM), or amnion was incorporated into MSC spheroids during formation (SPHwAM). Conditioned media was collected after 4 days and immunomodulatory

cytokines were quantified with Milliplex® Human Cytokine/Chemokine Magnetic Bead Panel Kit. Heatmaps of the z-scored data indicate relatively low cytokines levels of amnion compared to all MSC groups (Figure 30 A). PLSDA analysis of z-scored secreted cytokines separated amnion alone from all MSC spheroid containing groups on latent variable 1 (LV1) (Figure 30 B&C) while LV2 exhibited significant differences from amnion-MSC transwell culture from all other MSC groups (Figure 30 B&D). Transwell culture of MSCs with amnion had the largest effect with increased IL-6, MCP1, G-CSF, MCP-3, IL-8, and GRO; and decreased IFN-a2, EGF, IL-12p40, IL-4, sCD40L in comparison to spheroids with amnion pre-incorporated (SPHwA) (Figure 31).

### *5.3.3 Co-culture and Transwell Culture of Activated Synoviocytes, MSCs, and Amnion*

Co-cultures with activated synoviocytes were conducted for 4 days and immunomodulatory cytokines were quantified in the conditioned media to investigate synergies in therapeutic efficacy in vitro. Spheroids appeared more dense and showed less spreading when amnion was incorporated in comparison to spheroids alone after 24 hours of co-culture (Figure 32D,H, & L).

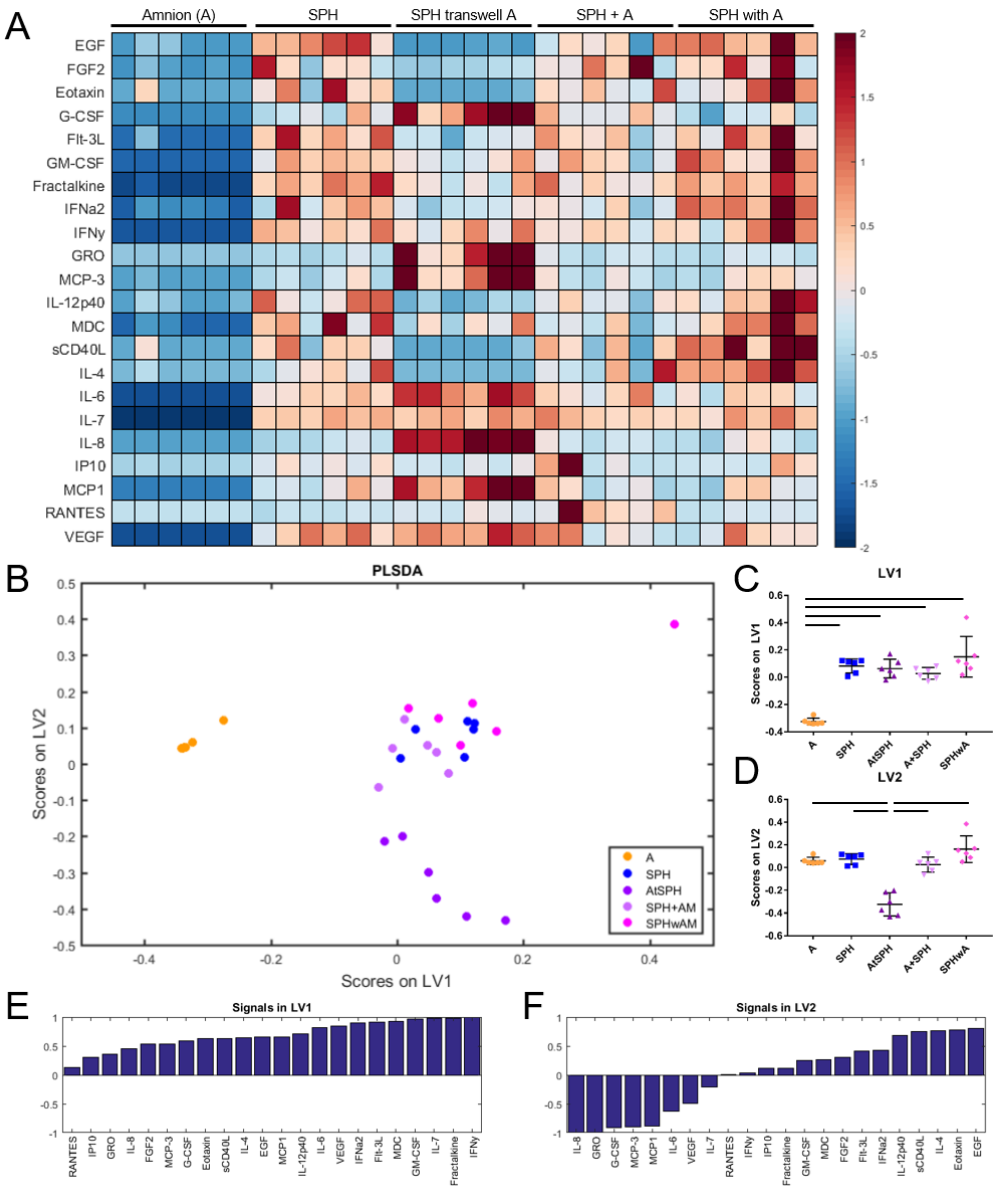


**Figure 30. Transwell culture with amnion but not incorporation or co-culture alters MSC spheroid secretome.** Amnion (A) and spheroids (SPH) were added to 96-well plates and separated by a transwell (AtSPH), co-cultured (SPH+AM), or amnion was incorporated into MSC spheroids (SPHwAM). All wells had the same amount of MSCs (22,500/well) or amnion (9.75 µg/well) in 200µL MSCGM. Conditioned media was collected after 4 days and immunomodulatory cytokines were quantified with a Milliplex® Magnetic Bead Panel Kit. Heatmaps of the z-scored data show relative cytokines levels (A). PLSDA analysis of z-scored secreted cytokines (B) separated amnion alone from all MSC spheroid containing groups on LV1 (C) while LV2 exhibited significant differences in amnion-MSC transwell culture from all other MSC groups (D). LV signal plots detail cytokine weight in each latent variable (LV) (E&F). Bars represent significant differences using multi-way ANOVA with Bonferroni correction and $\alpha$=0.05.

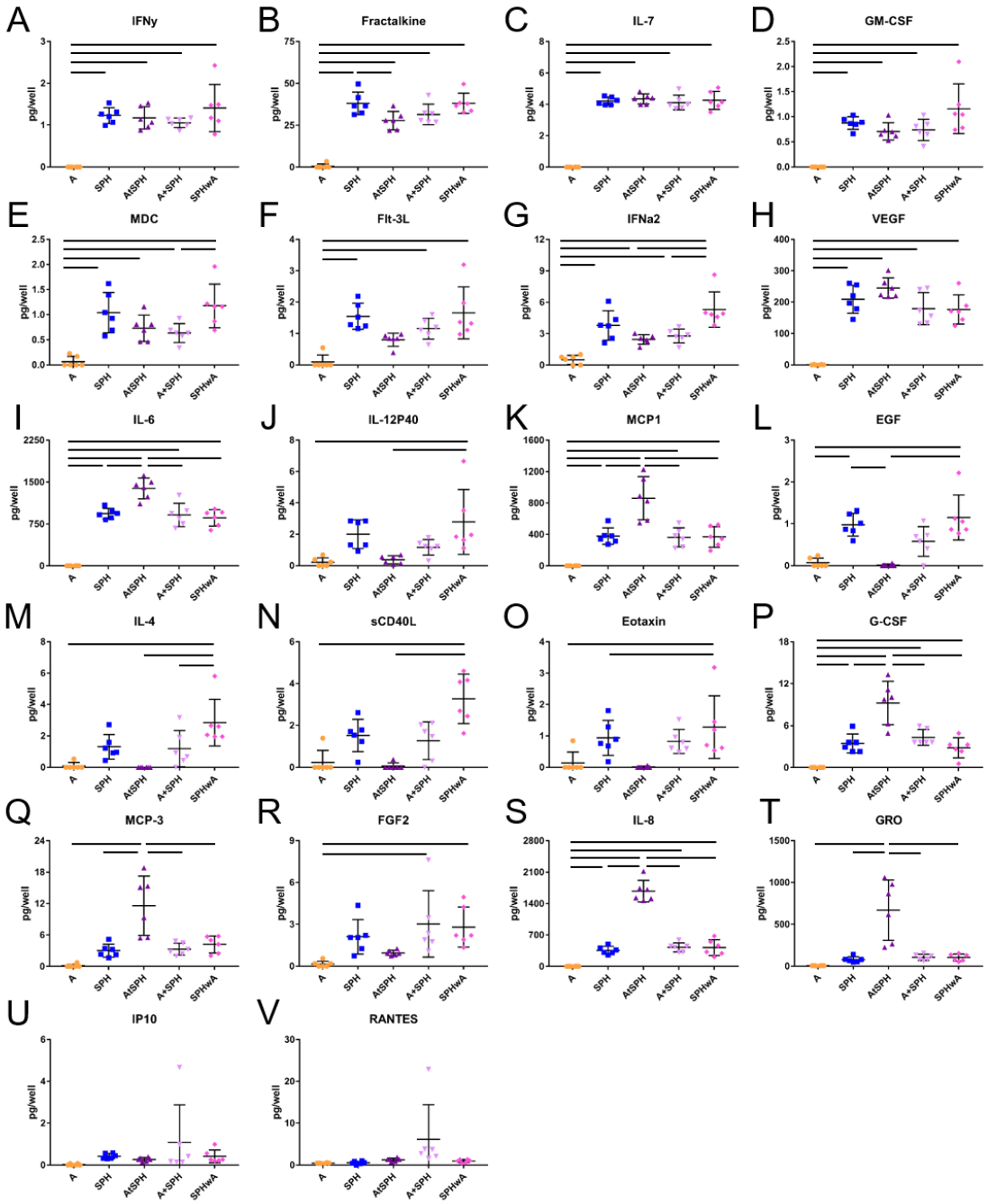


**Figure 31. Transwell culture with amnion alters MSC secretome more than co-culture or spheroid incorporation.** Amnion (A) and spheroids (SPH) were added to 96-well TCPS plates in MSCGM and separated by a transwell (AtSPH), co-cultured (SPH+AM), or amnion was incorporated into MSC spheroids during formation (SPHwAM). All wells had the same amount of MSCs (22,500/well) or amnion (9.75 µg/well) in 200µL MSCGM. Conditioned media was collected after 4 days and immunomodulatory cytokines were quantified with a Milliplex® Magnetic Bead Panel Kit. Bars represent significant differences based on multi-way ANOVA with Bonferroni correction and $\alpha$=0.05.

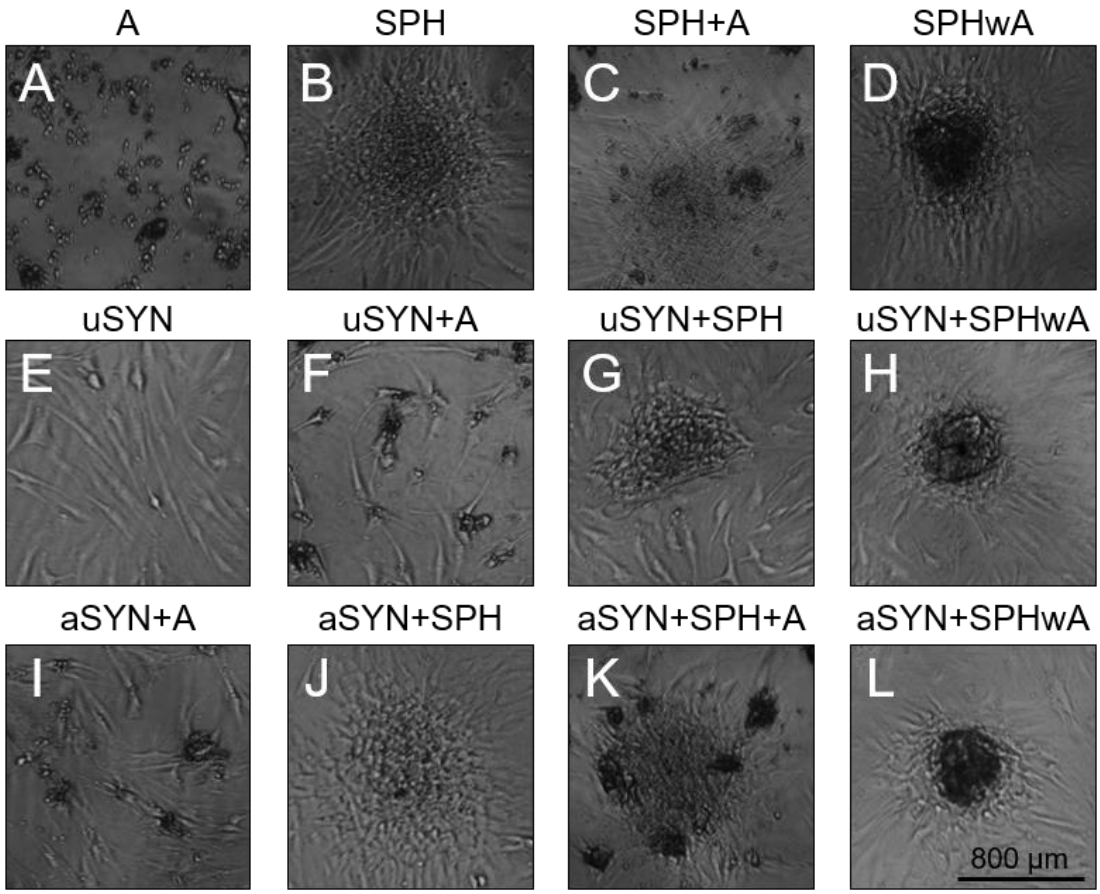


**Figure 32. Amnion and hMSC Spheroid Co-cultures with Activated Synoviocytes.** Amnion (A) and hMSC spheroids (SPH) were added together (SPH+A) or spheroids with amnion incorporated (SPHwA) were co-cultured with unactivated (uSYN) or activated synoviocytes (aSYN). Images taken at 4x magnification on day 1 show changes in spheroid density and slower spreading in spheroids with amnion incorporated (D,H, & L).

### *5.3.4 Synoviocyte Co-cultures of Spheroids and Amnion*

Synoviocyte co-cultures and transwell cultures were used to model OA-associated inflammation in vitro. Amnion (A) and spheroids (SPH) were added together (SPH+A), or spheroids with amnion incorporated (SPHwAM) were added directly to activated synoviocytes (aSYN). Activation was separated on LV1 with PLSDA analysis

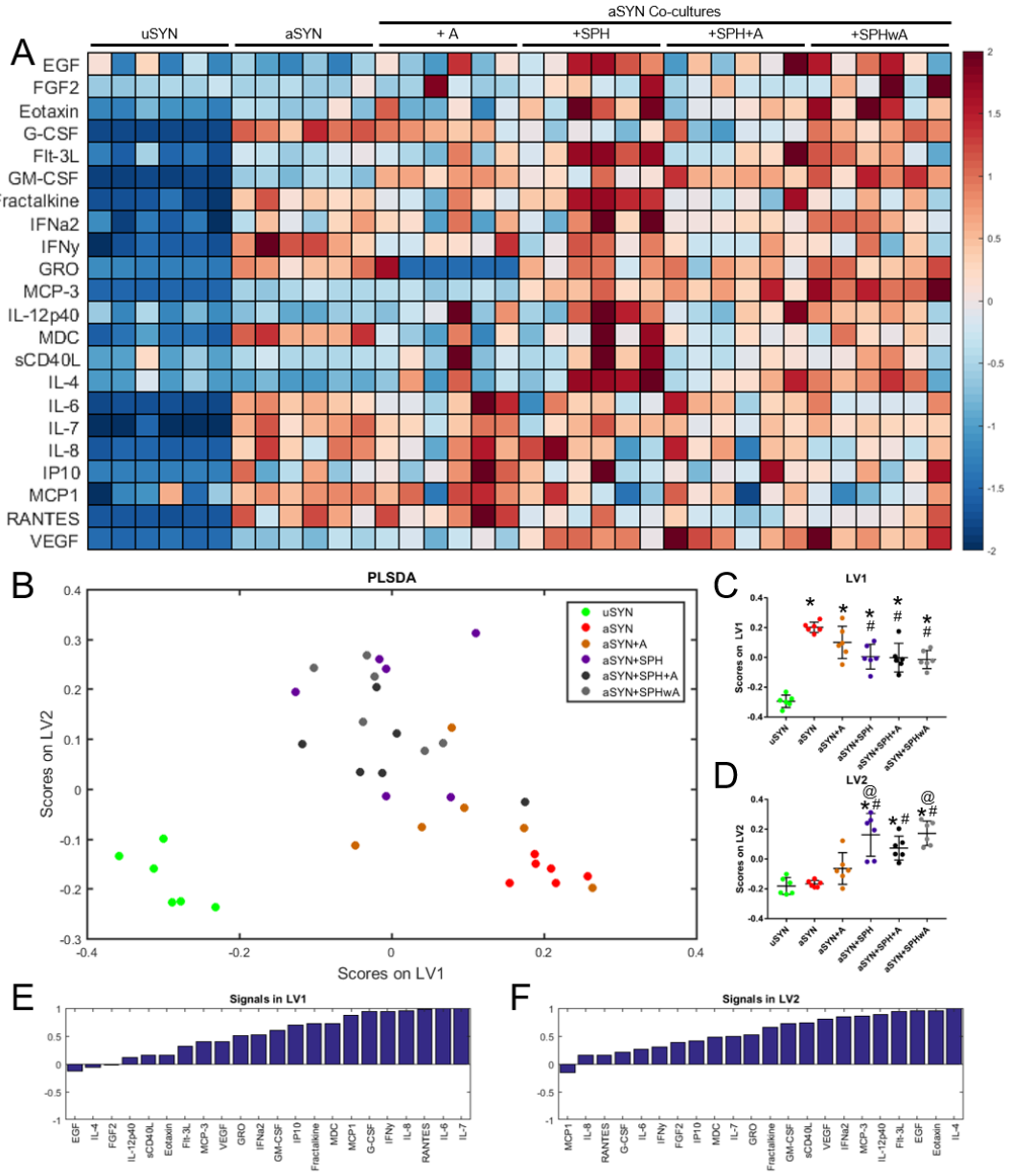


**Figure 33. Co-cultures of MSC spheroids with aSYN is better at reducing the inflammatory environment than amnion but has limited efficacy.** Amnion (A) and spheroids (SPH) were added together (SPH+AM) or spheroids with amnion incorporated (SPHwAM) were added directly to activated synoviocytes (aSYN). Immunomodulatory cytokines in conditioned media collected after 4 days were quantified with a Milliplex® Magnetic Bead Panel Kit. Heatmaps of the z-scored data show relative cytokine levels (A). PLSDA analysis of z-scored cytokines (B) separated activated from unactivated culture on LV1 where spheroid culture reduced activation-associated inflammation (C) while LV2 separated SPH cultures (D). LV signal plots detail cytokine weight in each latent variable LV) (E&F). Significant differences based on multi-way ANOVA with Bonferroni correction and $\alpha$=0.05. * vs uSYN, # vs aSYN, @ vs aSYN+A, %vs aSYN+SPH.

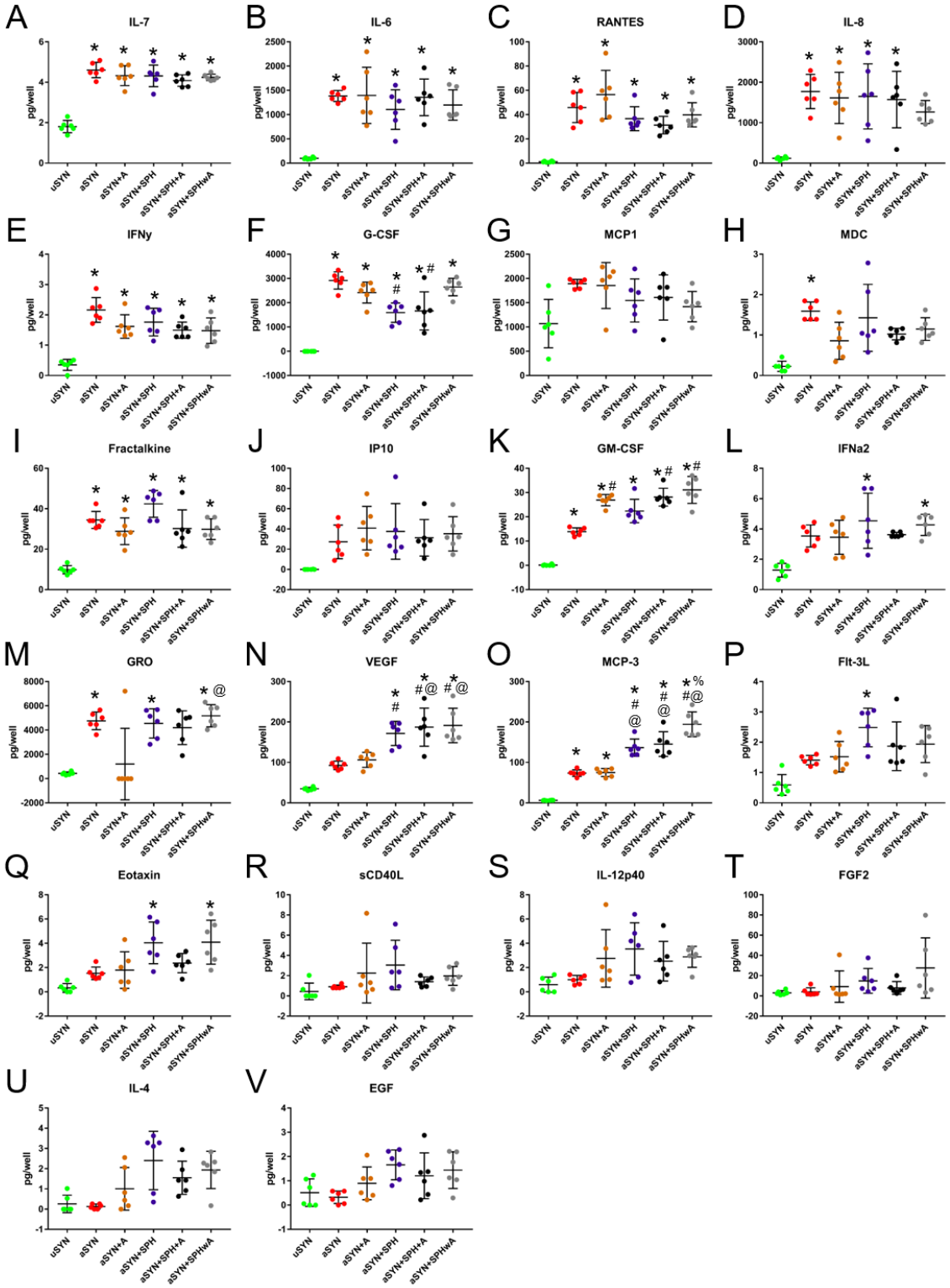
A
IL-7
B
IL-6
C
RANTES
D
IL-8
E
IFNy
F
G-CSF
G
MCP1
H
MDC
I
Fractalkine
J
IP10
K
GM-CSF
L
IFNa2
M
GRO
N
VEGF
O
MCP-3
P
Flt-3L
Q
Eotaxin
R
sCD40L
S
IL-12p40
T
FGF2
U
IL-4
V
EGF
pg/well
uSYN
aSYN
aSYN+A
aSYN+SPH
aSYN+SPH+A
aSYN+SPHwA

**Figure 34. Co-cultures of spheroids and amnion have little effect on inflammatory cytokine production from activated synoviocytes and spheroids are more effective at reducing the inflammatory environment than amnion alone.** Amnion (A) and spheroids (SPH) were added together (SPH+AM) or spheroids with amnion incorporated (SPHwAM) were added directly to activated synoviocytes (aSYN). Immunomodulatory cytokines in conditioned media collected after 4 days were quantified with a Milliplex® Magnetic Bead Panel Kit. Activation upregulated a number of cytokines (graphs sorted based on LV1), but only G-CSF was significantly reduced by spheroid co-culture in comparison to aSYN alone. Spheroid co-cultures increased GM-CSF, VEG-F, and MCP-3 in comparison to synoviocytes alone. Significant differences based on multi-way ANOVA with Bonferroni correction and $\alpha$=0.05. * vs uSYN, # vs aSYN, @ vs aSYN+A, %vs aSYN+SPH.

where spheroid culture reduced activation-associated inflammation, and LV2 separated SPH cultures (Figure 33). Activation increased synoviocyte IL-7, IL-6, RANTES, IL-8, IFN-ɣ, G-CSF, MDC, Fractalkine, GM-CSF, and GRO (**Figure 34**). Spheroid treatment alone and the combination of spheroid and amnion added reduced G-CSF and increased IFN-α2, Flt-3L and eotaxin, but not spheroids incorporated with amnion (**Figure 34**). All treatments were reduced but not significantly different from either activated or unactivated cultures for MDC while only amnion or the combination of spheroids and amnion were not significantly different from uSYN or aSYN for GRO (**Figure 34**). All co-culture treatments increased GM-CSF and spheroid culture increased VEGF and MCP-3 (**Figure 34**). Altogether, co-culture with spheroids had little effect on reducing the inflammatory environment of activated synoviocyte.

Transwells with the same concentrations of MSCs and amnion were also compared to determine the dependence of contact on MSC and amnion immunomodulation (Figure 35). Transwell culture of spheroids significantly decreased MDC, Fractalkine, IFN-ɣ in comparison to aSYN and reduced IFNα-2 to levels not significantly different from aSYN or uSYN (**Figure 36**). Transwell culture with amnion also significantly reduced IFNα-2

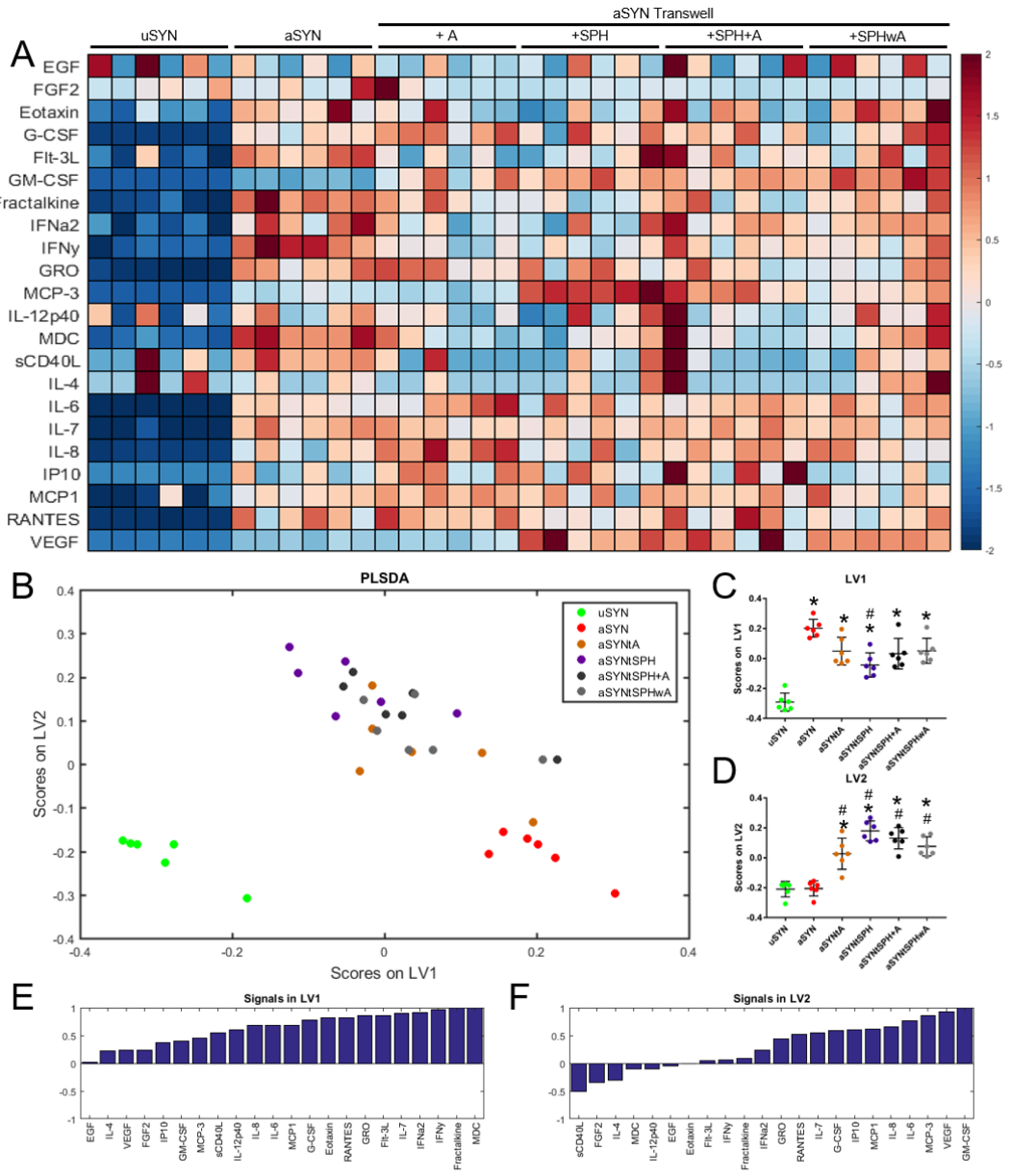


**Figure 35. Transwell culture of spheroids reduces activated synoviocytes inflammatory secretome.** Amnion (A) and spheroids (SPH) were added in transwells together (SPH+AM) or spheroids with amnion incorporated (SPHwAM) with activated synoviocytes (aSYN). Immunomodulatory cytokines in conditioned media collected after 4 days were quantified with a Milliplex® Magnetic Bead Panel Kit. Heatmaps of the z-scored data show relative cytokines levels (A). PLSDA analysis of z-scored cytokines (B) separated activated from unactivated culture on LV1 where spheroid culture reduced activation-associated inflammation (C) and LV2 separated all treatments from uSYN and aSYN (D). LV signal plots detail cytokine weight in each latent variable (LV) (E&F). Significant differences based on multi-way ANOVA with Bonferroni correction and $\alpha$=0.05. * vs uSYN, # vs aSYN, @ vs aSYN+A, %vs aSYN+SPH.

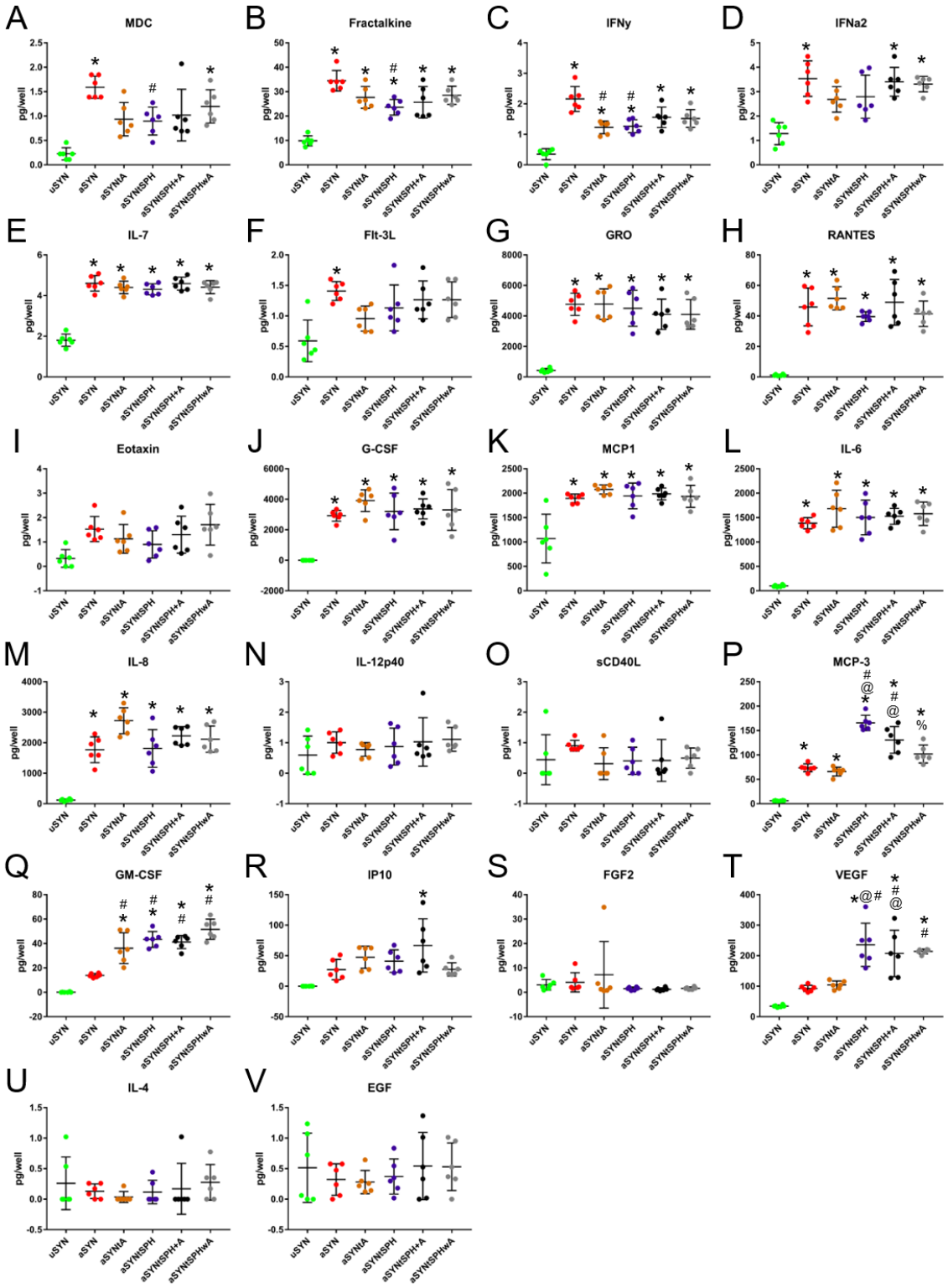
A
MDC
B
Fractalkine
C
IFNγ
D
IFNα2
E
IL-7
F
Flt-3L
G
GRO
H
RANTES
I
Eotaxin
J
G-CSF
K
MCP1
L
IL-6
M
IL-8
N
IL-12p40
O
sCD40L
P
MCP-3
Q
GM-CSF
R
IP10
S
FGF2
T
VEGF
U
IL-4
V
EGF
pg/well
uSYN
aSYN
aSYNtA
aSYNtSPH
aSYNtSPH+A
aSYNtSPHwA

**Figure 36. Transwell culture with spheroids or amnion reduces activated synoviocytes inflammatory secretome, but they do not have a synergistic effect.** Amnion (A) and spheroids (SPH) were added in transwells together (SPH+AM) or spheroids with amnion incorporated (SPHwAM) with activated synoviocytes (aSYN). Immunomodulatory cytokines in conditioned media collected after 4 days were quantified with a Milliplex® Magnetic Bead Panel Kit. Both amnion and spheroids alone had some effectiveness in reducing aSYN secretion of inflammatory cytokines, but not in combination with each other. Significant differences based on multi-way ANOVA with Bonferroni correction and α=0.05. * vs uSYN, # vs aSYN, @ vs aSYN+A, %vs aSYN+SPH.

and MDC was not significantly different from aSYN or uSYN (**Figure 36**). Flt-3L and

GM-CSF was not significantly different with any treatment compared to aSYN or uSYN,

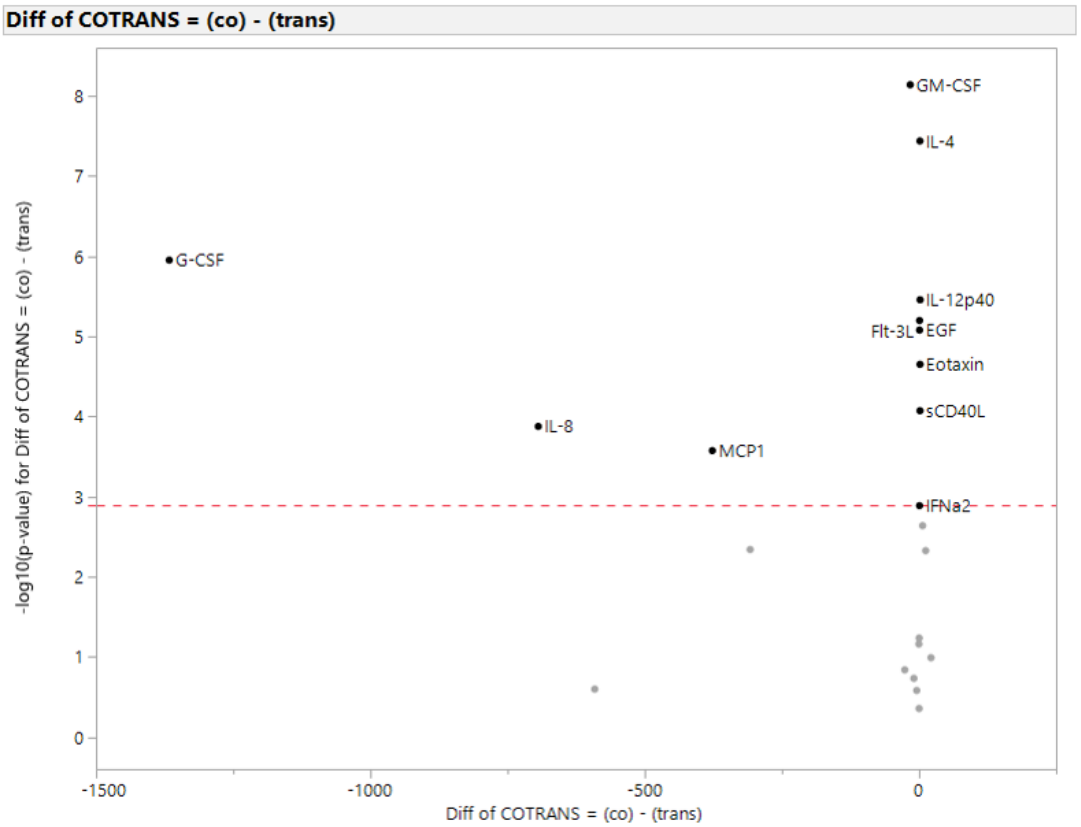


**Figure 37. Transwell cultures with spheroids and amnion yields significantly different immunomodulation of activated synoviocytes secretome than co-culture.** One-way analysis of variance (ANOVA) comparing co-culture and transwell cultures of activated synviocytes with amnion and MSC spheroids shows significant differences between multiple immunomodulatory cytokines.

but was increased in aSYN compared to uSYN (**Figure 37**). Similar to co-culture studies, all spheroid cultures had increased MCP-3 and VEG-F (**Figure 37**).

Surprisingly, transwell culture of amnion or spheroids alone more effectively reduced OA-associated inflammation in activated synoviocyte cultures than combinatorial approaches with MSCs and amnion. A one-way ANOVA comparing co-culture to transwells showed significant differences in a number of cytokines including G-CSF, GM-CSF, IL-4, IL-12p40, Flt-3L, EGF, Eotaxin, sCD40-L, IFNα2, MCP-1, and IL-8 (**Figure 37**). Altogether, there was no synergistic effect observed in vitro combining MSC spheroids with amnion, but both modulated inflammation in this in vitro model. The efficacy of both treatments was reduced in direct contact with activated synoviocytes via co-culture in comparison to transwell cultures.

### *5.3.5 Investigation of Amnion and MSC Spheroids in Rat Model of OA*

A rat post-traumatic model of osteoarthritis involving medial meniscal transection (MMT) was used to test the therapeutic efficacy of MSC spheroids and single cells with and without amnion or with amnion-loaded MSC spheroids. RoosterBio MSCs were used for all amnion containing studies, but single cells and spheroids of both RoosterBio and Texas A&M cells were used as controls for comparison since pilot studies of MSCs were performed with Texas A&M cells. Single injections of MSCs at day 1 resulted in few changes in tibial cartilage. The only differences in quantitative EPIC-μCT analysis of cartilage between sham and MMT control groups were in the surface roughness of the medial and central thirds of the tibial plateau (Figure 38). MMT control groups exhibited

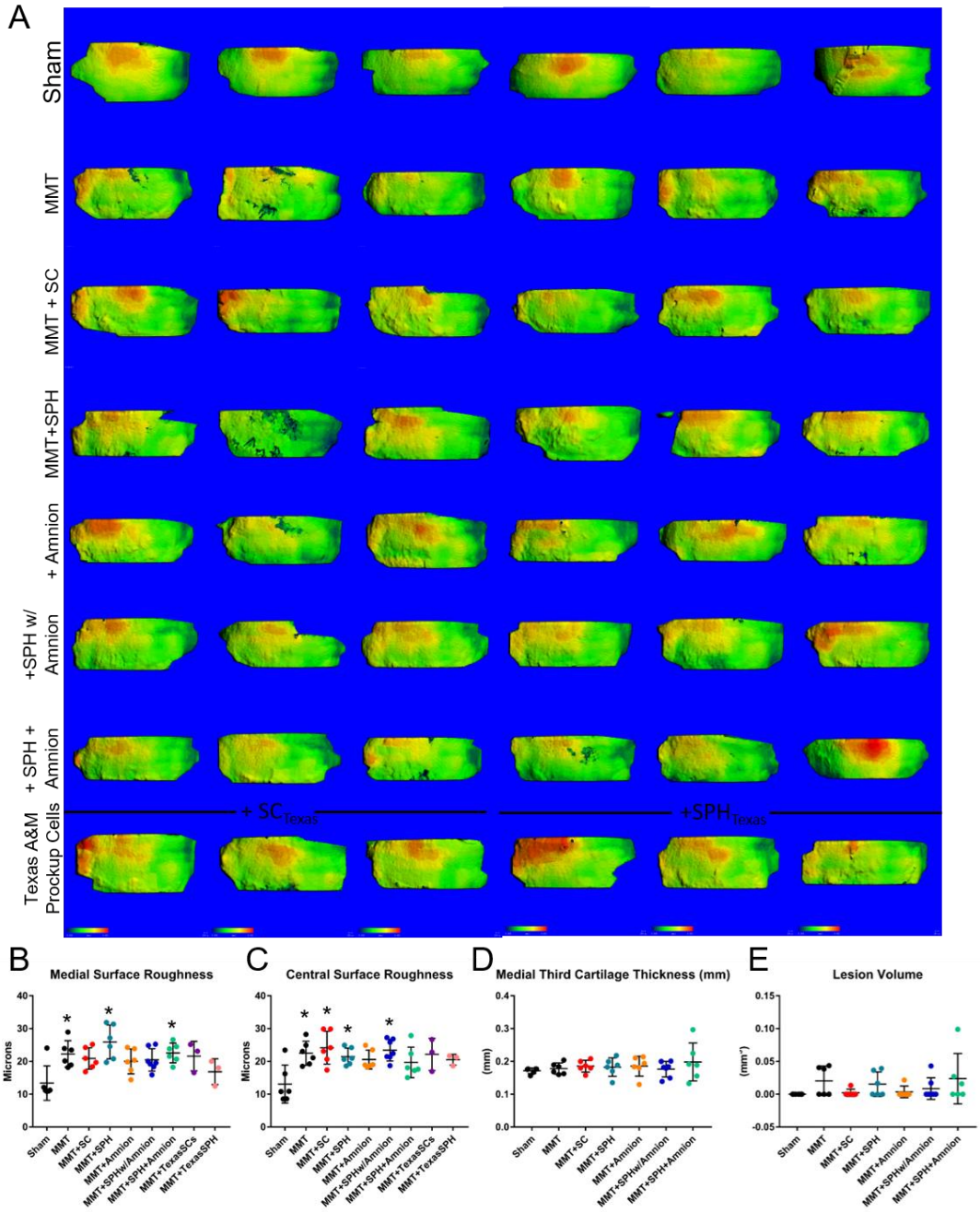


**Figure 38. EPIC-µCT data depicting the therapeutic effect of MSC single cells and spheroids and amnion in MMT joints compared to controls.** MSC single cells (SC) or spheroids (SPH) from RoosterBio or Texas A&M were intra-articularly injected 24-hours after MMT and animals were sacrificed 21 days after surgery. Thickness maps of the tibial plateau show few lesions in treatment or control groups. Only amnion treated rats or those treated with MSC SC or SPH from Texas A & M didn't have increased surface roughness in the medial (B) or central (C) thirds of the medial plateau. There was no significant difference in the medial cartilage thickness (D) or lesion volume (E) in any group. Significant difference from sham depicted with * for ANOVA with Bonferroni and $\alpha$=0.05.

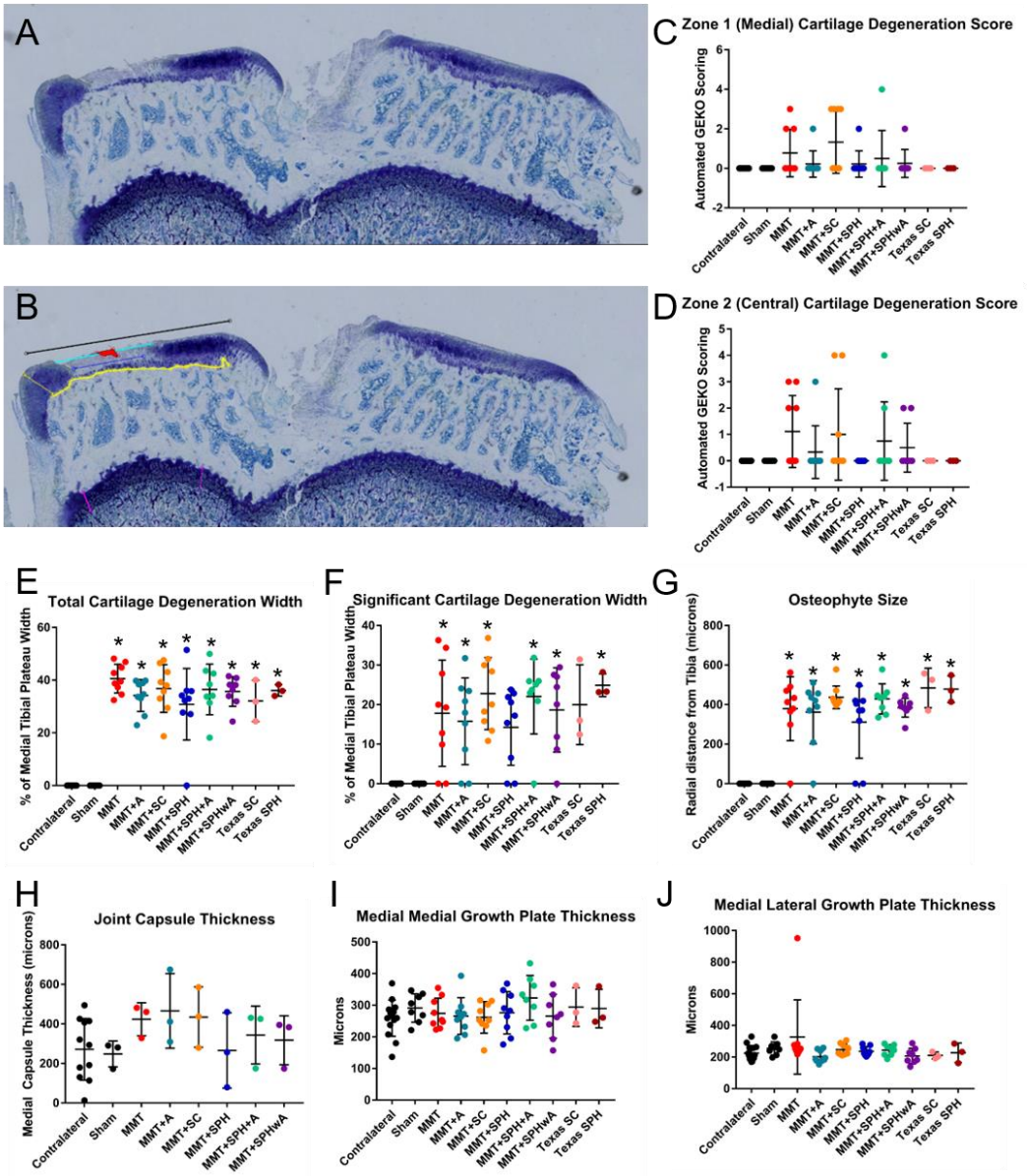


**Figure 39. Semi-automated histological scoring to quantify the effect of MSCs and amnion in MMT joints compared to controls.** A MATLAB GUI was used to score toluidine blue stained tibial plateaus (A) using measurements of the entire medial plateau (black line), total cartilage degeneration width (aqua line), significant cartilage width (blue line), the cartilage-bone interface (bold yellow line), medial subchondral growth plate thickness (magenta lines), osteophyte size (thin yellow line) and synovial lining thickness of whole joints (not pictured). There were no significant differences in the cartilage degeneration scores in the medial (C) or central thirds (D), joint capsule thickness (H), or growth plate thickness in the medial (I) or lateral (J) thirds. All MMT surgerized joints had increased total cartilage degeneration width (E) and osteophyte size (G) in comparison to sham. Only RoosterBio spheroids or single cells from Texas A&M did not have increased significant cartilage degeneration widths (F). *vs Sham. ANOVA with Bonferroni.$\alpha$=0.05.

few lesions and degeneration did not significantly progress beyond early fibrillations quantified by surface roughness in most samples (Figure 38).

Semi-automated scoring of microscope images was also conducted on the surgerized tibias following Toluidine Blue staining. There were no significant differences in the systematically determined cartilage degeneration scores in the medial or central thirds, joint capsule thickness, or growth plate thickness. Total cartilage degeneration width, which quantified the difference for any cartilage damage including surface fibrillations, decellularization, or GAG loss was increased in all surgerized joints compared to sham controls. Osteophyte size, as determined by chondral thickening on the medial edge of the tibial pleateau was also increased in all MMT joints. Only RoosterBio spheroids or single cells from Texas A&M did not have increased significant cartilage degeneration widths in the medial or tibial thirds in comparison to the sham. Altogether, there was little effect of any treatment group and although MMT legs were significantly different than sham controls, progression of MMT-induced damage was slower than previous experiments in terms of lesion volume and cartilage thickness.

## 5.4 Discussion

There is an unmet clinical need for disease modifying OA therapies that can address the complex chronic inflammation associated with osteoarthritis. While previous studies with hMSCs have been promising, variability in clinical outcomes demonstrate the necessity of robust translatable approaches to optimize MSC therapeutic efficacy. Multiple studies using MSCs in various disease models have demonstrated that the cells act primarily through paracrine mechanisms rather than directed differentiation [217]. In this

study, we evaluated a strategy to locally present naturally-derived amniotic membrane matrix within MSC constructs to augment MSC immunomodulatory activity.

The MSC secretome is highly dependent on the cellular microenvironment and clinical studies of MSC-based therapies have been most effective in treating acute inflammatory diseases rather than chronic inflammation [218-221]. Treating MSCs with IFN-ɣ enhanced therapeutic efficacy in multiple models [222, 223], and sustained presentations via IFN-γ-loaded heparin microparticles in MSC spheroids enhanced immunomodulatory paracrine production and polarization of macrophages towards an M2 phenotype [156]. Strategies involving treating chronic inflammation with any pro-inflammatory cytokines are often met with apprehension, however, due to the fear of amplifying the disease state.

Alternatively, previous studies by MiMedx Group have demonstrated that multiple factors eluted from dehydrated amnion can also modulate stem cell paracrine activity, enhancing MSC production of SCF, FH, IL-6, IL-1ra, FGF-1, and ICAM-1 [164]. Surprisingly, in this study amnion incorporation into MSC spheroids did not alter the cytokine profile in comparison to MSC spheroids alone, but transwell culture of amnion and spheroids increased IL-6, MCP-1, G-CSF, MCP-3, IL-8, and GRO; and decreased EGF in comparison to spheroids alone. The variance between co-culture and transwell could be due to a multitude of factors. The extracellular matrix has multiple functions, one of which is to differentially modulate cytokine presentation through preferential binding and sequestration of ligands [224]. Amnion retains natural structural components, such as collagens (types I, III, IV, V, VI), fibrinogen, laminin, nidogen and proteoglycans capable of binding cytokines [161]. Binding of some ligands is influenced by proximity and

contact, and the amnion may be acting as a sink for cytokines that could otherwise be upregulated. Future studies should determine if amnion depletes immunomodulatory cytokines in MSC conditioned media to elucidate this potential mechanism of action.

Hyaluronic acid is also present in amnion and acts as a ligand for the CD44 receptors expressed by MSCs [225]. CD44 is a cell-surface glycoprotein involved in cell-cell and cell-adhesion interactions and has an inverse correlation with E-cadherins [226]. 3D aggregation of MSCs was found to upregulate E-cadherin expression, which in turn was responsible for enhanced vascular endothelial growth factor (VEGF) secretion via the ERK/AKT signaling pathway [139]. Thus, balanced function of CD44 and E-cadherin may be essential for spheroid functionality.

Amnion also contains multiple anti-inflammatory cytokines, including IL-1Ra, a receptor antagonist for IL-1; and two anti-inflammatory elastase inhibitors – secretory leukocyte proteinase inhibitor (SLP1) and elafin [225, 227]. Since MSC immunomodulation is directly dependent on the levels of inflammatory cytokines [126, 128], combinatorial approaches of MSCs and ECM with endogenous anti-inflammatory properties may reduce MSC-mediated paracrine activity.

Alternatively, direct contact with MSCs may enhance amnion degradation, potentially reducing its efficacy over the four days of culture. Future temporal studies of co-cultures and transwells of amnion and MSCs could aid in elucidating the mechanistic differences between contact-induced changes.

Similar dependence on contact, or lack thereof, was observed in transwell and co-culture of amnion and MSCs with activated synoviocytes. More differences were observed

in transwell cultures and both amnion and spheroids individually reduced inflammation due to synoviocyte activation, but combinations of amnion and spheroids were less effective (**Figure 36**). The only significant difference amnion incorporation into spheroids had was significantly decreasing MSC secreted monocyte chemotactic protein, MCP-3. Although MCP-3 has been detected in the synovium of RA patients, its role in both OA and RA remain unclear [228]. Combinations of this study and the previous transwell study with MSC spheroids and activated synoviocytes described in aim 2 suggests that amnion and spheroids modulate synoviocyte inflammation through different mechanisms since MSCs had a dose dependent improvement in reducing inflammation at higher concentrations and adding amnion reduced the efficacy of spheroid modulation (**Figure 36**).

Delivery of MSCs and amnion to an osteoarthritic rat model did not significantly reduce OA degeneration at 21 days post-surgery (Figure 38 & Figure 39). Previous work in the Guldberg lab has demonstrated that a single intra-articular injection of micronized amnion at 4mg/animal attenuates osteoarthritis development in the medial meniscal transection (MMT) rat model of OA when evaluated at 21 days [166]. The amnion delivered in this study was at approximately one ninth of that dose since that was the maximum concentration that could effectively be incorporated into $10^6$ MSCs delivered as spheroids. A recent study in ACL-transected rats showed that single injections of MSCs was insufficient to modulate OA progression, but that weekly injection of MSCs significantly reduced OA progression [209]. The same study also found that alterations in OA progression were not significantly different between treatments at what they deemed an early time point of 4-weeks, but treatments showed significant improvements and

reduction in cartilage degeneration at 8 and 12 weeks [209]. The results of this study showed no clear advantage or disadvantage with amnion and MSC co-delivery, but differences in therapeutic potential may be more evident with weekly injections and longer study duration.

## 5.5 Conclusion

The results of this study demonstrate that both cell and ECM-mediated immunomodulation are affected by cell-cell and cell-ECM contact in activated synoviocyte cultures. While both amnion and MSC spheroids individually enhanced suppression of inflammatory cytokines secreted by activated synoviocytes in vitro, combinatorial approaches were less effective. Overall, understanding the mechanisms involved in both MSC spheroid and amnion immunomodulation may aid in the development of novel strategies capable of reducing OA-associated inflammation. Although very few changes in treatment were evident in our animal study, further investigation of weekly injections taken out to longer periods may elucidate potential interactions of amnion and MSC therapies. Altogether, our findings suggest that both amnion and MSC spheroids have therapeutic benefits in reducing OA-associated inflammation, and that harnessing the capabilities of both may be best augmented with separate or sequential treatments rather than combinatorial approaches.

# CHAPTER 6. CONCLUSIONS & FUTURE CONSIDERATIONS

Taken together, the data presented in this dissertation establish novel approaches to both improve cartilage regeneration and address the chronic inflammation associated with osteoarthritis. In Chapter 3, culture of primary chondrocytes on decellularized cartilage microcarriers was found to both support expansion and enhance retention of a chondrocytic phenotype. Furthermore, the culture platform with native cartilage ECM does not require trypsinization, allowing for ECM proteins to be retained during culture before direct implantation into chondral defects. In Chapter 4, the immunomodulatory capabilities of MSCs were investigated for their ability to modulate OA-associated inflammation. Robust characterization of the influence of culture format, donor variability, and media composition demonstrated that aggregated MSCS have enhanced sensitivity to changes in the local microenvironment, which can be tailored to enhance immunomodulatory paracrine activity. Moreover, MSC single cells and spheroids reduced inflammation in activated synoviocyte cultures in a dose-dependent manner and transwell rather than direct co-culture improved this response. Surprisingly, although paracrine activity was upregulated in spheroid culture, more MSCs spheroids were required to result in the same therapeutic outcomes as MSCs delivered as single cells, but both groups exhibited reduction in OA progression when injected in a 3-week rodent model of OA. Finally, in Chapter 5, combinatorial approaches with amnion and MSCs did not enhance immunomodulation of OA inflammation in vitro or in vivo, and only transwell culture of amnion with MSCs altered the secretory activity.

## 6.1 Contributions to the Field

This two-fold approach aimed to improve current OA therapies by (1) creating novel ECM-microcariers for chondrocyte expansion and delivery; (2) investigating MSCs and amnion as sources for immunomodulation of OA. Thus, this work presents significant contributions to areas of research in cartilage tissue engineering, biomaterial design, immunoengineering, and the translation of cell-based therapeutics, as described below.

### *6.1.1 Fabrication of ECM Microcarriers*

Decellularized cartilage scaffolds fail to repair cartilage defects due to inadequate cellular infiltration and tissue integration [107]. By milling decellularized cartilage, this work resulted in the creation of novel ECM microcarriers that (1) allow for additional cell-ECM contact, (2) support cell proliferation and chondrogenic phenotype, and (3) retain endogenous ECM components. While many synthetic microcarriers have been characterize, most are not suitable for direct implantation and do not provide the tissue specific cues found endogenously in the cartilage ECM. Turner and Flynn previously described the fabrication of decellularized adipose ECM microcarriers [229]. Pepsin-digested adipose ECM was combined with sodium alginate and microbeads were crosslinked through calcium chloride (to cross-link alginate) and rose bengal (to crosslink ECM) before aliginate was removed with sodium citrate [230]. In a later study by Flynn, decellularized adipose microbeads were formed via electrospraying digested adipose tissue, which eliminated the need for chemical cross-linking [231]. Although ECM digests retain some bioactivity, solubilizing ECM via pepsin digests causes a loss of native collagen structure, molecular integrity, and native mechanical properties [101, 232]. By directly using milled ECM as microcarriers, our approach reduces loss of native tissue integrity and the biochemical microenvironment.

In addition to expansion of primary cells, decellularized tissues can stimulate differentiation of stem cells for a multitude of applications, including chondrogenesis [233]. While many groups have milled decellularized tissues to form specific geometries, incorporate into other biomaterials, add directly to cell cultures, or implant into tissue defects, ours is the first study demonstrating the direct use of decellularized ECM as microcarriers [80, 100, 103, 105, 157, 233]. Overall, we expect that the novel, facile approach to fabricate ECM microcarriers developed in this study can be easily integrated to a variety of tissues and cell types, demonstrating the vast versatility of this system.

### *6.1.2 Characterization of In Vitro Model of Synovial Inflammation*

Fibroblast-like synoviocytes in the synovial lining are key effectors in both OA and rheumatoid arthritis (RA) by producing proteases and cytokines that degrade cartilage and recruit other inflammatory cells, both amplifying and perpetuating inflammation [234]. Multiple groups have used synoviocytes to test OA therapeutics, but there is no consistent activation protocol to stimulate synoviocyte inflammation, and multiple cytokines and chemokines have been reported at a large array of concentrations [197-200, 235, 236]. By comparing activation with various cytokines at multiple concentrations in different medias, we thoroughly characterized in vitro activation of synoviocytes and their dose dependent response through analyzing the synoviocyte secretome. Twenty-four-hour activation of primary synoviocytes with 5ng/mL IL-1β and 5ng/mL TNF-α consistently resulted in detectable inflammation after 4 days of culture in fresh media. Reduction of inflammation with multiple therapeutics (MSCs and amnion) at various doses was also detectable with this platform in both direct (co-culture) and in-direct (transwell) contact. This robust analysis may aid in standardization for testing disease modifying OA therapies *in vitro*.

## 6.2 Clinical Translation

The ultimate goal of this thesis is to characterize the phenotype of cells in response to culture parameters and ECM materials in order to engineer transplantable cell constructs to improve OA therapies. To date there are no disease modifying OA therapies that can prevent disease progression, but by addressing the limited regenerative potential of cartilage and the complex inflammatory environment of OA, findings in this thesis may help improve therapeutic efficacy.

### *6.2.1 Development of A Novel ACI Therapy*

Current autologous chondrocyte implantation strategies require a massive number of cells (1.6 million cells per $cm^2$ defect) [60]. In order to obtain these substantial numbers, chondrocytes from non-load bearing areas must be expanded for 14-21 days, over which period many cells lose their phenotype, de-differentiate, and form fibrocartilage upon implantation [61]. By filling the defect site with chondrocyte-laden microcarriers, the approach developed in Chapter 2 of this thesis could provide physiologically relevant ECM and require fewer cells, shortening the expansion time and loss of nascent ECM production during culture by eliminating the need for trypsinization. Culture on our DC-μCs also decreased de-differentiation over 7 days of culture and reduced hypertrophic differentiation, two major impediments to successful outcomes of traditional ACI therapies [63]. Additionally, multiple other decellularized tissues have already been approved for clinical use, which will help pave the way for navigating the regulatory requirements by the FDA for decellularized microcarriers [237]. Thus, the decellularized cartilage microcarriers developed in this thesis have promising clinical applicability as a readily

translatable delivery vehicle with low adoption barriers for both cell culture technicians and orthopedic surgeons.

### *6.2.2 Approaches to Address OA Inflammation*

The complex nature of inflammation in OA lends itself to combinatorial, multi-faceted approaches. In vitro assays in this project suggest both MSCs and amnion modulate OA inflammation through multiple signaling pathways. Although combinatorial approaches with amnion and MSCs at the tested doses used herein did not result in synergistic enhancement of immunomodulation, future studies in this area could investigate more frequent injections over a longer period to elucidate potential interactions of amnion and MSC therapies. Altogether, our findings suggest that both amnion and MSC spheroids have therapeutic benefits in reducing OA-associated inflammation, and that harnessing the capabilities of both may be best augmented with separate or sequential treatments rather than combinatorial approaches. The dose dependent improvement with both amnion and spheroids in cultures with activated synoviocytes also suggests that increased injection frequency and concentration may enhance therapeutic efficacy of both treatments.

### *6.2.3 Screening Cellular Therapies*

Discrepancies in processing, culture conditions, passage number, and donor characteristics have all contributed to variability in transplanted cell populations for multiple clinical studies [196]. While three-dimensional aggregate culture has long been utilized to mimic cell-cell and cell-matrix interactions of in vivo physiology, more recently 3D cultures have emerged as a new tool for early drug discovery and therapeutics[238].

Our studies comparing donor variability, seeding densities, culture platforms, and media composition all demonstrate that spheroid format is more sensitive to these changes than 2D monolayer by exhibiting an altered secretory profile. These findings suggest that spheroid culture may not only be advantageous as a screening tool for drugs, but also an effective means to compare cell sources for multiple clinical applications. By evaluating changes in MSC spheroid secretome due to donor variability or responses to disease relevant microenvironments, we may better predict therapeutic potential of cell sources. This could reduce the cost and time required to test sources that were otherwise indistinguishable in monolayer culture. Thus, the approach described in Chapter 3 could better characterize cell therapy manufacturing processes, improving quality-control, efficiency, and reproducibility for clinical use.

## 6.3 Future Directions

Altogether, the findings of this work motivate further studies to evaluate the transplantation of chondrocyte ECM-microcarrier constructs *in vivo* and to better characterize the mechanisms involved in immunomodulation in both ECM and cell-based therapies.

### *6.3.1 Screening models to evaluate chondrocyte and ECM transplantation*

Animal studies are critical for the development of effective treatments for cartilage injuries. Evaluation of chondrocyte implantation therapies requires direct implantation of expanded cells into chondral defects. While multiple animal models of osteoarthritis exist, many do not recapitulate the local environment, repair processes, or relative defect size needed to model human autologous chondrocyte transplantation.

Direct injury to articular cartilage, including creation of focal defects, joint destabilization, or injection of chondrotoxic agents are common methods to induce cartilage loss and osteoarthritis in animal models [239-242]. Focal defects are necessary to investigate the incorporation of cell-ECM constructs mimicking ACI and MACI therapies. Although both joint destabilization and chondrotoxic agents lead to variability in defect size, location, and volume, they may aid in mimicking an OA environment prior to formation of focal defects. Alternatively, trauma accounts for approximately 12% of osteoarthritis and chondral defects progress to osteoarthritis with time [243, 244].

Rodent models are cost effective and their genetic backgrounds have been well characterized, but their joints are small with thin cartilage which is difficult to consistently surgerize. A custom-built device has improved consistency in trochlear defect size in rats, but defects spontaneously regenerated the surfacing articular cartilage [245]. Larger animal models with thicker articular cartilage permit study of both partial thickness and full thickness chondral repair, as well as osteochondral repair. Lapine models are attractive because of their relatively low cost, increased cartilage thickness, and genotypically similar subjects are available [246]. Although the thin cartilage is likely easier to damage and repair than human cartilage, intrinsic repair is limited in the larger 3-4 mm defects that are commonly used [247]. Although these larger defects penetrate the subchondral bone, lapine models are still practical for early-stage pre-clinical evaluation [246]. Larger animal models with dogs, goats, pigs, and horses exhibit load-bearing, chondral thickness, and limited regeneration potential more similar to human OA, but their cost is prohibitive for early-stage therapeutic investigations. Therefore, future investigation of integration and

repair of osteoarthritic defects with the chondrocyte-laden decellularized cartilage microcarriers should be conducted in a lapine defect model of OA.

### *6.3.2 Mechanisms to Quantify Inflammation in the Synovial Fluid of Small Animal Models*

The *in vitro* co-culture and transwell studies of MSCs and activated synoviocytes demonstrates that MSCs can modulate OA-associated inflammation through multiple pathways. This characteristic lends itself to further characterization of OA-inflammation *in vivo*. Understanding the molecular mechanisms of OA-associated inflammation could allow for better therapeutics tailored to the specific microenvironment. Synovial fluid biomarkers including cartilage degradation products, catabolic enzymes, inflammatory mediators, chemokines, and other molecules have been used to characterize OA disease state and severity [248]. Additionally, monitoring temporal changes in inflammatory cytokines during therapeutic evaluations would not only yield a better understanding of the disease state, but could also be used to modulate treatments based on differentiation for responders/non-responders.

Synovial fluid extraction in rodent models of OA is difficult due to the small volume available. Lavage, a process of washing the joint with saline prior to fluid extraction, significantly dilutes the biomarkers. A previous study performed by the Guldberg lab using lavage of rat knees detected changes in MCP-1 concentration in the synovial fluid between MMT and amnion treated knees, but the other 9 cytokines that were quantified in the 10-panel ELISA kit were undetectable in either the treatment or control groups [166].

Recently, a promising approach to detect synovial cytokines in rodents was developed using a magnet to capture superparamagnetic nanoparticles conjugated to antibodies specific to cartilage degradation product CTXII (c-terminus telopeptide of type II collagen) [248]. Rats with monoiodoacetate (MIA) induced OA were sacrificed after 30 days. Particles were then injected to the knee joint, allowed to equilibrate for 2 hours, and then collected using insertion of a magnetic rod through a catheter. Particles were then released by washes with a diamagnetic supernatant and biomarker and targeting molecules were disrupted using heat, change in pH, and enzymatic cleavage. Magnetic particles were then separated using a magnetic and CTXII was quantified via an ELISA. Although magnetic capture was significantly more sensitive than lavage, there are many limitations to the multiple wash and release steps required which may reduce ELISA binding and sensitivity.

Alternatively, the beads used in the MILLIPLEX MAP Cytokine/Chemokine Magnetic Bead Panel Kits are already developed for magnetic isolation and capture, are sensitive to low concentrations and changes therein, have ligands for multiple cyotokines already conjugated, and would eliminate the wash steps previously necessary for ELISA quantification. Therefore, future studies should determine the ability to capture MILLIPLEX beads following intra-articular injection, the concentration of beads necessary to quantify changes in rodent models of OA, and investigate if beads could be used in longitudinal survival studies. These studies could elucidate a comprehensive screening tool to provide dynamic feedback to both measure and treat OA inflammation and disease progression.

## 6.4 Conclusions

The results of this dissertation provide a basis for future exploration of the clinical potential of matrix-assisted autologous chondrocyte implantation with chondrocyte-laden decellularized cartilage microcarriers. Future studies evaluating the integration, retention, and effect on OA progression in a rabbit chondral defect model could provide valuable information for the translation of ECM-microcarrier culture and subsequent transplantation for multiple diseases in addition to OA applications. The increased sensitivity of MSC spheroids to variations in culture conditions and donor-dependent responses could be useful in screening cell sources for translational applications and may better illustrate the variability in therapeutic outcomes that are masked in single cell monolayer culture. While in vitro and in vivo models of OA-associated inflammation provided some insight into both MSC and amnion mediated immunomodulation, monitoring temporal changes in inflammatory cytokines during therapeutic evaluations would not only yield a better understanding of the disease state, but could also be used to tailor treatments to optimize outcomes for osteoarthritis therapies.

# REFERENCES


1. Benjamin, M. and E.J. Evans, *Fibrocartilage.* J Anat, 1990. **171**: p. 1-15.

2. Goldring, M.B., K. Tsuchimochi, and K. Ijiri, *The control of chondrogenesis.* J Cell Biochem, 2006. **97**(1): p. 33-44.

3. Shum, L. and G. Nuckolls, *The life cycle of chondrocytes in the developing skeleton.* Arthritis Res, 2002. **4**(2): p. 94-106.

4. Muir, H., *The chondrocyte, architect of cartilage. Biomechanics, structure, function and molecular biology of cartilage matrix macromolecules.* Bioessays, 1995. **17**(12): p. 1039-48.

5. Riesle, J., et al., *Collagen in tissue-engineered cartilage: types, structure, and crosslinks.* J Cell Biochem, 1998. **71**(3): p. 313-27.

6. Flannery, C.R., et al., *Articular cartilage superficial zone protein (SZP) is homologous to megakaryocyte stimulating factor precursor and Is a multifunctional proteoglycan with potential growth-promoting, cytoprotective, and lubricating properties in cartilage metabolism.* Biochem Biophys Res Commun, 1999. **254**(3): p. 535-41.

7. Saxne, T. and D. Heinegard, *Cartilage oligomeric matrix protein: a novel marker of cartilage turnover detectable in synovial fluid and blood.* Br J Rheumatol, 1992. **31**(9): p. 583-91.

8. Roughley, P.J., *The structure and function of cartilage proteoglycans.* Eur Cell Mater, 2006. **12**: p. 92-101.

9. Detterline, A.J., et al., *Treatment options for articular cartilage defects of the knee.* Orthop Nurs, 2005. **24**(5): p. 361-6; quiz 367-8.

10. Dillon, C.F., et al., *Prevalence of knee osteoarthritis in the United States: arthritis data from the Third National Health and Nutrition Examination Survey 1991-94.* J Rheumatol, 2006. **33**(11): p. 2271-9.

11. *Prevalence of disabilities and associated health conditions among adults--United States, 1999.* MMWR Morb Mortal Wkly Rep, 2001. **50**(7): p. 120-5.

12. Lawrence, R.C., et al., *Estimates of the prevalence of arthritis and other rheumatic conditions in the United States. Part II.* Arthritis Rheum, 2008. **58**(1): p. 26-35.

13. Kotlarz, H., et al., *Insurer and out-of-pocket costs of osteoarthritis in the US: evidence from national survey data.* Arthritis Rheum, 2009. **60**(12): p. 3546-53.

14. Goldring, M.B. and S.R. Goldring, *Osteoarthritis.* J Cell Physiol, 2007. **213**(3): p. 626-34.

15. Li, Y., L. Xu, and B.R. Olsen, *Lessons from genetic forms of osteoarthritis for the pathogenesis of the disease.* Osteoarthritis Cartilage, 2007. **15**(10): p. 1101-5.

16. Martin, J.A. and J.A. Buckwalter, *Aging, articular cartilage chondrocyte senescence and osteoarthritis.* Biogerontology, 2002. **3**(5): p. 257-64.

17. *Autologous Chondrocyte Implantation Policy*, in *0247*, A. Inc., Editor. 2015.

18. Houard, X., M.B. Goldring, and F. Berenbaum, *Homeostatic mechanisms in articular cartilage and role of inflammation in osteoarthritis.* Curr Rheumatol Rep, 2013. **15**(11): p. 375.

19. Ayral, X., et al., *Synovitis: a potential predictive factor of structural progression of medial tibiofemoral knee osteoarthritis -- results of a 1 year longitudinal arthroscopic study in 422 patients.* Osteoarthritis Cartilage, 2005. **13**(5): p. 361-7.

20. Krasnokutsky, S., et al., *Quantitative magnetic resonance imaging evidence of synovial proliferation is associated with radiographic severity of knee osteoarthritis.* Arthritis Rheum, 2011. **63**(10): p. 2983-91.

21. Felson, D.T., et al., *Bone marrow edema and its relation to progression of knee osteoarthritis.* Ann Intern Med, 2003. **139**(5 Pt 1): p. 330-6.

22. Roemer, F.W., et al., *Presence of MRI-detected joint effusion and synovitis increases the risk of cartilage loss in knees without osteoarthritis at 30-month follow-up: the MOST study.* Ann Rheum Dis, 2011. **70**(10): p. 1804-9.

23. Bondeson, J., et al., *The role of synovial macrophages and macrophage-produced mediators in driving inflammatory and destructive responses in osteoarthritis.* Arthritis Rheum, 2010. **62**(3): p. 647-57.

24. Dean, G., et al., *Mast cells in the synovium and synovial fluid in osteoarthritis.* Br J Rheumatol, 1993. **32**(8): p. 671-5.

25. Skrzeczynska-Moncznik, J., et al., *Chemerin and the recruitment of NK cells to diseased skin.* Acta Biochim Pol, 2009. **56**(2): p. 355-60.

26. Sellam, J. and F. Berenbaum, *The role of synovitis in pathophysiology and clinical symptoms of osteoarthritis.* Nat Rev Rheumatol, 2010. **6**(11): p. 625-35.

27. Sokolove, J. and C.M. Lepus, *Role of inflammation in the pathogenesis of osteoarthritis: latest findings and interpretations.* Ther Adv Musculoskelet Dis, 2013. **5**(2): p. 77-94.

28. Shakibaei, M., et al., *Curcumin protects human chondrocytes from IL-l1beta-induced inhibition of collagen type II and beta1-integrin expression and activation of caspase-3: an immunomorphological study.* Ann Anat, 2005. **187**(5-6): p. 487-97.

29. Stove, J., et al., *Interleukin-1beta induces different gene expression of stromelysin, aggrecan and tumor-necrosis-factor-stimulated gene 6 in human osteoarthritic chondrocytes in vitro.* Pathobiology, 2000. **68**(3): p. 144-9.

30. Meszaros, E. and C.J. Malemud, *Prospects for treating osteoarthritis: enzyme-protein interactions regulating matrix metalloproteinase activity.* Ther Adv Chronic Dis, 2012. **3**(5): p. 219-29.

31. Vincenti, M.P. and C.E. Brinckerhoff, *Transcriptional regulation of collagenase (MMP-1, MMP-13) genes in arthritis: integration of complex signaling pathways for the recruitment of gene-specific transcription factors.* Arthritis Res, 2002. **4**(3): p. 157-64.

32. Mengshol, J.A., et al., *Interleukin-1 induction of collagenase 3 (matrix metalloproteinase 13) gene expression in chondrocytes requires p38, c-Jun N-terminal kinase, and nuclear factor kappaB: differential regulation of collagenase 1 and collagenase 3.* Arthritis Rheum, 2000. **43**(4): p. 801-11.

33. Pulsatelli, L., et al., *Chemokine production by human chondrocytes.* J Rheumatol, 1999. **26**(9): p. 1992-2001.

34. Alaaeddine, N., et al., *Production of the chemokine RANTES by articular chondrocytes and role in cartilage degradation.* Arthritis Rheum, 2001. **44**(7): p. 1633-43.

35. Lotz, M., R. Terkeltaub, and P.M. Villiger, *Cartilage and joint inflammation. Regulation of IL-8 expression by human articular chondrocytes.* J Immunol, 1992. **148**(2): p. 466-73.

36. Guerne, P.A., D.A. Carson, and M. Lotz, *IL-6 production by human articular chondrocytes. Modulation of its synthesis by cytokines, growth factors, and hormones in vitro.* J Immunol, 1990. **144**(2): p. 499-505.

37. Aigner, T., et al., *Gene expression profiling of serum- and interleukin-1 beta-stimulated primary human adult articular chondrocytes--a molecular analysis based on chondrocytes isolated from one donor.* Cytokine, 2005. **31**(3): p. 227-40.

38. Massicotte, F., et al., *Can altered production of interleukin-1beta, interleukin-6, transforming growth factor-beta and prostaglandin E(2) by isolated human subchondral osteoblasts identify two subgroups of osteoarthritic patients.* Osteoarthritis Cartilage, 2002. **10**(6): p. 491-500.

39. Sohn, D.H., et al., *Plasma proteins present in osteoarthritic synovial fluid can stimulate cytokine production via Toll-like receptor 4.* Arthritis Res Ther, 2012. **14**(1): p. R7.

40. Farahat, M.N., et al., *Cytokine expression in synovial membranes of patients with rheumatoid arthritis and osteoarthritis.* Ann Rheum Dis, 1993. **52**(12): p. 870-5.

41. Melchiorri, C., et al., *Enhanced and coordinated in vivo expression of inflammatory cytokines and nitric oxide synthase by chondrocytes from patients with osteoarthritis.* Arthritis Rheum, 1998. **41**(12): p. 2165-74.

42. Steenvoorden, M.M., et al., *Fibroblast-like synoviocyte-chondrocyte interaction in cartilage degradation.* Clin Exp Rheumatol, 2007. **25**(2): p. 239-45.

43. Alaaeddine, N., et al., *Osteoarthritic synovial fibroblasts possess an increased level of tumor necrosis factor-receptor 55 (TNF-R55) that mediates biological activation by TNF-alpha.* J Rheumatol, 1997. **24**(10): p. 1985-94.

44. Ye, Z., et al., *c-Jun N-terminal kinase - c-Jun pathway transactivates Bim to promote osteoarthritis.* Can J Physiol Pharmacol, 2014. **92**(2): p. 132-9.

45. Lopez-Armada, M.J., et al., *Cytokines, tumor necrosis factor-alpha and interleukin-1beta, differentially regulate apoptosis in osteoarthritis cultured human chondrocytes.* Osteoarthritis Cartilage, 2006. **14**(7): p. 660-9.

46. Heraud, F., A. Heraud, and M.F. Harmand, *Apoptosis in normal and osteoarthritic human articular cartilage.* Ann Rheum Dis, 2000. **59**(12): p. 959-65.

47. Saklatvala, J., *Tumour necrosis factor alpha stimulates resorption and inhibits synthesis of proteoglycan in cartilage.* Nature, 1986. **322**(6079): p. 547-9.

48. Seguin, C.A. and S.M. Bernier, *TNFalpha suppresses link protein and type II collagen expression in chondrocytes: Role of MEK1/2 and NF-kappaB signaling pathways.* J Cell Physiol, 2003. **197**(3): p. 356-69.

49. Lefebvre, V., C. Peeters-Joris, and G. Vaes, *Modulation by interleukin 1 and tumor necrosis factor alpha of production of collagenase, tissue inhibitor of metalloproteinases and collagen types in differentiated and dedifferentiated articular chondrocytes.* Biochim Biophys Acta, 1990. **1052**(3): p. 366-78.

50. Xue, J., et al., *Tumor necrosis factor-alpha induces ADAMTS-4 expression in human osteoarthritis chondrocytes.* Mol Med Rep, 2013. **8**(6): p. 1755-60.

51. Honorati, M.C., L. Cattini, and A. Facchini, *VEGF production by osteoarthritic chondrocytes cultured in micromass and stimulated by IL-17 and TNF-alpha.* Connect Tissue Res, 2007. **48**(5): p. 239-45.

52. Verma, P. and K. Dalal, *ADAMTS-4 and ADAMTS-5: key enzymes in osteoarthritis.* J Cell Biochem, 2011. **112**(12): p. 3507-14.

53. Suh, J., et al., *Injury and repair articular cartilage; related scientific issues.* Operative Techniques in Orthopeadics, 1997. **7**: p. 270-278.

54. Tabas, I. and C.K. Glass, *Anti-inflammatory therapy in chronic disease: challenges and opportunities.* Science, 2013. **339**(6116): p. 166-72.

55. Kon, E., et al., *Non-surgical management of early knee osteoarthritis.* Knee Surg Sports Traumatol Arthrosc, 2012. **20**(3): p. 436-49.

56. Clegg, D.O., et al., *Glucosamine, chondroitin sulfate, and the two in combination for painful knee osteoarthritis.* N Engl J Med, 2006. **354**(8): p. 795-808.

57. Sofat, N., et al., *Recent clinical evidence for the treatment of osteoarthritis: what we have learned.* Rev Recent Clin Trials, 2011. **6**(2): p. 114-26.

58. Madry, H., U.W. Grun, and G. Knutsen, *Cartilage repair and joint preservation: medical and surgical treatment options.* Dtsch Arztebl Int, 2011. **108**(40): p. 669-77.

59. Tuan, R.S., *A second-generation autologous chondrocyte implantation approach to the treatment of focal articular cartilage defects.* Arthritis Res Ther, 2007. **9**(5): p. 109.

60. Brittberg, M., et al., *Treatment of deep cartilage defects in the knee with autologous chondrocyte transplantation.* N Engl J Med, 1994. **331**(14): p. 889-95.

61. Henderson, I., et al., *Autologous chondrocyte implantation: superior biologic properties of hyaline cartilage repairs.* Clin Orthop Relat Res, 2007. **455**: p. 253-61.

62. Niemeyer, P., et al., *Influence of cell quality on clinical outcome after autologous chondrocyte implantation.* Am J Sports Med, 2012. **40**(3): p. 556-61.

63. Niemeyer, P., W. Koestler, and N.P. Sudkamp, *[Problems and complications of surgical techniques for treatment of full-thickness cartilage defects]*. Z Orthop Unfall, 2011. **149**(1): p. 45-51.

64. Bachmeier, C.J., et al., *A comparison of outcomes in osteoarthritis patients undergoing total hip and knee replacement surgery.* Osteoarthritis Cartilage, 2001. **9**(2): p. 137-46.

65. Shan, L., et al., *Total hip replacement: a systematic review and meta-analysis on mid-term quality of life.* Osteoarthritis Cartilage, 2014. **22**(3): p. 389-406.

66. Shan, L., et al., *Intermediate and long-term quality of life after total knee replacement: a systematic review and meta-analysis.* J Bone Joint Surg Am, 2015. **97**(2): p. 156-68.

67. Aglietti, P., et al., *The Insall-Burstein total knee replacement in osteoarthritis: a 10-year minimum follow-up.* J Arthroplasty, 1999. **14**(5): p. 560-5.

68. Parker, D.A., M.J. Dunbar, and C.H. Rorabeck, *Extensor mechanism failure associated with total knee arthroplasty: prevention and management.* J Am Acad Orthop Surg, 2003. **11**(4): p. 238-47.

69. Aggarwal, V.K., et al., *Revision total knee arthroplasty in the young patient: is there trouble on the horizon?* J Bone Joint Surg Am, 2014. **96**(7): p. 536-42.

70. Long, W.J., et al., *Total knee replacement in young, active patients: long-term follow-up and functional outcome: a concise follow-up of a previous report.* J Bone Joint Surg Am, 2014. **96**(18): p. e159.

71. Hanada, K., et al., *BMP-2 induction and TGF-beta 1 modulation of rat periosteal cell chondrogenesis.* J Cell Biochem, 2001. **81**(2): p. 284-94.

72. Liu, X., et al., *In vivo ectopic chondrogenesis of BMSCs directed by mature chondrocytes.* Biomaterials, 2010. **31**(36): p. 9406-14.

73. Mueller, M.B., et al., *Hypertrophy in mesenchymal stem cell chondrogenesis: effect of TGF-beta isoforms and chondrogenic conditioning.* Cells Tissues Organs, 2010. **192**(3): p. 158-66.

74. Shen, B., et al., *The role of BMP-7 in chondrogenic and osteogenic differentiation of human bone marrow multipotent mesenchymal stromal cells in vitro.* J Cell Biochem, 2010. **109**(2): p. 406-16.

75. Lories, R.J. and F.P. Luyten, *The bone-cartilage unit in osteoarthritis.* Nat Rev Rheumatol, 2011. **7**(1): p. 43-9.

76. Ge, Z., et al., *Functional biomaterials for cartilage regeneration.* J Biomed Mater Res A, 2012.

77. Raghunath, J., et al., *Biomaterials and scaffold design: key to tissue-engineering cartilage.* Biotechnol Appl Biochem, 2007. **46**(Pt 2): p. 73-84.

78. Ahmed, T.A. and M.T. Hincke, *Strategies for articular cartilage lesion repair and functional restoration.* Tissue Eng Part B Rev, 2010. **16**(3): p. 305-29.

79. Gilbert, T.W., T.L. Sellaro, and S.F. Badylak, *Decellularization of tissues and organs.* Biomaterials, 2006. **27**(19): p. 3675-83.

80. Badylak, S.F., D.O. Freytes, and T.W. Gilbert, *Extracellular matrix as a biological scaffold material: Structure and function.* Acta Biomater, 2009. **5**(1): p. 1-13.

81. van der Rest, M. and R. Garrone, *Collagen family of proteins.* FASEB J, 1991. **5**(13): p. 2814-23.

82. Bernard, M.P., et al., *Nucleotide sequences of complementary deoxyribonucleic acids for the pro alpha 1 chain of human type I procollagen. Statistical evaluation of structures that are conserved during evolution.* Biochemistry, 1983. **22**(22): p. 5213-23.

83. Bernard, M.P., et al., *Structure of a cDNA for the pro alpha 2 chain of human type I procollagen. Comparison with chick cDNA for pro alpha 2(I) identifies structurally conserved features of the protein and the gene.* Biochemistry, 1983. **22**(5): p. 1139-45.

84. Exposito, J.Y., et al., *Sea urchin collagen evolutionarily homologous to vertebrate pro-alpha 2(I) collagen.* J Biol Chem, 1992. **267**(22): p. 15559-62.

85. Constantinou, C.D. and S.A. Jimenez, *Structure of cDNAs encoding the triple-helical domain of murine alpha 2 (VI) collagen chain and comparison to human and chick homologues. Use of polymerase chain reaction and partially degenerate oligonucleotide for generation of novel cDNA clones.* Matrix, 1991. **11**(1): p. 1-9.

86. Gilbert, T.W., J.M. Freund, and S.F. Badylak, *Quantification of DNA in biologic scaffold materials.* J Surg Res, 2009. **152**(1): p. 135-9.

87. Atala, A., et al., *Tissue-engineered autologous bladders for patients needing cystoplasty.* Lancet, 2006. **367**(9518): p. 1241-6.

88. Barber, F.A., M.A. Herbert, and D.A. Coons, *Tendon augmentation grafts: biomechanical failure loads and failure patterns.* Arthroscopy, 2006. **22**(5): p. 534-8.

89. Butler, C.E. and V.G. Prieto, *Reduction of adhesions with composite AlloDerm/polypropylene mesh implants for abdominal wall reconstruction.* Plast Reconstr Surg, 2004. **114**(2): p. 464-73.

90. Catena, F., et al., *Lichtenstein repair of inguinal hernia with Surgisis inguinal hernia matrix soft-tissue graft in immunodepressed patients.* Hernia, 2005. **9**(1): p. 29-31.

91. Coons, D.A. and F. Alan Barber, *Tendon graft substitutes-rotator cuff patches.* Sports Med Arthrosc, 2006. **14**(3): p. 185-90.

92. Harper, C., *Permacol: clinical experience with a new biomaterial.* Hosp Med, 2001. **62**(2): p. 90-5.

93. Lee, M.S., *GraftJacket augmentation of chronic Achilles tendon ruptures.* Orthopedics, 2004. **27**(1 Suppl): p. s151-3.

94. Metcalfe, C. and K.S. Poon, *Long-term results of surgical techniques and procedures in men with benign prostatic hyperplasia.* Curr Urol Rep, 2011. **12**(4): p. 265-73.

95. Parker, D.M., et al., *Porcine dermal collagen (Permacol) for abdominal wall reconstruction.* Curr Surg, 2006. **63**(4): p. 255-8.

96. Sclafani, A.P., et al., *Evaluation of acellular dermal graft in sheet (AlloDerm) and injectable (micronized AlloDerm) forms for soft tissue augmentation. Clinical observations and histological analysis.* Arch Facial Plast Surg, 2000. **2**(2): p. 130-6.

97. Smart, N., A. Immanuel, and M. Mercer-Jones, *Laparoscopic repair of a Littre's hernia with porcine dermal collagen implant (Permacol).* Hernia, 2007. **11**(4): p. 373-6.

98. Ueno, T., et al., *Clinical application of porcine small intestinal submucosa in the management of infected or potentially contaminated abdominal defects.* J Gastrointest Surg, 2004. **8**(1): p. 109-12.

99. Nelson, C.M. and M.J. Bissell, *Of extracellular matrix, scaffolds, and signaling: tissue architecture regulates development, homeostasis, and cancer.* Annu Rev Cell Dev Biol, 2006. **22**: p. 287-309.

100. Reing, J.E., et al., *The effects of processing methods upon mechanical and biologic properties of porcine dermal extracellular matrix scaffolds.* Biomaterials, 2010. **31**(33): p. 8626-33.

101. Reing, J.E., et al., *Degradation products of extracellular matrix affect cell migration and proliferation.* Tissue Eng Part A, 2009. **15**(3): p. 605-14.

102. Ahn, H.H., et al., *Porcine small intestinal submucosa sheets as a scaffold for human bone marrow stem cells.* Int J Biol Macromol, 2007. **41**(5): p. 590-6.

103. Sellaro, T.L., et al., *Maintenance of hepatic sinusoidal endothelial cell phenotype in vitro using organ-specific extracellular matrix scaffolds.* Tissue Engineering, 2007. **13**(9): p. 2301-2310.

104. Gong, Y.Y., et al., *A sandwich model for engineering cartilage with acellular cartilage sheets and chondrocytes.* Biomaterials, 2011. **32**(9): p. 2265-73.

105. Hoganson, D.M., et al., *Differentiation of human bone marrow mesenchymal stem cells on decellularized extracellular matrix materials.* J Biomed Mater Res A, 2014. **102**(8): p. 2875-83.

106. Yang, Q., et al., *A cartilage ECM-derived 3-D porous acellular matrix scaffold for in vivo cartilage tissue engineering with PKH26-labeled chondrogenic bone marrow-derived mesenchymal stem cells.* Biomaterials, 2008. **29**(15): p. 2378-87.

107. Stabile, K.J., et al., *An acellular, allograft-derived meniscus scaffold in an ovine model.* Arthroscopy, 2010. **26**(7): p. 936-48.

108. Azarin, S.M. and S.P. Palecek, *Development of Scalable Culture Systems for Human Embryonic Stem Cells.* Biochem Eng J, 2010. **48**(3): p. 378.

109. Varani, J., et al., *Cell growth on microcarriers: comparison of proliferation on and recovery from various substrates.* J Biol Stand, 1986. **14**(4): p. 331-6.

110. Malda, J., et al., *Expansion of bovine chondrocytes on microcarriers enhances redifferentiation.* Tissue Eng, 2003. **9**(5): p. 939-48.

111. Rafiq, Q.A., et al., *Culture of human mesenchymal stem cells on microcarriers in a 5 l stirred-tank bioreactor.* Biotechnol Lett, 2013. **35**(8): p. 1233-45.

112. Surrao, D.C., et al., *Can microcarrier-expanded chondrocytes synthesize cartilaginous tissue in vitro?* Tissue Eng Part A, 2011. **17**(15-16): p. 1959-67.

113. Pettersson, S., et al., *Human articular chondrocytes on macroporous gelatin microcarriers form structurally stable constructs with blood-derived biological glues in vitro.* J Tissue Eng Regen Med, 2009. **3**(6): p. 450-60.

114. Malda, J., et al., *Expansion of human nasal chondrocytes on macroporous microcarriers enhances redifferentiation.* Biomaterials, 2003. **24**(28): p. 5153-61.

115. Pettersson, S., et al., *Cell expansion of human articular chondrocytes on macroporous gelatine scaffolds-impact of microcarrier selection on cell proliferation.* Biomed Mater, 2011. **6**(6): p. 065001.

116. Schrobback, K., et al., *Adult human articular chondrocytes in a microcarrier-based culture system: expansion and redifferentiation.* J Orthop Res, 2011. **29**(4): p. 539-46.

117. Cetinkaya, G., et al., *Derivation, characterization and expansion of fetal chondrocytes on different microcarriers.* Cytotechnology, 2011. **63**(6): p. 633-43.

118. Singh, M., et al., *Microsphere-based scaffolds for cartilage tissue engineering: using subcritical CO(2) as a sintering agent.* Acta Biomater, 2010. **6**(1): p. 137-43.

119. Georgi, N., C. van Blitterswijk, and M. Karperien, *Mesenchymal Stromal/Stem Cell-or Chondrocyte-Seeded Microcarriers as Building Blocks for Cartilage Tissue Engineering.* Tissue Eng Part A, 2014.

120. Dessau, W., et al., *Extracellular matrix formation by chondrocytes in monolayer culture.* J Cell Biol, 1981. **90**(1): p. 78-83.

121. Canavan, H.E., et al., *Cell sheet detachment affects the extracellular matrix: a surface science study comparing thermal liftoff, enzymatic, and mechanical methods.* J Biomed Mater Res A, 2005. **75**(1): p. 1-13.

122. Francois, M., et al., *Human MSC suppression correlates with cytokine induction of indoleamine 2,3-dioxygenase and bystander M2 macrophage differentiation.* Mol Ther, 2012. **20**(1): p. 187-95.

123. Maggini, J., et al., *Mouse bone marrow-derived mesenchymal stromal cells turn activated macrophages into a regulatory-like profile.* PLoS One, 2010. **5**(2): p. e9252.

124. Chiesa, S., et al., *Mesenchymal stem cells impair in vivo T-cell priming by dendritic cells.* Proc Natl Acad Sci U S A, 2011. **108**(42): p. 17384-9.

125. Djouad, F., et al., *Mesenchymal stem cells inhibit the differentiation of dendritic cells through an interleukin-6-dependent mechanism.* Stem Cells, 2007. **25**(8): p. 2025-32.

126. Nauta, A.J., et al., *Mesenchymal stem cells inhibit generation and function of both CD34+-derived and monocyte-derived dendritic cells.* J Immunol, 2006. **177**(4): p. 2080-7.

127. Corcione, A., et al., *Human mesenchymal stem cells modulate B-cell functions.* Blood, 2006. **107**(1): p. 367-72.

128. Di Nicola, M., et al., *Human bone marrow stromal cells suppress T-lymphocyte proliferation induced by cellular or nonspecific mitogenic stimuli.* Blood, 2002. **99**(10): p. 3838-43.

129. Aggarwal, S. and M.F. Pittenger, *Human mesenchymal stem cells modulate allogeneic immune cell responses.* Blood, 2005. **105**(4): p. 1815-22.

130. Duffy, M.M., et al., *Mesenchymal stem cell inhibition of T-helper 17 cell-differentiation is triggered by cell-cell contact and mediated by prostaglandin E2 via the EP4 receptor.* Eur J Immunol, 2011. **41**(10): p. 2840-51.

131. Ge, W., et al., *Regulatory T-cell generation and kidney allograft tolerance induced by mesenchymal stem cells associated with indoleamine 2,3-dioxygenase expression.* Transplantation, 2010. **90**(12): p. 1312-20.

132. Zhao, W., et al., *TGF-beta expression by allogeneic bone marrow stromal cells ameliorates diabetes in NOD mice through modulating the distribution of CD4+ T cell subsets.* Cell Immunol, 2008. **253**(1-2): p. 23-30.

133. English, K., et al., *IFN-gamma and TNF-alpha differentially regulate immunomodulation by murine mesenchymal stem cells.* Immunol Lett, 2007. **110**(2): p. 91-100.

134. Ren, G., et al., *Mesenchymal stem cell-mediated immunosuppression occurs via concerted action of chemokines and nitric oxide.* Cell Stem Cell, 2008. **2**(2): p. 141-50.

135. Prasanna, S.J., et al., *Pro-inflammatory cytokines, IFNgamma and TNFalpha, influence immune properties of human bone marrow and Wharton jelly mesenchymal stem cells differentially.* PLoS One, 2010. **5**(2): p. e9016.

136. Opitz, C.A., et al., *Toll-like receptor engagement enhances the immunosuppressive properties of human bone marrow-derived mesenchymal stem cells by inducing indoleamine-2,3-dioxygenase-1 via interferon-beta and protein kinase R.* Stem Cells, 2009. **27**(4): p. 909-19.

137. Waterman, R.S., et al., *A new mesenchymal stem cell (MSC) paradigm: polarization into a pro-inflammatory MSC1 or an Immunosuppressive MSC2 phenotype.* PLoS One, 2010. **5**(4): p. e10088.

138. Sart, S., et al., *Three-dimensional aggregates of mesenchymal stem cells: cellular mechanisms, biological properties, and applications.* Tissue Eng Part B Rev, 2014. **20**(5): p. 365-80.

139. Lee, E.J., et al., *Spherical bullet formation via E-cadherin promotes therapeutic potency of mesenchymal stem cells derived from human umbilical cord blood for myocardial infarction.* Mol Ther, 2012. **20**(7): p. 1424-33.

140. Dromard, C., et al., *Human adipose derived stroma/stem cells grow in serum-free medium as floating spheres.* Exp Cell Res, 2011. **317**(6): p. 770-80.

141. Kapur, S.K., et al., *Human adipose stem cells maintain proliferative, synthetic and multipotential properties when suspension cultured as self-assembling spheroids.* Biofabrication, 2012. **4**(2): p. 025004.

142. Baraniak, P.R. and T.C. McDevitt, *Scaffold-free culture of mesenchymal stem cell spheroids in suspension preserves multilineage potential.* Cell Tissue Res, 2012. **347**(3): p. 701-11.

143. Li, Y., et al., *Three-dimensional spheroid culture of human umbilical cord mesenchymal stem cells promotes cell yield and stemness maintenance.* Cell Tissue Res, 2015. **360**(2): p. 297-307.

144. Pennock, R., et al., *Human cell dedifferentiation in mesenchymal condensates through controlled autophagy.* Sci Rep, 2015. **5**: p. 13113.

145. Lee, W.Y., et al., *The use of injectable spherically symmetric cell aggregates self-assembled in a thermo-responsive hydrogel for enhanced cell transplantation.* Biomaterials, 2009. **30**(29): p. 5505-13.

146. Ma, D., et al., *Engineering injectable bone using bone marrow stromal cell aggregates.* Stem Cells Dev, 2011. **20**(6): p. 989-99.

147. Wang, C.C., et al., *Spherically symmetric mesenchymal stromal cell bodies inherent with endogenous extracellular matrices for cellular cardiomyoplasty.* Stem Cells, 2009. **27**(3): p. 724-32.

148. Molendijk, I., et al., *Intraluminal Injection of Mesenchymal Stromal Cells in Spheroids Attenuates Experimental Colitis.* J Crohns Colitis, 2016. **10**(8): p. 953-64.

149. Kabiri, M., et al., *3D mesenchymal stem/stromal cell osteogenesis and autocrine signalling.* Biochem Biophys Res Commun, 2012. **419**(2): p. 142-7.

150. Bhang, S.H., et al., *Angiogenesis in ischemic tissue produced by spheroid grafting of human adipose-derived stromal cells.* Biomaterials, 2011. **32**(11): p. 2734-47.

151. Zhang, Q., et al., *Three-dimensional spheroid culture of human gingiva-derived mesenchymal stem cells enhances mitigation of chemotherapy-induced oral mucositis.* Stem Cells Dev, 2012. **21**(6): p. 937-47.

152. Santos, J.M., et al., *Three-dimensional spheroid cell culture of umbilical cord tissue-derived mesenchymal stromal cells leads to enhanced paracrine induction of wound healing.* Stem Cell Res Ther, 2015. **6**: p. 90.

153. Bartosh, T.J., et al., *Aggregation of human mesenchymal stromal cells (MSCs) into 3D spheroids enhances their antiinflammatory properties.* Proc Natl Acad Sci U S A, 2010. **107**(31): p. 13724-9.

154. Ylostalo, J.H., et al., *Human mesenchymal stem/stromal cells cultured as spheroids are self-activated to produce prostaglandin E2 that directs stimulated macrophages into an anti-inflammatory phenotype.* Stem Cells, 2012. **30**(10): p. 2283-96.

155. Zimmermann, J.A. and T.C. McDevitt, *Pre-conditioning mesenchymal stromal cell spheroids for immunomodulatory paracrine factor secretion.* Cytotherapy, 2014. **16**(3): p. 331-45.

156. Zimmermann, J.A., M.H. Hettiaratchi, and T.C. McDevitt, *Enhanced Immunosuppression of T Cells by Sustained Presentation of Bioactive Interferon-gamma Within Three-Dimensional Mesenchymal Stem Cell Constructs.* Stem Cells Transl Med, 2017. **6**(1): p. 223-237.

157. Fishman, J.M., et al., *Immunomodulatory effect of a decellularized skeletal muscle scaffold in a discordant xenotransplantation model.* Proc Natl Acad Sci U S A, 2013. **110**(35): p. 14360-5.

158. Garfias, Y., et al., *Amniotic membrane is an immunosuppressor of peripheral blood mononuclear cells.* Immunol Invest, 2011. **40**(2): p. 183-96.

159. Mamede, A.C., et al., *Amniotic membrane: from structure and functions to clinical applications.* Cell Tissue Res, 2012. **349**(2): p. 447-58.

160. Ji, S.Z., et al., *An epidermal stem cells niche microenvironment created by engineered human amniotic membrane.* Biomaterials, 2011. **32**(31): p. 7801-11.

161. Koob, T.J., et al., *Biological properties of dehydrated human amnion/chorion composite graft: implications for chronic wound healing.* Int Wound J, 2013. **10**(5): p. 493-500.

162. Diaz-Prado, S., et al., *Potential use of the human amniotic membrane as a scaffold in human articular cartilage repair.* Cell Tissue Bank, 2010. **11**(2): p. 183-95.

163. Krishnamurithy, G., et al., *Human amniotic membrane as a chondrocyte carrier vehicle/substrate: in vitro study.* J Biomed Mater Res A, 2011. **99**(3): p. 500-6.

164. Massee, M., et al., *Dehydrated human amnion/chorion membrane regulates stem cell activity in vitro.* J Biomed Mater Res B Appl Biomater, 2015.

165. Zheng, Y., et al., *Topical administration of cryopreserved living micronized amnion accelerates wound healing in diabetic mice by modulating local microenvironment.* Biomaterials, 2017. **113**: p. 56-67.

166. Willett, N.J., et al., *Intra-articular injection of micronized dehydrated human amnion/chorion membrane attenuates osteoarthritis development.* Arthritis Res Ther, 2014. **16**(1): p. R47.

167. Bendele, A.M., *Animal models of osteoarthritis.* J Musculoskelet Neuronal Interact, 2001. **1**(4): p. 363-76.

168. Janusz, M.J., et al., *Induction of osteoarthritis in the rat by surgical tear of the meniscus: Inhibition of joint damage by a matrix metalloproteinase inhibitor.* Osteoarthritis Cartilage, 2002. **10**(10): p. 785-91.

169. Wei, T., et al., *Analysis of early changes in the articular cartilage transcriptisome in the rat meniscal tear model of osteoarthritis: pathway comparisons with the rat anterior cruciate transection model and with human osteoarthritic cartilage.* Osteoarthritis Cartilage, 2010. **18**(7): p. 992-1000.

170. Ashraf, S., P.I. Mapp, and D.A. Walsh, *Contributions of angiogenesis to inflammation, joint damage, and pain in a rat model of osteoarthritis.* Arthritis Rheum, 2011. **63**(9): p. 2700-10.

171. Thote, T., et al., *Localized 3D analysis of cartilage composition and morphology in small animal models of joint degeneration.* Osteoarthritis Cartilage, 2013. **21**(8): p. 1132-41.

172. Gerwin, N., et al., *The OARSI histopathology initiative - recommendations for histological assessments of osteoarthritis in the rat.* Osteoarthritis Cartilage, 2010. **18 Suppl 3**: p. S24-34.

173. Glowacki, J., *In vitro engineering of cartilage.* J Rehabil Res Dev, 2000. **37**(2): p. 171-7.

174. Minas, T. and R. Chiu, *Autologous chondrocyte implantation.* The American journal of knee surgery, 2000. **13**(1): p. 41-50.

175. Schnabel, M., et al., *Dedifferentiation-associated changes in morphology and gene expression in primary human articular chondrocytes in cell culture*, in *Osteoarthritis and Cartilage*. 2002. p. 62-70.

176. Brittberg, M., *Cell Carriers as the Next Generation of Cell Therapy for Cartilage Repair.* The American Journal of Sports Medicine, 2009. **38**(6): p. 1259-1271.

177. Bartlett, W., et al., *Autologous chondrocyte implantation versus matrix-induced autologous chondrocyte implantation for osteochondral defects of the knee: a prospective, randomised study.* J Bone Joint Surg Br, 2005. **87**(5): p. 640-5.

178. Bahuaud, J., et al., *[Implantation of autologous chondrocytes for cartilagenous lesions in young patients. A study of 24 cases]*. Chirurgie, 1998. **123**(6): p. 568-71.

179. Behrens, P., et al., *[New therapy procedure for localized cartilage defects. Encouraging results with autologous chondrocyte implantation]*. MMW Fortschr Med, 1999. **141**(45): p. 49-51.

180. Panagopoulos, A., L. van Niekerk, and I. Triantafillopoulos, *Autologous chondrocyte implantation for knee cartilage injuries: moderate functional outcome and performance in patients with high-impact activities.* Orthopedics, 2012. **35**(1): p. e6-14.

181. Marcacci, M., et al., *Arthroscopic autologous chondrocyte transplantation: technical note.* Knee Surg Sports Traumatol Arthrosc, 2002. **10**(3): p. 154-9.

182. Ossendorf, C., et al., *Treatment of posttraumatic and focal osteoarthritic cartilage defects of the knee with autologous polymer-based three-dimensional chondrocyte grafts: 2-year clinical results.* Arthritis Res Ther, 2007. **9**(2): p. R41.

183. Selmi, T.A., et al., *Autologous chondrocyte implantation in a novel alginate-agarose hydrogel: outcome at two years.* J Bone Joint Surg Br, 2008. **90**(5): p. 597-604.

184. Richardson, J.B., et al., *Repair of human articular cartilage after implantation of autologous chondrocytes.* J Bone Joint Surg Br, 1999. **81**(6): p. 1064-8.

185. Gong, Y.Y., et al., *A sandwich model for engineering cartilage with acellular cartilage sheets and chondrocytes.* Biomaterials, 2011. **32**(9): p. 2265-2273.

186. Yang, Q., et al., *A cartilage ECM-derived 3-D porous acellular matrix scaffold for in vivo cartilage tissue engineering with PKH26-labeled chondrogenic bone marrow-derived mesenchymal stem cells.* Biomaterials, 2008. **29**(15): p. 2378-2387.

187. Hoshiba, T., et al., *Maintenance of cartilaginous gene expression on extracellular matrix derived from serially passaged chondrocytes during in vitro chondrocyte expansion.* Journal of Biomedical Materials Research Part A, 2012. **100A**(3): p. 694-702.

188. Reing, J.E., et al., *The effects of processing methods upon mechanical and biologic properties of porcine dermal extracellular matrix scaffolds.* Biomaterials, 2010. **31**(33): p. 8626-8633.

189. Temu, T.M., et al., *The mechanism of ascorbic acid-induced differentiation of ATDC5 chondrogenic cells.* Am J Physiol Endocrinol Metab, 2010. **299**(2): p. E325-34.

190. Livak, K.J. and T.D. Schmittgen, *Analysis of relative gene expression data using real-time quantitative PCR and the 2(-Delta Delta C(T)) Method.* Methods, 2001. **25**(4): p. 402-8.

191. Gilbert, T.W., T.L. Sellaro, and S.F. Badylak, *Decellularization of tissues and organs.* Biomaterials, 2006. **27**(19): p. 3675-3683.

192. Malda, J., et al., *Expansion of human nasal chondrocytes on macroporous microcarriers enhances redifferentiation.* Biomaterials, 2003. **24**(28): p. 5153-5161.

193. Sophia Fox, A.J., A. Bedi, and S.A. Rodeo, *The Basic Science of Articular Cartilage: Structure, Composition, and Function.* Sports Health, 2009. **1**(6): p. 461-468.

194. Bassi, E.J., C.A. Aita, and N.O. Camara, *Immune regulatory properties of multipotent mesenchymal stromal cells: Where do we stand?* World J Stem Cells, 2011. **3**(1): p. 1-8.

195. Yi, T. and S.U. Song, *Immunomodulatory properties of mesenchymal stem cells and their therapeutic applications.* Arch Pharm Res, 2012. **35**(2): p. 213-21.

196. Tolar, J., et al., *Concise review: hitting the right spot with mesenchymal stromal cells.* Stem Cells, 2010. **28**(8): p. 1446-55.

197. Byron, C.R., et al., *In vitro expression of receptor activator of nuclear factor-kappaB ligand and osteoprotegerin in cultured equine articular cells.* Am J Vet Res, 2010. **71**(6): p. 615-22.

198. Andreassen, S.M., et al., *mRNA expression of genes involved in inflammation and haemostasis in equine fibroblast-like synoviocytes following exposure to lipopolysaccharide, fibrinogen and thrombin.* BMC Vet Res, 2015. **11**: p. 141.

199. Wada, J.A. and M. Sata, *Generalized convulsive seizures induced by daily electrical stimulation of the amygdala in cats. Correlative electrographic and behavioral features.* Neurology, 1974. **24**(6): p. 565-74.

200. Xu, H., et al., *Astragaloside IV suppresses inflammatory mediator production in synoviocytes and collageninduced arthritic rats.* Mol Med Rep, 2016. **13**(4): p. 3289-96.

201. Reece, D.S., et al. *Novel Method of Evaluating Cartilage Surface Roughness in a Rat OA Model using Contrast Based CT Imaging*. in *Orthopedic Research Society*. 2014.

202. Wood, L.B., et al., *Identification of neurotoxic cytokines by profiling Alzheimer's disease tissues and neuron culture viability screening.* Sci Rep, 2015. **5**: p. 16622.

203. Li, Y.P., et al., *Human mesenchymal stem cells license adult CD34+ hemopoietic progenitor cells to differentiate into regulatory dendritic cells through activation of the Notch pathway.* J Immunol, 2008. **180**(3): p. 1598-608.

204. Zhang, B., et al., *Mesenchymal stem cells induce mature dendritic cells into a novel Jagged-2-dependent regulatory dendritic cell population.* Blood, 2009. **113**(1): p. 46-57.

205. White, D.E., *Analyzing multicellular interactions: a hybrid computational and biological pattern recognition approach*, in *Biomedical Engineering*. 2015, Georgia Institute of Technology. p. 220.

206. Rijk, P.C., *Meniscal allograft transplantation--part I: background, results, graft selection and preservation, and surgical considerations.* Arthroscopy, 2004. **20**(7): p. 728-43.

207. Allen, K.D., et al., *Gait and behavior in an IL1beta-mediated model of rat knee arthritis and effects of an IL1 antagonist.* J Orthop Res, 2011. **29**(5): p. 694-703.

208. Harris, R., J.B. Millard, and S.K. Banerjee, *Radiosodium clearance from the knee joint in rheumatoid arthritis.* Ann Rheum Dis, 1958. **17**(2): p. 189-95.

209. Ozeki, N., et al., *Not single but periodic injections of synovial mesenchymal stem cells maintain viable cells in knees and inhibit osteoarthritis progression in rats.* Osteoarthritis Cartilage, 2016. **24**(6): p. 1061-70.

210. Mei, L., et al., *Culture-expanded allogenic adipose tissue-derived stem cells attenuate cartilage degeneration in an experimental rat osteoarthritis model.* PLoS One, 2017. **12**(4): p. e0176107.

211. Yang, X., et al., *Intraarticular Injection of Allogenic Mesenchymal Stem Cells has a Protective Role for the Osteoarthritis.* Chin Med J (Engl), 2015. **128**(18): p. 2516-23.

212. Clouet, J., et al., *From osteoarthritis treatments to future regenerative therapies for cartilage.* Drug Discov Today, 2009. **14**(19-20): p. 913-25.

213. Gerwin, N., C. Hops, and A. Lucke, *Intraarticular drug delivery in osteoarthritis.* Adv Drug Deliv Rev, 2006. **58**(2): p. 226-42.

214. Martel-Pelletier, J., L.M. Wildi, and J.P. Pelletier, *Future therapeutics for osteoarthritis.* Bone, 2012. **51**(2): p. 297-311.

215. English, K., *Mechanisms of mesenchymal stromal cell immunomodulation.* Immunol Cell Biol, 2013. **91**(1): p. 19-26.

216. Kloefkorn, H.E. and K. Allen, *Examining the Nexus Amongst Joint Degeneration, Disability, and Chronic Pain Using a Rodent Model of Post-Traumatic Knee Osteoarthritis.* University of Florida, 2016.

217. von Bahr, L., et al., *Analysis of tissues following mesenchymal stromal cell therapy in humans indicates limited long-term engraftment and no ectopic tissue formation.* Stem Cells, 2012. **30**(7): p. 1575-8.

218. Valles, G., et al., *Topographical cues regulate the crosstalk between MSCs and macrophages.* Biomaterials, 2015. **37**: p. 124-33.

219. Abdeen, A.A., et al., *Matrix composition and mechanics direct proangiogenic signaling from mesenchymal stem cells.* Tissue Eng Part A, 2014. **20**(19-20): p. 2737-45.

220. Le Blanc, K., et al., *Mesenchymal stem cells for treatment of steroid-resistant, severe, acute graft-versus-host disease: a phase II study.* Lancet, 2008. **371**(9624): p. 1579-86.

221. Wang, D., et al., *Umbilical cord mesenchymal stem cell transplantation in active and refractory systemic lupus erythematosus: a multicenter clinical study.* Arthritis Res Ther, 2014. **16**(2): p. R79.

222. Duijvestein, M., et al., *Pretreatment with interferon-gamma enhances the therapeutic activity of mesenchymal stromal cells in animal models of colitis.* Stem Cells, 2011. **29**(10): p. 1549-58.

223. Polchert, D., et al., *IFN-gamma activation of mesenchymal stem cells for treatment and prevention of graft versus host disease.* Eur J Immunol, 2008. **38**(6): p. 1745-55.

224. Lu, P., et al., *Extracellular matrix degradation and remodeling in development and disease.* Cold Spring Harb Perspect Biol, 2011. **3**(12).

225. Niknejad, H., et al., *Properties of the amniotic membrane for potential use in tissue engineering.* Eur Cell Mater, 2008. **15**: p. 88-99.

226. Xu, Y. and Q. Yu, *E-cadherin negatively regulates CD44-hyaluronan interaction and CD44-mediated tumor invasion and branching morphogenesis.* J Biol Chem, 2003. **278**(10): p. 8661-8.

227. Hao, Y., et al., *Identification of antiangiogenic and antiinflammatory proteins in human amniotic membrane.* Cornea, 2000. **19**(3): p. 348-52.

228. Haringman, J.J., et al., *Chemokine and chemokine receptor expression in paired peripheral blood mononuclear cells and synovial tissue of patients with rheumatoid arthritis, osteoarthritis, and reactive arthritis.* Ann Rheum Dis, 2006. **65**(3): p. 294-300.

229. Turner, A.E. and L.E. Flynn, *Design and characterization of tissue-specific extracellular matrix-derived microcarriers.* Tissue Eng Part C Methods, 2012. **18**(3): p. 186-97.

230. Turner, A.E., et al., *The performance of decellularized adipose tissue microcarriers as an inductive substrate for human adipose-derived stem cells.* Biomaterials, 2012. **33**(18): p. 4490-9.

231. Yu, C., et al., *Decellularized adipose tissue microcarriers as a dynamic culture platform for human adipose-derived stem/stromal cell expansion.* Biomaterials, 2017. **120**: p. 66-80.

232. Lin, Y.K. and D.C. Liu, *Effects of pepsin digestion at different temperatures and times on properties of telopeptide-poor collagen from bird feet.* Food Chemistry, 2006. **94**(4): p. 621-625.

233. Sutherland, A.J., et al., *Decellularized cartilage may be a chondroinductive material for osteochondral tissue engineering.* PLoS One, 2015. **10**(5): p. e0121966.

234. Bartok, B. and G.S. Firestein, *Fibroblast-like synoviocytes: key effector cells in rheumatoid arthritis.* Immunol Rev, 2010. **233**(1): p. 233-55.

235. Chen, D.P., et al., *Activation of human fibroblast-like synoviocytes by uric acid crystals in rheumatoid arthritis.* Cell Mol Immunol, 2011. **8**(6): p. 469-78.

236. Ribel-Madsen, S., et al., *A synoviocyte model for osteoarthritis and rheumatoid arthritis: response to Ibuprofen, betamethasone, and ginger extract-a cross-sectional in vitro study.* Arthritis, 2012. **2012**: p. 505842.

237. Scarritt, M.E., N.C. Pashos, and B.A. Bunnell, *A review of cellularization strategies for tissue engineering of whole organs.* Front Bioeng Biotechnol, 2015. **3**: p. 43.

238. Ivanov, D.P. and A.M. Grabowska, *Spheroid arrays for high-throughput single-cell analysis of spatial patterns and biomarker expression in 3D.* Sci Rep, 2017. **7**: p. 41160.

239. Katayama, R., et al., *Repair of articular cartilage defects in rabbits using CDMP1 gene-transfected autologous mesenchymal cells derived from bone marrow.* Rheumatology (Oxford), 2004. **43**(8): p. 980-5.

240. Lind, M., et al., *Cartilage repair with chondrocytes in fibrin hydrogel and MPEG polylactide scaffold: an in vivo study in goats.* Knee Surg Sports Traumatol Arthrosc, 2008. **16**(7): p. 690-8.

241. Murphy, J.M., et al., *Stem cell therapy in a caprine model of osteoarthritis.* Arthritis Rheum, 2003. **48**(12): p. 3464-74.

242. Clements, K.M., et al., *Cellular and histopathological changes in the infrapatellar fat pad in the monoiodoacetate model of osteoarthritis pain.* Osteoarthritis Cartilage, 2009. **17**(6): p. 805-12.

243. Messner, K. and W. Maletius, *The long-term prognosis for severe damage to weight-bearing cartilage in the knee: a 14-year clinical and radiographic follow-up in 28 young athletes.* Acta Orthop Scand, 1996. **67**(2): p. 165-8.

244. Brown, T.D., et al., *Posttraumatic osteoarthritis: a first estimate of incidence, prevalence, and burden of disease.* J Orthop Trauma, 2006. **20**(10): p. 739-44.

245. Anraku, Y., et al., *The chondrogenic repair response of undifferentiated mesenchymal cells in rat full-thickness articular cartilage defects.* Osteoarthritis Cartilage, 2008. **16**(8): p. 961-4.

246. Chu, C.R., M. Szczodry, and S. Bruno, *Animal models for cartilage regeneration and repair.* Tissue Eng Part B Rev, 2010. **16**(1): p. 105-15.

247. Furukawa, T., et al., *Biochemical studies on repair cartilage resurfacing experimental defects in the rabbit knee.* J Bone Joint Surg Am, 1980. **62**(1): p. 79-89.

248. Yarmola, E.G., et al., *Comparing intra-articular CTXII levels assessed via magnetic capture or lavage in a rat knee osteoarthritis model.* Osteoarthritis Cartilage, 2017. **25**(7): p. 1189-1194.